ADDIS ABABA UNIVERSITY
ADDIS ABABA INSTITUTE OF TECHNOLOGY
SCHOOL OF MECHANICAL AND INDUSTRIAL ENGINEERING

Development and Characterization of the Mechanical Properties of Al2024 alloy Reinforced with SiO_2 and Bagasse Ash Composite

A Master Thesis Submitted to Graduate School of Addis Ababa University In Partial Fulfillment of the Requirements for the Award of Degree of Masters of Science (M.Sc.) In Mechanical Engineering (Manufacturing Engineering)

By: **Senait Menbere Lencho**

Advisor: **Prof. Shantha Kumar** (Associate Professor)

Co-Advisor: **Mr. Henok Zewdu** (PhD Candidate)

July, 2021

Addis Ababa, Ethiopia

ADDIS ABABA UNIVERSITY
ADDIS ABABA INSTITUTE OF TECHNOLOGY
SCHOOL OF MECHANICAL AND INDUSTRIAL ENGINEERING

Development and Characterization of the Mechanical Properties of Al2024 alloy Reinforced with SiO_2 and Bagasse Ash Composite

By: Senait Menbere Lencho
Submitted in accordance with the requirements for the degree
Master of Science (M.Sc.)

Approved by: Board of Examiners

Prof. Shantha Kumar, Advisor	Signature	10.09.2021 Date
Mr. Henok Zewdu, Co-Advisor	Signature	11/09/2021 Date
Dr. Desalegn Wagaso, Internal Examiner	Signature	20/09/21 Date
Dr. Mesfin Gizaw, External Examiner	Signature	21/09/21 Date
Dr. Yilma Tadesse, Dean of the School	Signature	22/09/21 Date

Addis Ababa University * Addis Ababa Institute of Technology * Director of Postgraduate Program

DECLARATION

I now declare that this thesis entitled "**Development and Characterization of the Mechanical Properties of Al2024 Alloy Reinforced with SiO_2 and Bagasse Ash Composite**" is prepared by me with the guidance of my advisors. The work contained here is my own except where explicitly stated otherwise in the text. This work had never been submitted in a complete or part, for any other degree or professional qualification.

Senait Menbere Lencho		10/09/2021
Student Name:	Signature	Date

This is to certify that the above declaration made by the candidate is correct to the best of our knowledge and belief. It has been submitted for examination with our approval.

Prof. Shantha Kumar		10/09/2021
Advisor	Signature	Date

Mr. Henok Zewdu		11/09/2021
Co-Advisor	Signature	Date

ACKNOWLEDGEMENT

First, I would like to express my heart full thanks to my almighty God: who is the basis for all the successful progress of my life as a whole and this research as a particular.

I want to express my deepest gratitude to my Supervisor, Professor Shantha Kumar, and co-advisor, Mr. Henok Zewdu, for their valuable support, encouragement, guidance, and valuable criticism during this thesis work. I want to thank the mechanical and industrial engineering staff of AAiT for their excellent hospitality and invaluable support during this entire journey of my study.

I want to give genuine gratitude to Addis Ababa University for the provided female scholarship opportunity.

I want to express my gratitude to Ethiopian airlines management and Mr. Henok, structural department head; Mr. Takele HR head; Mr. Befekadu Buche, and the structural department crew for their limitless cooperation and support of experimental materials of the thesis with providing the required materials.

I want to thank Ethiopian Technical University in general and Mr. Gezahegn, the Manufacturing Engineering department head and all machine shop crew.

I want to thank the Wenji sugar factory for providing all the necessary materials & equipment intended for fabricating the test samples.

I also want to acknowledge Mr. Fisha (Defense University Engineering College, Mechanical Engineering department) for facilitating material lab and their valuable support during lab tests on UTM.

Last but not least, I would like to express my gratitude to my family and fellow friends who were supporting and encouraging me during this entire study period.

ABSTRACT

Silica sand and sugarcane bagasse-ash (BA) are used as reinforcement for Aluminum alloy (Al2024) based hybrid composites. The Aluminum matrix hybrid composites were fabricated by stir cast at 750°C. The reinforcement weighted by volume fraction ratio 5%, 10% & 15% of matrix and reinforcements, <63µm particle size, stirring the slurry at 650rpm for 10 minutes were the parameters used for the fabrications of aluminum matrix hybrid composites. The development and experimental findings of aluminum matrix hybrid composite mechanical properties were performed by adding silica sand and bagasse ash as reinforcement with different composition proportions. The addition of this reinforcement with nine compositions proportion, in range of 5-15% with 5% interval. For a maximum improvement of the material properties, solution heat-treatment (T3-temper) was performed. The effects of the reinforcements have been examined through different mechanical tests. These tests were implemented using Rockwell hardness indenter, bending, and tensile strength by universal testing machines, and optical microscopy was used to characterize the microstructure of composite specimens. Specimens were prepared as per the ASTM E18-15 for Rockwell hardness and E8M/16a for tensile, E290 for bending test specimen standards. The samples are modeled using Solid works 2017, and its analysis was performed by ANSYS 19.2. The analysis result showed a higher effect of the reinforcing bagasse-ash with different compositions in aluminum matrix reinforced composites. Enhanced mechanical properties have been achieved in the 3rd case compared to the 1st and the 2nd BA & SiO_2 combination. It shows that the selection of BA & SiO_2 as reinforcement has one of the essential criteria for fabricating aluminum matrix reinforced composites. The result showed that the hardness of the composites increased slightly with an increase in bagasse ash content with a maximum increment of 15%. The maximum mechanical properties were observed for the Al2024 reinforced composite at 5% bagasse ash and10% silicon dioxide compositions. Tensile strength increased to a maximum value of 560MPa, and also flexural strength increased to a maximum value of 482MPa at 10% SiO_2 and 5% bagasse ash compositions. Hybrid composite superior properties are observed in tensile strength, flexural strength, and hardness than single reinforced Al2024/ SiO_2 metal matrix composites. Also, for the application of fuselage-skin panels, the reinforced and heat-treated Al2024/SiO_2/BA-T3 improved a better stress resistance performance than the unreinforced Al2024-T3/T351 through FEA.

Keywords: Al-2024, SiO_2, Bagasse Ash, ASTM, Stir Casting, Optical Microscope, FEA

TABLE OF CONTENTS

LIST OF FIGURES

LIST OF TABLE

LIST OF ABBREVIATIONS AND ACRONYMS

ASTM	America Society for Testing and Material
AMCs	Aluminum matrix composites
CMCs	Ceramic matrix composites
FEA	Finite Element Analysis
IJERT	International Journal of Engineering Research & Technology
IJMET	International Journal of Mechanical Engineering and Technology
MMCs	Metal Matrix Composites
ROM	Rule of Mixture
UTM	Universal Testing Machine
UD	Unidirectional
w_{r}	Weight of Reinforcement
w_m	Weight of Matrix
w_c	Weight of Composite
W_{r}	Weight Fraction Reinforcement
W_m	Weight Fraction Matrix
W_c	Weight Fraction Composite
ρ_m	Density of Matrix
ρ_c	Density of Composite
v_{r}	Volume of Reinforcement
v_m	Volume of Matrix
v_c	Volume of Composite
V_{r}	Volume Fraction Reinforcement
V_m	Volume Fraction Matrix
V_c	Volume Fraction composite
σ	Stress
ε	Strain
E_C	Elastic modulus of the composite
E_m	Elastic modulus of the matrix
V	poisons ratio

CHAPTER ONE

1. Introduction

1.1 Background of the Study

Recently, composite materials are used mainly in structures, high-performance racing cars, automobiles, helicopters, and commercial aeroplanes [1]. Composite materials are commonly a mixture of dual or extra unlike constituents that have different characteristics called matrix & reinforcement are used together to develop and achieve the best or new set of characteristics properties of materials [2]. The most frequently used reinforcements are ceramics, ashes, etc., as a type of fiber, whiskers, or particle used in metal matrices. Common types of matrices are Al, Ti, Mg, and Cu. Some commonly used ceramic reinforcements are SiC, Al_2O_3, BC, SiO_2, WC, etc. [3]. Among several discontinuously dispersed solids used, the waste ash (which consists of a high amount of silica & alumina) is the lowest density & low-cost reinforcement accessible in massive amounts as a dense unwanted byproduct [4].

In general, there are three categories of composites which are namely; Metal Matrix composite (MMCs), Polymer matrix composite (PMCS), and ceramic matrix composite (CMCs). From the last couple of decades, metal matrix composite has found worldwide application with a significant class of weight and design proficiency for structural material assigned in every range of engineering applications. MMCs are composite materials which composed of two or more metal or non-metallic materials. Mainly, the matrix material is mixed with the metal or other materials to enhance the mechanical properties such as strength, hardness, corrosion resistance, and wear resistance [5]. Therefore, composites with ash as reinforcement are expected to beat the cost problem for broad usage in the fabrication of small engines and automotive applications.

Metal alloys such as Titanium, Magnesium, and Aluminum have high-temperature resistance, lightweight, which makes them preferable for structural application. Recently most practitioners are engaged their research on aluminum matrices composite material since it is primarily used for the structural application of the aerospace industry. Ceramic particles reinforced the Al-alloy to improve the mechanical and tribological properties of the material. Such materials will bring the following properties: lower density, reduced weight ratio, high strength, better malleability, good machinability, good corrosion resistance, increased wear resistance, better hardness, good thermal & electrical conductivity [6,7]. These MMCs fabricated by the liquid (solid) state method. To fabricate MMCs the process selection also shows a significant role. The liquid state method is the most inexpensive way of producing MMCs. In general, stir casting of the fluid state technique is engaged because of its homogeneous mixing & affordable process of casting compare with other methods[8].

1.2 Problem Statement

Aluminum alloys have unique feature mechanical and tribological properties. They have excellent mechanical properties: which make them useful in various applications like automotive, marine, engine assembly, aeronautics, and other engineering applications [1]. In the aviation industry, aluminum alloys are broadly used for structural materials. They have a high lightweight and high strength and stiffness, high fatigue resistance, good damage tolerance, good corrosion resistance, good thermal conductivity, and many properties as the needed application area [2]. Some use areas of aluminum alloys in aerospace applications are fuselage frame, stringer, skin, bulkhead, wing structural parts, skin, etc. Such aluminum alloys are identified as 2xxx, 4xxx, 5xxx, 6xxx, and 7xxx. The well-known aerospace structural application material is the Al 2xxx series. Al 2xxx series are Al-Cu alloys, contain between 2 to 10% Cu with smaller addition of other elements. The presence of Cu in this alloy reduces ductility and shows lesser corrosion resistance. As a result, some of these alloys can be the most challenging aluminum alloys to be weld. They are highly used in aerospace applications, but now because of these problems and high density, less strength, less stiffness than the new composite materials, which are favoured for the need for performance optimization materials for aerospace applications. Then the Al-Cu alloys are beginning to be replaced.

Recently, most researches focus on the performance enhancement of aircraft fuselage structure [9]. By design optimization of the different structural parts and replacing with composite materials to get a better performance or strength, reduce weight and improve the overall efficiency of the aircraft instead of the currently used aluminum alloy, which is used chiefly as aerospace material [10]. Also, extending the structure lifetime is the other big issue for their research. Even though it has lesser corrosion resistance, low stiffness strength and higher density, it has the best performance for the aircraft fuselage structural and wing parts. It has an irreplaceable character compared to other composite materials. Such characters are resistant to fire, can operate in a broader range of temperatures, have no moisture absorption, have better thermal and electrical conductivity, and resist emission (radioactivity) damage [11]. Therefore, instead of replacing the capable materials for the application area, it is better to characterize and develop their performance by reinforcing with the hard-ceramic particle and BA particle.

1.3 Objective of the Study

1.3.1 General Objective

The general objective is to study the development and characterization of the mechanical properties of Al2024 alloy reinforced with silica sand and bagasse ash by varying the volume fraction ratio of alloy and reinforcement particles by using the stir casting technique.

1.3.2 Specific Objectives

- To fabricate Al2024 /SiO2/BA matrix composite
- To investigate the mechanical properties such as tensile, hardness, flexural tests of Al2024 / SiO2 / Bagasse ash mixture composite
- To examine and compare the microstructural properties and composition tests using an optical microscope of composite materials with improving mechanical properties.
- To model and analyze FEA by using the mechanical property of the composite for fuselage-skin panel

1.4 Scope of the Study

The scope of this study is to successfully fabricate AA2024/ SiO_2/ BA composite using the stir casting method and analyze its results using FEA. The study also quantified the mechanical property performance of the fabricated composite according to ASTM standard, considering the fuselage application for the structural part system to increase the mechanical performance of aircraft engineering material. Moreover, the study analyzed the fuselage structure load using the finite element method. The characterization of mechanical properties of Al2024/ SiO_2/Bagasse ash by varying the volume fraction ratio was investigated and compared.

1.5 Significance of the Study

The significance of this study could be serving as a valuable reference for further investigation of hard ceramic and agro-west reinforced aluminum matrix composite to improve the mechanical performance for both academicians and aircraft industry researchers. The land usage of sugarcane bagasse waste is minimized and reduces pollution of the environment at large.

This thesis will help:

- ✓ As a teaching material and base for further research
- ✓ For minimizing pollution and reducing fuel consumption, especially in the automobile and aerospace industries
- ✓ It substitutes the metals with composite materials by comparing properties

1.6 Limitation of the Study

Among many obstacles, the major one is few experimental setups not available. For example, starting from the manufacturing of composite test specimens to the experimental tests, there are many problems like there is no access to build stir casting mechanism because of the high cost required to be made. In addition, there is no suitable experimental load setup for tensile & bending tests to be applied. Therefore, it was obligated to use the available materials, which need to build the stir cast mechanism and test the experiment specimens.

1.7 Research Question

RQ1. Is it possible to develop and characterize the aluminum alloy with ceramic particles and agro-waste ash?

RQ2. Is it possible to improve aluminum alloy's mechanical and tribological properties by reinforcing it with silica sand and bagasse ash?

RQ3. What would be the effect of reinforcement volume fraction ratio in the composite?

RQ4. Is it possible to use enhanced composite for fuselage structural applications?

1.8 Organization of the Thises

This thesis is an organized of five chapters and its content is about the manufacturing, characterization and investigations of the mechanical properties of aluminum composite Al2024 / SiO2/ Bagasse ash

The thesis is structured as follows:

Chapter 1 presents about the introduction of AMMC, the statement of the problem and thesis objectives, scope, and limitations, and methodology.

Chapter 2 is divided into five sections on previous works, the first section briefs AMC's based on mechanical properties, the second section review AMC's based on reinforcement particle size and amount, the third section is concentrate based on AMC's based on stir casting parameters, the fourth section review Al2024 based on heat treatment. In addition, the last section review composite based fuselage structural parts as an application area.

Chapter 3 provides a detailed description of materials used in the study, the methodology followed during the research work. The modeling procedures, the steps, and the conditions of finite element analysis are also presented in this chapter.

Chapter 4 presents the outcomes of both simulation and experimental studies. Meanwhile, it also details discussions on the results on simulation and experimental results.

Chapter 5 presents the conclusion and directions for future works.

CHAPTER TWO
2. Literature Review

This chapter presents a detailed discussion about the previous work related to aluminum composites and methods used to investigate the mechanical properties of Al-alloy reinforced with hard ceramic and agro-waste ash particulates, and others. Some of them, which are considered essential for this thesis work, are discussed below.

2.1 Composites Material

Composites are classified based on the behaviour of the matrix they own. Fabrication methods are also different according to the chemical and physical properties of the matrix and reinforcing particle. Composite materials are primarily used in structures, high-performance racing cars, automobiles, and helicopters, most recently for the application of commercial aeroplanes. Composite materials are commonly a mixture of two or additional unlike materials that have different characteristics called matrix & reinforcement are used together to develop and achieve the best or new set of features properties of materials [2]. The best usually used reinforcements are ceramics, metals, ashes, etc., as a type of fibre, whiskers, or particles used in metal matrices. Common types of matrices are Al, Ti, Mg, Cu, and so on [12]. Some frequently used reinforcements are SiC, Al2O3, BC, SiO2, WC, etc. Among several discontinuously dispersed solids used, ash reinforcement the one & mostly low-cost and low-density reinforcement is accessible in bulky amounts as a solid waste byproduct [4].

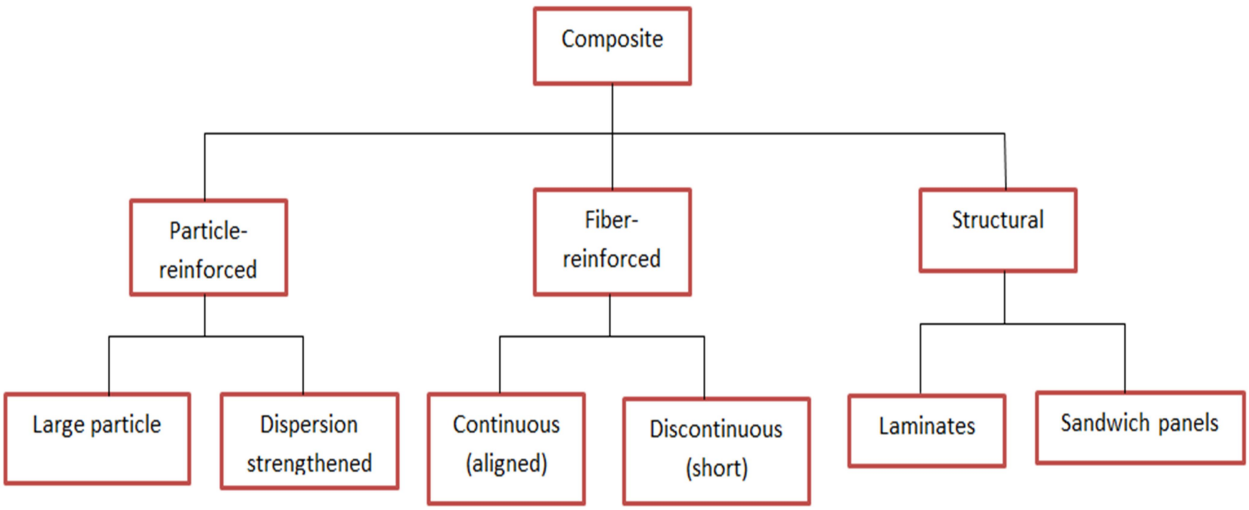

Figure 2.1: Classification of composite [13]

a) **Metal matrix composite (MMCs)**

As the name implies, MMCs have a metal matrix. Such metal composites include Mg, Al, and Ti. These metals ensure specific mechanical properties, greater stiffness, high shear and compressive strength, more excellent transverse stability, and good temperature capacity [14]. The reasons why AMCs utilized in the area of aerospace and automotive are their performance, economic and environmental benefits. Aluminum matrices reinforced with particulate reinforcement material become more critical because of their isotropic property, less cost, and a wide variety of custom-made properties to fabricate secondary constituents [15]. Widely used reinforcements are particulate reinforcements as they are easily manufactured and relatively chip they would be available as a waste product. Metal matrix composite reinforcements could generally classify into five main groups: continuous and discontinuous fibre, whisker, wires, and particulates. MMCs reinforcements are commonly ceramics. The ceramic reinforcements are carbides, oxides & nitrides, which are uses because of their admirable mixtures of specific strength & stiffness at both ambient and increased temperature. In metal matrices, commonly used particulate ceramic reinforcements are SiC, SiO2, TuC, BC, etc. [12].

b) **Ceramic matrices composite (CMCs)**

CMCs have ceramic matrix-like alumina, aluminum silicate, calcium reinforced by SiC. The benefit of ceramic matrices consists of an excellent capacity temperature limit for ceramic, high strength, hardness also lesser density [16]. Ceramic materials are naturally having high-temperature resistance and tend near to fracture and brittle. There are four types of ceramic matrices: glass, conventional ceramic, cement, and concreted carbon substituent.

c) **Polymer matrix composites (PMCs)**

PMCs are the most innovative composite include polymer thermosetting or thermoplastic strengthened by fibre. They provide excellent stiffness & strength with corrosion resistance. Due to the low density of the components, the PMCs frequently confirm admirable specific properties [17].

2.1.1 Metal and Ceramic Matrix Composites

Metal matrix composites (MMCs) offer numerous advantages compared to their base metals, like higher specific strengths and modules, higher elevated temperature resistance, lower coefficients of thermal expansion, and better wear resistance. As a disadvantage, they are more expensive than their base metals and have lesser stiffness. MMCs also have some advantages compared to PMCs, no moisture absorption, higher thermal and electrical conductivities, and fair resistance [18].

Due to their high price, commercial applications for MMCs are sparse. However, since they are counted as a capable material for future hypersonic aircraft vehicles, MMCs and CMCs remain essential materials. Ceramics hold numerous wanted properties, like great compression strengths, high moduli, high-temperature capability, & excessive hardness, high wear resistance, and low thermal conductivity.

Due to their very low breakage stiffness, CMCs are limited in structural uses [19].

Table 2.1 Relative Comparisons of Material Groups Material [19]

Material Class	Tension Strength	Compression Strength	Stiffness	Ductility	Temperature Capability	Density
Metals	High	High	Medium	High	High	High
Ceramics	Low	High	Very High	Nil	Very High	Medium
Polymers	Very Low	Very Low	Very Low	High	Low	Low
PMC	Very High	High	Very High	Low	Medium	Low
MMC	High	High	Very High	Low	High	Medium
CMC	Medium	High	Very High	Low	Very High	Medium

PMC – Polymer Matrix Composite MMC – Metal Matrix Composite CMC – Ceramic Matrix Composite

2.1.2 Aluminum Alloys for composites

Al-2024

The Al2024 alloy has high strength at room temperature and even at a raised temperature. It shows superior capability, good machinability, and fair to good workability [20]. Al2024 alloy offers a low ductility at room temperature and is commonly heat-treated in different states to outfit specific applications. It catches wide use in many aeronautic structural components, bridges, military vehicles, and weapons manufacture due to its outstanding strength. Then, additional improvements to increase the mechanical properties of this alloy will open up new areas of research [21].

2xxx series alloys

In 2xxx Series, Cu is the primary alloying component, frequently with Mg as a second count. These mixtures need solution heat treatment to attain optimal properties; in solution, heat-treated state, mechanical properties are comparable to, & sometimes surpass, those of low-carbon steel [22]. In some cases, precipitation heat treatment (ageing) is engaged to more increment of mechanical properties.

Al-alloys in the 2xxx series are particularly well appropriate for used parts. And structures necessitate high strength-to-weight ratios and are usually used to make and aircraft wheels, truck, aircraft fuselage and wing skins, truck suspension parts, structural parts, and those demanding good strength at temperature up to 150 °C or 300 °F.

2.2 Reinforcements

2.2.1 Particulate reinforcements

Microstructures of metal & ceramics composites, which demonstrate particles of individual phase dispersed in the other, these materials so-called particle-reinforced composites [23]. Triangular, round, and Square shapes reinforcement were identified, but the sizes of all their sides were detected to be equal. The volume and size absorption of the dispersion differentiates it from distribution-hardened-

materials.

In particulate reinforced composites, the particles reinforce the system by the hydrostatic oppression of fillers in the matrix & by their toughness comparative to the matrix. Three-dimensional strengthening particles in composites provide isotropic properties of the material due to the three systematical orthogonal planes. Meanwhile, it is not identical; the material properties obtain compassion to the essential properties and the array's geometric shapes and bonding properties. The composite strength was typically based on the size of the particles, the inter-particle arrangement, and the volume fraction of the reinforcement [24].

2.2.2 Ceramic reinforcements

The acquaintance of a ceramic reinforcement into metal matrix products the composite material produces the desired mixture of mechanical & physical properties, which cannot achieve with unreinforced alloys [25]. In developing AMC**s** for performance optimization with less consideration on production cost, SiC, Al_2O_3, B_4C, WC, Gr, CNC, and SiO_2 are synthetic ceramics particulate between those SiC and Al_2O_3 are widely utilized reinforcement particulates. Matrices reinforced with high modules short fibers, whiskers or particulates have improved strength and stiffness and are isotropic. Conventional AMCs reinforced with those ceramics' particulates improve strength and specific stiffness over the unreinforced alloy [26].

2.2.3 Quartz (Silica)

SiO_2 - The glass types typically contain about 70 to 98% silica. Quartz is even purer, and quartz fibers are made from natural quartz crystals that contain 99.9% silica, possessing nearly all the properties of pure solid quartz. They are highly elastic and stretched to 1% of their length before breakpoint. Both silica and quartz are not affected by acid attacks & has resistant to moisture. As thermal properties of silica: - the natural choice as fibers in several applications [27]. Silica has good insulating properties and melting temperature extends up to 1600ºC.

In addition, they have a low coefficient of thermal expansion, which makes them withstand high temperatures. It is a rigid material, which is in large quantities available as a natural resource. It has a rhombohedra mineral structure with a hardness of 7 on the Mohs scale and a low density ranging from 2 to 2.66. It provides excellent hardness when combined with the soft copper alloy, thus making it better suitable for use where hardness is required. SiO_2 has improved corrosion resistance, high chemical stability. Compositions of the mineral have SiO_2, which is the furthermost common among other materials, & existed simple compound state. Earth's crust holds 60% SiO_2 rocks, sand, clay and is mainly composed of small quartz minerals. Silica sand is white in its purest form [28].

2.2.4 Agro-waste (secondary) reinforcements

At present, there have been efforts custom-made to producing low-cost AMCs. The use of ashes produced from controlled burning of agro-wastes as reinforcement is receiving serious attention. Agro-

waste products such as bagasse, rice husk, bamboo leaves, groundnut, and coconut shell, after gathering frequently rejected in the environment due to poor recycling technologies. And responsiveness leading to diverse environmental challenges [29]. Thus, research efforts targeted at translating these agro-waste products to productive uses will significantly appeal to the scientific and technological community, particularly in developing countries where the effects of poor environmental waste management policies are highly touched.

2.2.5 Bagasse ash (BA)

The development of the MMCs is of great interest in industrial applications because of their high specific strength, stiffness, wear and heat resistance, compared to unreinforced Aluminium alloy. Among several discontinuous dispersion applied in MMCs, Bagasse ash is the one which is the cheapest and low-density strengthening material accessible in bulky quantities as waste solid from the sugar processing mill [30]. Hence, the composites with BA as reinforcement beat the cost problem for extensive uses in small engine & automotive applications. Therefore, it is estimated that the combination of BA particles with Al-alloy would help. However, alternative use of this inexpensive unwanted by-product &, additionally, has the efficiency of saving energy-intensive Aluminium and decreasing the price of Aluminium products. Strengthening Aluminium metal by BA as the source of SiO2 and alumina particulate will yield a material that displays the mixture of mechanical & physical properties of both the Al- matrix & the SiO_2 [5].

2.2 AMCs Based on Mechanical Property

Al-Cu-Mg alloy investigates using the reinforcement bean pods ash through the double stir casting method. This investigation concentrated on using bean pod ash at Nano-particle size to determine the micro-structural & mechanical behaviour of reinforced Al-alloy [31]. Nano-particles used in the change of 1- 4 wt. % to produce the aluminum matrix composite. The experiment presented interphase bonding was accomplished and very strong, with a significant increase in the tensile strength by 35% and hardness at 44.1% at 4wt%. Density also decreased as the wt.% of BPA Nano-particles increase in the alloy. The presence of BPA Nano-particles in matrix alloy results in a much smaller grain size in as-cast composite compared to the matrix alloy.

The effect of particulate reinforcements on the mechanical performance of Al2024/WC metal matrix composite by using liquid metallurgy. The WC reinforcement particles in Al2024 alloy with changing wt. % from 0% - 5% by weight. For the casting, the production of MMCs composite vortex method was used [32]. Vortex method of cast fabrication engaged to the reinforcement poured in the vortex generated by stirring the melted metal employing a mechanical stirrer. To determine the mechanical character of composite hardness test, tensile test, elasticity, compression test conducted as ASTM measurement standard. The study results showed that as the WC reinforcement amount rose by 3%, it shows significant increments in UTS about 57.5%, hardness about 9%, and young's modulus about

47.6%, compressive strength, and decreasing its ductility. In the study, significant mechanical property improvement was achieved.

Bagasse ash (BA) reinforcing particle on mechanical properties of Al-Cu-Mg alloy studied [33]. BA particles varied from 0 -10 wt. Percentage, 2–10wt%. With an interval of 2 wt. Pct. BA particulate size was 64µm. Lubricated pin-on-disc tests were conducted to examine the wear performance of the Al alloy/BA particulate composites. Hardness, microstructure, and wear test performed. The physical and mechanical properties determined include density, ultimate tensile strength, yield strength, compression strength, hardness values, and impact energy. As a result, the hardness value of reinforced Al-Cu-Mg/BA increased with increasing the wt. of BA particles because of the particle dislocation of particle boundary of ceramic particles. These increases in strength and hardness values are attributed to the distribution of hard and brittle ceramic phases in the ductile metal matrix. The microstructure shows a damaged surface, and a large amount of plastic deformation appeared on the surface of unreinforced alloy. The wear rates of Al-Cu-Mg/BA mixtures get lower than that of the matrix alloy and further decrease with increasing BA content. Though BA strengthened Al-Cu-Mg alloy revealed damaged surface which is not smooth, and scratches and parallel lines observed Wear rate rises as the applied load & sliding speed increase. The microstructure obtained reveals dark ceramic and white metal phases, which resulted in an increase in the dislocation density at the particles–matrix interfaces [34]. Therefore, as a result, the show improves wear properties are achievable for the Aluminum alloy by adding BA particles as reinforcement material. These results show that better properties are attainable by adding bagasse ash to Al–Cu–Mg alloy.

Other Aluminium alloys Al7%Si with Bagasse ash reinforced composite manufactured at governing the mechanical and density properties. Bagasse ash contain high alumina & silica substances of up to 77.29% & 10.95%, correspondingly and used as reinforcement & in different composition from 0vol% - 30vol% at interval 5vol%. As a density, tensile test, hardness test, impact test, and fatigue tests were conducted [35]. The results revealed the density reductions by a vol. fraction of reinforcement by the minimum rate at 30vol% bagasse ash. The mechanical properties tests results

presented the UTS, Young modulus, impact strength varies and their max. The value achieved at 10vol% BA and hardness varies maxi. Value 90.767HRV at 20vol% BA and then decreased to 75.067HRV at 30vol% BA, the number of cycles increased from 0.620x106 for the control sample to 1.797x106 at 15% BA and decreased to 0.066x106 at 30% BA. It implies fatigue strength of the composites increases with an increase in ash addition up to 15% BA and decreases with further add up to 30%. The particulate reinforced composites show improved fatigue behavior compared to unreinforced alloy. Such improvement is attributed to higher stiffness reinforcement material in the composites & the elongation (%) taking almost equal (approximately the same between 9.5% to 10.6%).

2.3 AMCs Based on the Particle Size and Amount

Metal matrix composites are strongly influenced by microstructural parameters of the reinforcement such as shape, size, orientation, distribution, and volume fraction. The finer the grain size better is the hardness and strength of composites.

Al356/bagasse ash (BA) particle reinforced composite with varying wt. % of 2 - 10 wt. % was manufactured with the stir casting method. The overall density of Al356/BA composite decreased with increasing wt. % of BA particle. The microstructural analysis of different wt. % BA particles reinforced as-cast composites revealed uniform distribution of ash particles with a significant refinement of the Aluminium matrix phase [24], in the case of 10wt.% BA particles in matrix clustered particles formed in a few places this could attribute to low density and high wt—% of particles. Brinell hardness values increased linearly with an increase in wt. % BA particles and composite containing 8wt. % of BA particles were observed to have a maxi. Value of 82 HRB. Compressive, tensile strength and brittleness increased with an increase in wt—% of BA particles. However, the impact strength of the composites decreased with an increase in wt. % of BA particles also increases.

Silica particulate reinforced Aluminum MMCs of different wt% (4, 6, and 8%) are successfully cast employing the stir casting process, and then results obtained from various experiments are compared with base material mechanical properties. The composites with particle volume fractions of less than 4–6% show the best comprehensive mechanical properties, i.e. tensile strength, yield stress, and percentage elongation. As the weight% of reinforcement increases, the wear loss decreases, suggesting that Al2O3 aluminum MMCs have good wear resistance compared with the base material. The hardness of the material increases only up to 4 wt% of SiO2 reinforcement, and then with increasing the wt%, the hardness drastically decreases. It might be due to the uneven distribution of the particles caused by the increase in wt%. Microstructure and mechanical properties deteriorate after excessive addition of particle reinforcement [36].

The influence of reinforcing particles size on the mechanical behaviour and microstructure character in pure Al-matrix composites were investigated [37]. The specimen was arranged by warm consolidation by 10 vol. % reinforcement particle with different size varieties, D (0–20 μm), (20–40μm), (40–80μm) and (80–100μm). The result shows that reinforcement particle size has the greatest influence on the mechanical properties of percentage elongation, ultimate tensile strength, and yield strength. When particle size reduced from $80 \leq D < 100$ μm - $0 < D < 20$ μm, ductility & tensile strength increased from 195 MPa - 295 MPa and 3%-4% correspondingly, because of the decreased size & fracturing particle. The wear rate also confirms the size influence, where enhanced wear is detected in composite specimens strengthened by rough particles. The small strain elastic behaviour of SiCp strengthened Al-Cu-Mg composites by different particulate sizes, by 1.4, 15.8, and 62.8 μm in measured strain distortion of 1.5% in both compression & tension [38]. In all the MMCs, the actual elastic happened at lesser stress in

compression property than in the tension. This dispersion of remaining stresses in a matrix of MMCs created because of the higher in thermal expansion coefficient between the matrix medium & the reinforcement particle [39].

2.4 Stir Casting Processes for Composite Fabrication

A simple and cost-effective method for manufacturing composites is essential aimed at increasing their use. Reinforcements such as particulate SiC, Al2O3, Bagasse ash, graphite, fly ash, etc., can easily be incorporated into the melt using an inexpensive and broadly accessible stir casting method. In a stir casting process, the particulate reinforcement is usually distributed into the aluminum melts in mechanical stirring.

There are process variables in the way of influence on the behaviours of composite materials [40]. Stirring speed is an essential factor in the stir casting process. This parameter influences the proper mixing of the particulate reinforcement in the matrix phase. The result of moving speed could reveal by the microstructure of composite materials. With increasing stirring speed rises the uniformity of particulates spreading, therefore causing a reduction in the average incline of corroboration beside the admission path. Stirring Time As stirring encourages even spreading corroboration partials and boundary pledge among the background and strengthening, the stirring stage plays a vital role in the mixing forming process. They fabricate a composite from aluminum alloy (A384). The different weight percentage of SiC particulate reinforcement powder of average 60μm found good hardness in composite at 10 minutes of stirring at 600 rpm [41].

The distribution of reinforced particles in the matrix also depends on the viscosity of the setting phase. The viscosity of the mixture is based on the working temperature and holding time of stirring. The viscosity of the Aluminum matrix decreases with a rise in the holding time of stirring. A decrease in viscosity will lead to an increase in the rate of the chemical response between matrix and reinforced particles as literature found promising results and wettability between mixture & reinforced particles by maintaining the temperature of 800 °C. To achieve good wettability between the reinforced particle and the matrix, it needed to pre-heat the reinforced particle. Pre-heating particle is also required to remove the moisture and gases from the particle, which might affect the property and characteristics of the composites [42]. Found good results on preheating of a reinforced particle at temperature 500 °C for 30 minutes.

The environment resistance, low density & satisfactory physical and mechanical properties of AMCs made them the most motivating material replacements for producing lightweight portions for various types of current manufacturing equipment [43]. Manufacture of aluminum & its alloys-based casting compound constituents through stir casting is the noticeable and inexpensive technique for improving and processing MMCs materials. The main trials of this method are to accomplish adequate wetting of particles by molten metal, get a uniform combination of ceramic particles, and decrease porosity in the

cast MMCs [44]. This article analyzes the stir casting for the manufacture of AMCs. Diverse progression factors of the stir casting route, like reinforcement feed rate, stirring temperature, stirrer speed, stirring time, preheat temperature of reinforcement and mould, wettability-promoting agent, and pouring of melt, and problems faced in the effective production of AMMC's by stir casting method.

2.5 Heat Treatment of AMCs

Good machinability and good corrosion resistance could be achieved by t- tempering for high structural application materials. Al2024 the high strength to weightiness ratio material uses in many structural aircraft applications, for machinery gear, rivet & screw products, automotive parts, piston & cylinder, etc.

In the 2xxx series, Cu is the principal element, frequently with Mg as a secondary alloying element. these alloys need solution treatment to attain the most favourable properties. In heat-treated solution conditions, the mechanical property achieved, like precipitation heat treatment or ageing, engaged in additional mechanical property increments [22]. Among all casting alloys, 2xx.x. Al-Cu can develop the highest strength by heat treatment and required heat treatment to improve its highest strength, elasticity and certify high confrontation to corrosion cracking. Because of their superior damage tolerance, excellent resistance to the growth of fatigue crack, Al-Cu alloys are used for the fuselage and lower wing skin on commercial aircraft. The 2024-T3 has superior fatigue performance when compared with 7075-T6 in the 105 cycle range. These performances give to widespread use of Al-Cu alloys in the tension-tension application [45].

T3 tempering

T3 temper condition is one of the heat-treating methods of alloy materials to improve their mechanical properties. It has three stages to implement. The first step is solution heat treatment in the second step is quenching in water media then the third step is natural ageing [6]. Al2024 mostly used this method to enhance the tensile yield strength, ultimate tensile strength, better corrosion resistance, and other properties, which makes Al2024 a suitable aircraft structural material.

The analysis was performed to evaluate the behaviour of the micro-hardness curve by ageing time and microstructural characterization with thermal treatments by interrupting every 1hr within 1-9hrs [6]. The results indicate the value of hardness and electrical conductivity with its reliance on ageing situations. The electrical conductivity versus hardness curve showed a substantial relationship and shows that the measure has great potential to use as a tool to control the thermal treatment of ageing.

Table.2.2: Solution heat-treatment temperature range & eutectic melting temperature for 2XXX alloys [46].

Alloy	Solution heat treatment Temperature range, ^{0}C	Initial eutectic melting Temperature, ^{0}C
2014	496-507	510
2017	496-507	513
2024	488-507	502

Table 2.3: Mechanical properties of Al 2024 at different tempers [47]

Temper	Temper detail	*Tensile strength* (MPa)	Yiel strength (MPa)	Hardness (HB)
O	Annealed	185	75	47
T3	Solution heat-treated, cold worked & natural aged.	485	345	120
T351	Solution heat-treated at 495^{0}C, quenched, stretched 1.5-3% & natural aged for several months	470	325	120
T4	Solution heat-treated, natural aged.	470	325	120
T6	Solution heat-treated & artificially aged at 190 ^{0}C for 12hrs.	475	395	
T8	Solution heat-treated, cold worked & artificially aged at 190 ^{0}C for 12hrs.	480	450	

The electrical conductivity value is consequent from its high sensitivity to microstructural factors that affect electron scattering. The electrical conductivity performance related to the hardness curve offers a good tool for process control and the study of the electrical behaviour of the 2024 alloy through real-time artificial ageing heat treatment due to the practicality of the measurements [21].

Artificial ageing of Al2024 T3 was conducted in two stages of solution heat treatment at 500 ^{0}C for 1hr & continued artificial ageing at 180^{0}C by holding to 2, 4, and 6 hrs. Vickers hardness test machine conducted to examine hardness test. The specified load of 5 kg is based on the testing material as a result showed that ageing time increases the hardness of Al2024 T3. The micro-photo result showed the designed particle became delicate with an extra ageing period which made the hardness of the material was rise [6].

Al2024 and Beryl ceramic reinforcing particulate composites were prepared by stir casting by changing the wt.% of beryl ceramic particulates from 0 wt.% - 10 wt.% in a stage of 2 wt.%. The cast Al2024 alloy and its composites have been subjected to solution heat treatment at a temperature of 495°C for 2 hrs and then quenched with ice. A Microstructural investigation was obtained to define the nature of the composite structure. The hardness test was conducted with Brinell to both the Al2024 alloy & its composites earlier and later solution heat treatment. A wear test was conducted on disc Pin to observe the wear behaviour of Al2024-alloy & the reinforced composites. The results

indicate that the wear rate of the reinforced aluminum composites is lesser than the Al2024 alloy. The wear rate improved with raising applied load & sliding distance and reduced with rising sliding velocity [6].

2.6 AMCs for Fuselage Application

Aluminum alloys are broadly used in aircraft fuselage construction. Aluminum alloys are valued because they have a high strength-to-weight ratio. Aluminum alloys are corrosion resistant and comparatively easy to make. The exemplary behaviour of aluminum is its lightweight.

Aircraft fuselage

A fuselage is the central body of an aeroplane & designed to accommodate the passengers, crew, and cargo. Moreover, it provides the structural connection for the tail & wings assembly. It is Vary widely in style, size, & shape based on the persistence of the built aeroplane. It has hollowed out to decrease the total weight of the craft, and it offers the structural building to which the tail, wings, and other types are attached [48].

Aeroplanes are commonly constructed from the fundamental constituents of fuselage, wings, tail components & control surfaces. Each member has one or more particular purposes & essentially designed to confirm specific tasks to carry out safely. Any minor catastrophe of any of these constituents might lead to a catastrophic disaster affecting massive damage of lives and materials [49].

Structural Members of Fuselage

Skin

The skin of an aeroplane can also manufacture from different materials, those materials aluminum, plywood, and composites. Skin and many other components are involved in the structural fuselage to support airframe function [50].

In the semi-monocoque fuselage, Stringers are used. Those longitudinal supporters are characteristically more frequent and lighter weight than the longerons. They are different in shape and, most of the time, made or formed from a single piece of aluminum. The skin develops the body and suitable attachments from stringers, which are having some rigidity characteristics. Longerons and Stringers are organized to prevent the fuselage from compression, tension, and bending [51].

Functions of skin (cover)

- It conducts the aerodynamic forces to the transverse & longitudinal supporting members by membrane & plate action
- It improves shearing stresses, which respond to the applied shear forces & torsional moments.
- It acts resisting the axial loads & applied to bend with the longitudinal members.
- While the structure is pressurized, it acts longitudinally in resisting the axial load with the transverse members in reacting to the circumferential or hoop load.

- It provides a shield for the subjects of the vehicle & an aerodynamic surface.

Longerons

Longeron's members longitudinally reinforce the skin. Longerons generally spread across several frame supporters & assist the skin support mainly bending load. Typically, it is made from aluminum alloy, each of a single piece or a developed construction.

Bulkheads

Bulkheads provided at the point of primer of intense forces from the landing gear and wing's tail surface. Bulkhead's structure is considerable and functions to allocate the applied load into fuselage skin.

Frames

Fuselage frames execute many functions like support stringer panel of fuselage skin, dispense concentrated loads, crack stoppers (fail-safe). Structures act as circumferential tear strips to safeguard fail-safe design besides propagation of skin crack [52,53].

Stiffened skin panel

A thin skin that stabilized in compression by longitudinal stringers, running across the panel width at regular intervals, describes stiffened panel construction [9]. It loaded by compression experiences limitation, at a definite value of limitation or load level, transverse bends occur all in unexpected buckling. Skins between stiffeners perform as a braced plate. If skin material is designed for the required strength, it is very thin & prone to buckling. Stiffeners are used locally to increase the second moment of area of the skin [54].

Loads Acting On Fuselage Components

Fuselage structural members intended to carry the load (to resist stress). In designing aircraft, each square inch of fuselage and wing, spar, every single rib, and even metal fit must be considered about the physical behaviours of the material that it is prepared. All parts of the aeroplane must design to handle the load to be exerted upon it [55].

Force acting on fuselage

The fuselage will experience a varied range of loads from the number of bases. The fuselage structure and load's weightiness will cause the fuselage to place the top portion in tension & the bottom part in compression to bend downwards from its support at the wing. The landing loads are significant. The bending loads are greater when the load is distributed towards the tail & nose. As a result, the aircraft weighed nearby to the Centre of gravity [56].

The forces that act on the aircraft's fuselage are categorized into four different types:

- Aerodynamic forces
- Gravity forces

- Ground reaction forces
- Internal pressure

Internal Pressure

Aircraft cabin pressurization is an accepted system of protecting occupants against the effects of hypoxia [55]. Inside a pressurized cabin, occupants can travel safely & comfortably for a more extended period, principally if the cabin elevation is sustained at 8000 feet or below, where the use of oxygen is not required. Particular difficulties happen in a place where the fuselage is necessary to be non-cylindrical. Internal pressure could generate huge bending loads in fuselage structures. The structures in these regions are essential to reinforce to resist these loads. Since fuselages are pressurized for safety, the designer must consider what will occur if the pressurization vanished. The loss due to depressurization depends on the degree of pressure loss.

Throughout airlift, an artificial pressure level has been preserved in the fuselage, which is crucial for moving people. The resulting pressure variance results in hoop stress in the fuselage skin [57].

In circumferential direction, hoop stress is largest:

$$\sigma\text{hoopcirc} = \frac{\triangle \text{PR}}{\text{t}} \quad \text{..... (2.1)}$$

In the longitudinal direction, the hoop stress is:

$$\sigma\text{hooplong} = \frac{\triangle \text{PR}}{2\text{t}} \quad \text{..... (2.2)}$$

The Δp (pressure difference) is the internal pressure minus the pressure at maximum travelling altitude. The internal pressure level is equal to a pressure altitude of 2400 m. As the Boeing 787 & Airbus A350, the latest designs use a higher internal pressure, which is also comfortable for travellers. This pressure is 1800 m of a pressure altitude. Hence, the pressure change increases from 49500 N/m2 to 61500 N/m2. It also increases the minimum skin thickness required to resist the pressure difference.

The aircraft fuselage function is to resist & transmit the applied loads, which run aerodynamic shape & defend aircraft system and payload. It supports main concentrated load like tailplane reaction, wing, inertia force & undercarriage reaction. To manage these loads simultaneously, considering the impact of the design on aspects like the weight is mostly the designer's role. Optimization of fuselage structure weight is an essential part of the design development as it influences the aeroplane's performance. Optimizing the definite inflexibility of the fuselage, payload (fuel volume) increases, and weight can be reduced [58].

The aircraft designer needs to ensure the structural reliability of the airframe without negotiating on the safety of the structure [59]. It involves different stress investigations of unlike components, which represent the features of the airframe. In addition, these analysis predictions have to demonstrate by structural testing during the progressive phase. The stress analysis of the stiffened panel was carried out by using the FEM approach [60]. Aluminum alloy 2024-T351 material was used for the stiffened

panel. The fuselage structure experiences hoop tension and longitudinal tension because of the internal pressurization. If there is a crack in the unstiffened fuselage under the flight condition, it could lead to catastrophic failure of the structure. The fatigue crack will usually initiate from the highest tensile stress locations. Therefore, rivet locations are the most probable locations for fatigue crack initiation. Miner's rule was employed for the fatigue damage calculation and life estimation of the structure.

Finally, the researcher concluded that a representative fuselage segment from a transport airframe was considered for the evaluation aluminum alloy 2024-T351 material used for the fuselage segment. The fuselage structure experiences hoop tension and longitudinal tension caused by internal pressurization.

Optimization of fuselage performance

Most of these days, research is done by substituting the existing structural material of aluminum alloy, which is assumed. Its significant problems are that the aluminum floor beam is a more significant weight and has lower stiffness than CFRP. This CFRP (carbon fibre reinforced plastics) was selected to design aircraft floor beams, the conceptual design for improving durability, weight reduction, strength, and cost on the floor beam. Depend on numerical simulation; the CFRP floor beam is lower weight compare to aluminum. For static analysis, ANSYS Workbench is used of CFRP cross beam and calculate equivalent stress under given boundary conditions. The obtained maximum von-mises stress is lesser from CFRP material yield strength. The expected outcome is to decrease the weight to strength ratio, design, cost & shape with a weight reduction of the fuselage; hence, the Aircraft floor beam designed is safe and efficient. Then it concludes that the CFRP floor beam is better and has high durability and strength compared to the aluminum floor beam [10]. The same improvement is observed on stiffened skin panels [9].

In another case, systematic design, analysis, and evaluation tool for both metal and composite fuselage configurations in Visual Basic Application to increase understanding into these material groups & to approximate the load and necessary structural sizes for both aluminum and composite fuselages. The fuselage geometry is customary parametrical and modelled as a simplified tube with variable cross-section without extension box and cut-outs. It is spread into inlets and skin boards [61]. The stress load cases are used for investigation. The running loads, like bending stress, longitudinal stress, circumferential stress, and shear stress, are calculated for the entire aircraft fuselage. A clear load pattern is created to evaluate the materials.

The materials were evaluated for strength, stability, and several other failure modes, like fatigue and crack growth. The skin panels are optimized for these evaluation methodologies, and after executing fuselage, weight is found for conventional aircraft structures [62].

Airframe engineers do not favour any cutouts in airframe constructions since the required reinforcement of the cutout raises both weight & costs to the overall design. Moreover, the size & shape of the cutout is a challenging route as it is an area of stress concentration, life requirements & stiffness, a problem area

for essential strength & there is insufficient design data. Cutouts are necessary for airframe structures to provide the following [61];

- ✓ Fuel access cutout at the bottom skin of fuselage & wing
- ✓ Retracting & landing gear opening at the bottom skin of the fuselage or wing.
- ✓ Lightening holes in webs
- ✓ Accessibility for maintenance & final assembly
- ✓ Fuselage window cutout

2.7 Summary of Literature Review

In the AMMCs research trend, mechanical properties improvement such as increased hardness, high-temperature oxidation resistance, tensile strength, and other tribological properties are achievable for the Aluminum alloy by adding ceramic and ash particles as used material. It was concluded that agro-waste BA could use reinforcement to improve mechanical properties such as tensile strength, hardness, bending strength, and lower aluminum alloy density.

The composite has smaller size reinforcement with more yield strength, hardness, and bending strength than composite having large-sized reinforcement particles. Composite with large particle sizes (>75 μm) have good wear resistance, but they are highly susceptible for crack initiation and for settling gravity because of their dense properties. When particle size decreases, composite tensile strength, fatigue life, ductility, hardness also increases. Less than 75μm uses as a better reinforcement particle size to improve aluminum alloys' mechanical and tribological properties [29,45,41]. In addition, the amount of (volume fraction ratio and weight percentage) reinforcement in the composite gives a noticeable result variation in the properties of composite materials. When reinforcement percentage increases in the composite from 1 up to 10% gives a better improved mechanical property of the composite. But when it increased,>10% particles in matrix clustered particles could form and lower density and high wt. % of particles could observe strength.

Quality of casting composite defined by stirring time (5-10 min) and stirring speed(550-700 rpm) reduce the porosity in the cast composite materials [40]. Preheating of the reinforcement particle at (500-1000 ^{0}c) leads to an increase in wettability and decent interfacial connection between the reinforced particle and matrix [41]. The feed rate of the reinforcement and pouring temperature are also many parameters in improving the mechanical properties of the composite constituents [64].

In the liquid phase, the processing stir cast method is most suitable for the production of MMCs. Improvement in the mechanical properties of the composite solid increased with the addition of reinforced particles. Good particulate-matrix interface bonding reduces the porosity and enhances the composite solid's hardness and impact.

2.8 Gaps Identified

The research was conducted for different purposes of aluminum composite for various applications, especially for the automotive part and small engines application. Many types of analysis were made by reinforcing Al2024 with other agro-waste ashes and with ceramic reinforcements. However, aluminum alloys reinforced with silica sand and bagasse ash particulate were not investigated to improve the mechanical and tribological properties of Al2024 alloy. In addition, most of the investigation was implemented for automotive and small engine parts. However, it was not implementing for high structural parts like fuselage structural parts.

Most investigators study the optimization of fuselage structural parts to achieve better less weight to strength ratio, manufacturability, cost reduction, etc., materials. For the aircraft fuselage structure with other CFRP and design modification or cutout methods used, it is the most stress concentration area instead of the available or currently used material characterization.

Then in this thesis, the characterization and improvement mechanical properties of currently available material for the fuselage structural application area.

CHAPTER THREE

3. Materials and Methods

This chapter presents the materials and equipment used, fabrication methods, specimen preparation, and experimental procedures used to fabricate aluminum alloy reinforced with SiO_2 and sugar cane bagasse ash.

3.1 Methodology

The general methods employed to achieve the objectives of this thesis are presented in figure 3.1.

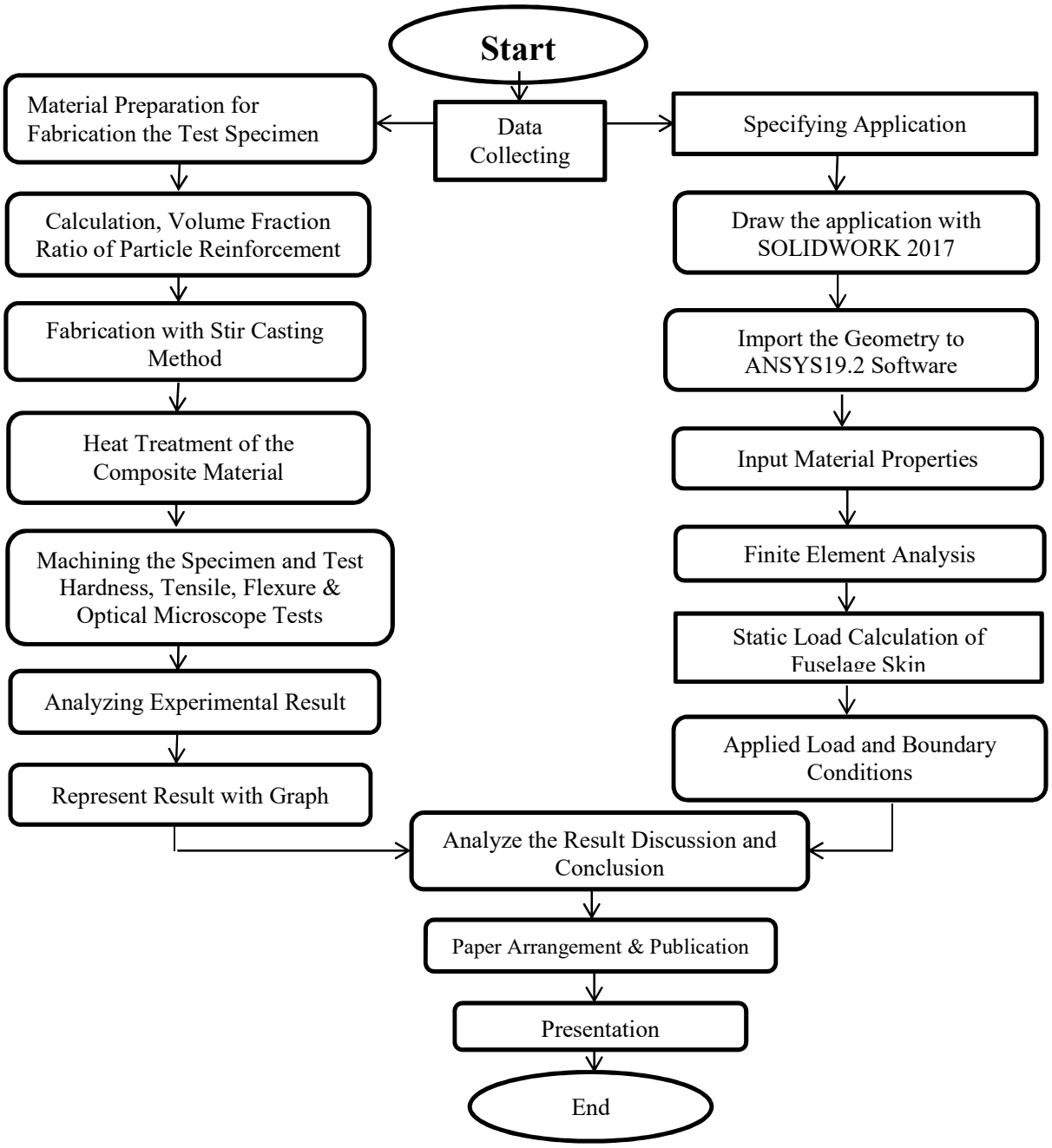

Figure 3.1 Methodologies

3.2 Composite Materials

3.2.1 Aluminum 2024

Aluminum alloy 2024 is an aluminum alloy, with copper as the primary alloying element. It is used in applications demanding high strength to weight ratio, as well as good fatigue resistance. It is weldable only through friction welding and has common machinability. Because of its poor corrosion resistance, it is often clad with aluminum or Al-Zn for protection, although this may decrease the fatigue strength. Due to its high strength and fatigue resistance, Al-2024 is widely used in aeroplane structures, especially fuselage and wing structures under tension.

The aluminum 2024 material was collected from Ethiopian airlines as a sheet metal form, and a spectroscopy test was performed at B & C aluminum.

Figure 3.2: Al2024 sheet metal

Table 3.1 Chemical composition of Al2024 spectroscopy test

No.	Al	Si	Fe	Cu	Mn	Mg	Cr	Zn	Pb	Ti
Avg.	93.06	0.028	0.168	>3.33	0.441	>2.67	0.014	0.151	<0.01	0.011

3.2.2 Reinforcement preparation

SiO_2

The silica sand material was collected from the Addis Ababa bottle and glass manufacturing Share Company. Also, it crashed and filtered with a sieve at < 63µm. Then before it is mixed with the molten metal, it is preheated at 700 ^{0}c to strengthen the composite better. The material used in this work is AA2024 metal matrix and SiO_2 as reinforcement particulates with different volume fraction ratios. Silica sand reinforcement was added to the molten alloy by different weight portions such as 5%, 10%, and 15%. The mesh size of silicon dioxide particulate is < 63 µm.

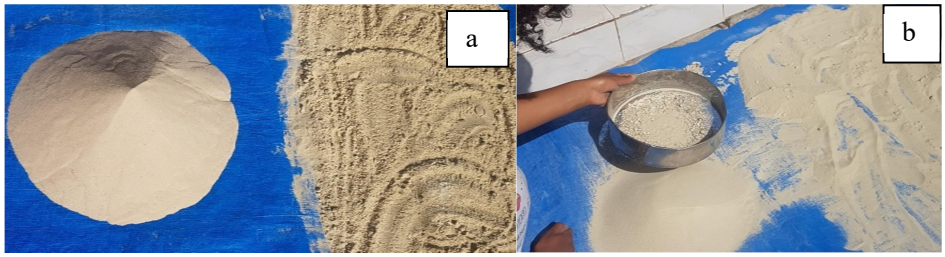

Figure 3.3: dried and sieved silica sand

Average density calculation by using Pycnometer Method

Calculating density of SiO_2

W1 = weight of empty bottle specific gravity

W2 = bottle + powder

W3 = bottle + powder + kerosene

W4 = bottle + kerosene

$$W5 = \frac{w2-w1}{(w2-w1)-(w3-w4)*0.79}$$

Specific gravity of kerosene = 0.79

Sample1. W1= 28.5341g

W2= 41.7913g

W3= 77.0270g

W4= 67.8865g

$$W5 = \frac{41.7913g-28.5341g}{(41.7913g-28.5341g)-(77.0270g-67.8865g)*0.79} = 2.196g$$

Sample 2. =2.195g

Sample 3. = 2.198g

Average = 2.196g

Table 3.2: Chemical composition of silica sand before heat treatment

Compound name	SiO_2	Al_2O_3	CaO	Fe_2O_3	MgO_2	K_2O
Avg. Composition by %	93.92	3	0.07	2.01	0.13	0.09

Bagasse ash

The bagasse, a waste material of sugarcane, was collected from the wenji sugar factory, located 110km from Addis Ababa.

Preparation of bagasse ash

First, the bagasse was washed with water to remove the dust and other deposits. In addition, it dried for 4 days with direct sunlight until it gets fully dry [65]. Next, it was burned at room temperature until it forms bagasse ash. Then it sieved at < 63µm particle size.

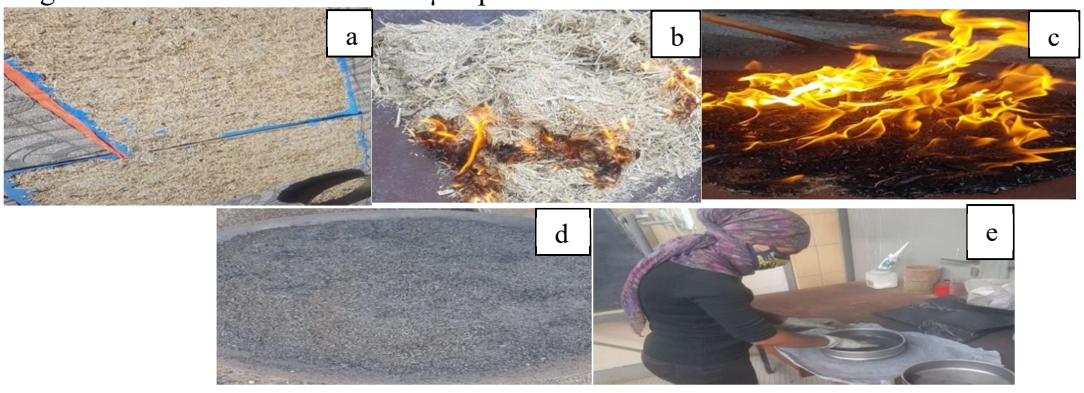

Figure 3.4: Bagasse ash preparation methods

Average density calculation by using pycnometer method

The calculating density of Bagasse Ash

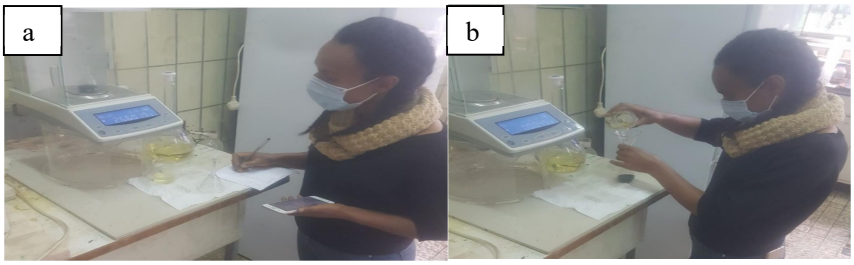

Figure.3.5: Measuring the density of BA & SiO_2 using a pycnometer

Sample1. W1= 28.5341g

W2= 31.4132g

W3= 69.4809g

W4= 67.8865g

$$W5 = \frac{31.4132g - 28.5341g}{(31{,}4132g - 28.5341g) - (69.4809g - 67.8865g) * 0.79}$$

= 1.778g

Sample 2. = 1.758g

Sample 3. = 1.797g

Average = 1.7776g

Table 3.3: Chemical composition of bagasse ash before heat treatment

Compound name	SiO_2	Al_2O_3	CaO	Fe_2O_3	Na2O	MgO_2	K_2O	P_2O_5	MnO	TiO_2
Avg. Composition by %	78.07	9.05	2.437	3.27	0.41	0.9	3.69	0.95	0.13	0.39

Table.3.4: Average density of materials

Material type	Sample 1	Sample 2	Sample 3	Sample 4	Sample 5	Average
SiO_2	2.196	2.194	2.196	2.198	2.198	2.196
BA	1.778	1.761	1.758	1.797	1.797	1.778

Additives

Magnesium powder was added to the composite in a small constant amount to each cast because of magnesium's property, which gives better wettability to the molten composite and good machining performance to the metal matrices composite [22]. It also reduces the surface rigidity and avoids the rejection of the particles from the melts. Without the addition of Mg, recovery of the particles into the melt is relatively low. Therefore, 2-5% Mg is commonly used in the Aluminum composite melts before a mixture of the particles. The interaction of the particles of an Aluminum composite would

change with adding Mg that could damage the mechanical properties of the composites [66]. However, adding the content above 1wt. percentage raises the viscosity of the slurry, and hence uniform particle circulation will be difficult. Wettability and reactivity determine the bonding between the constituents and, thereby, significantly affect the final properties of the composite material [67].

Salt (Duge)

The salt was added to deoxidize the molten composite and to remove the slag from the molten composite.

3.3 The Volume Fraction of the Particle and the Matrix Content of the Composite

3.3.1 Rule of Mixtures

The volume fraction of bagasse ash and silica sand is 0.05, 0.1, 0.15, each of them for a different composition. The density of BA, SiO_2, and Al2024 is 1.778 g/m^3, 2.196g/m^3, and 2.6555 g/m^3, respectively.

Given the volume portions of particle, V_p, and matrix, Vm, the density of composites, ρc, could calculate by the following equation.

$$\rho c = \rho_r V_r + \rho m Vm \quad \text{..... (3.1)}$$

If the density of reinforcement particle (ρ_r) and matrix (ρm) is known. The subscripts c, r, and m represent Composite, reinforcement, and matrix, respectively.

Where weight fraction of the reinforcing particles (Wr) and weight fraction of matrix (Wm) are defined as below respectively:

$$\text{Wr} = \frac{\text{density of reinforcement}}{\text{density of composite}} * \text{the volume fraction of reinforcement} = \frac{\rho r}{\rho c} * \text{ vr} \quad \text{.....(3.2)}$$

$$\text{Wm} = \frac{\text{density of matrix}}{\text{density of composite}} * \text{the volume fraction of matrix} = \frac{\rho m}{\rho c} * \text{vm} \quad \text{..... (3.3)}$$

The summation of the vol. fractions of all components in a composite must be equivalent to one. In the two constituents system containing one reinforcement particle and one matrix, then, the volume of the composite is:

$$VC = V\text{r} + Vm = 1$$

Where Vol. fraction of the reinforcing particle component (Vr) and Volume fraction of the matrix component (Vm) is defined as below respectively:

$$\text{vr} = \frac{\text{volume of reinforcement}}{\text{volume of composite}} = \frac{\text{Vr}}{\text{Vc}} \quad \text{..... (3.4)}$$

$$\text{vm} = \frac{\text{volume of matrix}}{\text{volume of composite}} = \frac{\text{Vm}}{\text{Vc}} \quad \text{..... (3.5)}$$

Matrix volume fractions Vm, Vc are matrix volume and composite volume, respectively.

Table 3.5: Composition by volume fraction ratio

Composite	Volume fraction ratio of materials
0	Al2024
1	Al2024 + Bagasse ash 5%
2	Al2024 + Bagasse ash 10%
3	Al2024 + Bagasse ash 15%
4	Al2024 + Silica sand 5%
5	Al2024 + Silica sand 10%
6	Al2024 + Silica sand 15%
7	Al2024 + Bagasse ash 5% + Silica sand 10%
8	Al2024 + Bagasse ash 10% + Silica sand 5%
9	Al2024 + Bagasse ash 10% + Silica sand 10%

3.3.2 The density of the composite

For the first composition of composite density calculation at different reinforcement vol. %

$\rho c = \rho_r V_r + \rho m V m$, Where: ρc – Density of composite, ρr – Density of reinforcement, ρm – Density of matrix, Vm – the volume of matrix

3.3.3 Reinforcement and matrix mass fraction

$\mathrm{Wr} = \frac{\rho r}{\rho c} * \mathrm{Vr}$, Where: Wr – the weight of reinforcement, ρc – Density of composite, Vr - Volume of composite, ρr - Density of reinforcement

Table 3.6: calculated results of Wc, Vm, Vr, Wm, and Wr

ρ= Density ***V***=volume ***c***,**r**,***m***= composite , rienforcment, matrix	**Wc**= weight of composite ***ρc***= Density of composite **Vc** = volume of composite	**Vm** = volume of matrix **Vc** = volume of composite **%Vmf**= volume mass fraction of matrix	**Vr** = volume of reinforcement **Vc** = volume of composite **%Vrf** = volum of reinforcement fraction	**Wm** = mass of matrix **Vm** = volume of matrix ***ρm*** = density of matrix	**Wr** = weight of rinforcement ***ρr*** = density of reinforcement **Vr** = volume of reinforcement
***ρc*=*ρr V*r + *ρmV*m**	**Wc= *ρc**Vc**	**Vm =Vc*%Vmf**	**Vr =Vc*%Vrf**	**Wm=*ρ*m*Vm**	**Wr=*ρ*r*Vr**
$\rho c1$=2.6116g/m^3	Wc1=5308.34g	Val =1930.9cm^3	VBA=101.6cm^3	Wal =5127.7g	WBA=180.7g
$\rho c2$=2.5677g/m^3	Wc2=5219.2g	Val =1829.36cm^3	VBA=203.26cm^3	Wal =48578g	WBA=361.398g
$\rho c3$=2.5239g/m^3	Wc3=5130.13g	Val =1727.72cm^3	VBA=304.89cm^3	Wal =4587.98g	WBA=542.1g
$\rho c4$=2.6325g/m^3	Wc4=5350.9g	Val =1930.9cm^3	VSiO2=101.6cm^3	Wal =5127.8g	WSiO2=223.18g
$\rho c5$=2.6095g/m^3	Wc5=5304.122g	Val =1829.358cm^3	VSiO2=203.26cm^3	Wal =4849.86g	WSiO2=446.36g
$\rho c6$= 2.5866g/m^3	Wc6=5257.58g	Val =1727.72cm^3	VSiO2=304.89cm^3	Wal =4587.8g	WSiO2=669.5g
$\rho c7$=2.5657g/m3	Wc7=5215.1g	Val =1727.73cm3	VBA=101.6cm3 $VSiO_2$=203.26cm3	Wal =4587.8g	WBA=180.7g $WSiO_2$=446.36g
$\rho c8$=2.5448g/m3	Wc8=5172.6g	Val =1727.8cm3	VBA=203.6cm3 $VSiO_2$=101.6cm3	Wal =4587.8g	WBA=361.398g $WSiO_2$=223.18g
$\rho c9$=2.5218g/m3	Wc9=5125.8g	Val =1626.1cm3	VBA=2.3.26cm3 $VSiO_2$=203.26cm3	Wal =4319g	WBA=361.398g $WSiO_2$=446.36g

3.4 Experimental Procedures and Steps

After collecting the required materials discussed in section 3.1, the next step is the fabrication of aluminum particle reinforced composite as per ASTM standard. In this section, the techniques adopted during the processing of the experimental analysis will be discuses.

3.4.1 Specimen pattern preparation

Tensile test specimen preparation as ASTM E8/E8M – 16a [68]. Including machining and shrinkage allowance for Aluminum metal up to 8in +2.286mm and up to 0.155in 3.937mm, respectively. The thickness of the specimen is 2.5mm as the sheet metal plate.

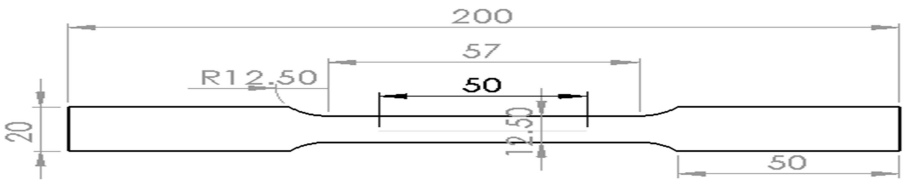

Figure 3.6: Tensile test specimen as ASTM E8M/16a

Hardness test specimen preparation As ASTM E18-15 Rockwell hardness for metallic material 5*5mm dimension.

Flexural/Bending Test Specimen ASTM 290 considering machining allowance up to 8in +2.286mm, shrinkage allowance up to 0.155in 3.937mm, and thickness of the specimen is 2mm.

Figure 3.7: flexural test specimens as ASTM E290

3.4.2 Sand mould preparation

The sand was brought from Ethiopian small and medium industry development enterprises around Mexico. Sand moulding is a metal casting process that includes the use of natural sand and the adequate proportion of clay (as a binder material) to keep the sand grains together or use the silica sand and artificial binder pair.

Design flexibility the size and weight of parts can range from a few millimetres & grams to meters & many tons. The size and weight of the cast are only limited by the restriction imposed by molten metal handling and supply.

High complexity shapes No other procedure offers the same range of potentials for shaping complex features than casting that can produce near net form components.

Wider material choice virtually all types of engineering alloys could cast as long as it could be melted.

Low-cost tooling- Tooling and equipment costs are low compare to some other metal manufacturing processes. Hence making it one of the cheapest methods to achieve near-net form components

Short lead time compared to others and hence ideal for short production runs.

Green sand:–The combination of silica sand or quartz, 15% clay bonding agent, about 5% water, and some other additives (molasses). The green sand is prepared from silica sand, water, and a certain quantity of clay (bentonite, kaolin). Greensand is the most popular sand type.

Green Sand Molding This process involves natural sand, which has a small percentage of clay. The green sand-casting process involves the following basic steps.

- Adequate amount of water added to the sand.
- After adding water, the green or natural sand is thoroughly conditioned and mixed with the help of a Mixer.
- Clay and water work as a binder: which holds the sand grains together.
- The sand is compressed around the pattern and rammed to become compact and tight; this is known as 'Green Strength.'

Advantages of green sand moulding

- Appropriate for long production runs
- Low-cost process
- Materials are available all around the world
- The process is versatile, and the sand is reusable

A mould frame (flask) consists of two parts: cope (the upper part) and drag (the lower position). Design of mould frame: with solid work software.

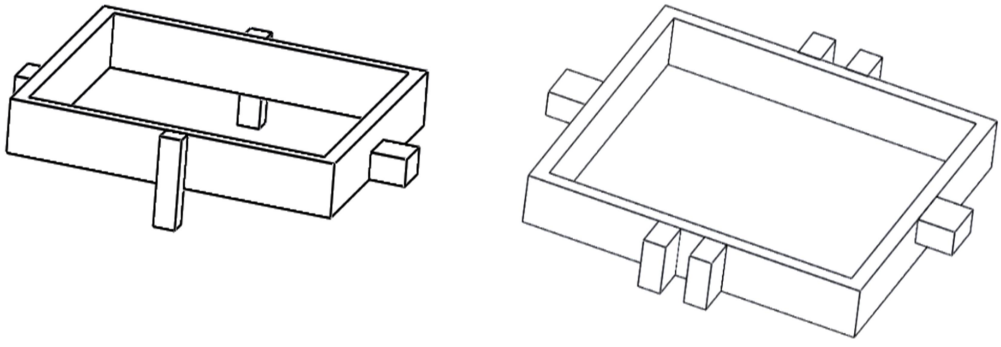

Cope **Drag**

Figure 3.8: Mold design

- The steps in the preparation of mould for the cast are based on [69].

Figure 3.9: Mold and Casting procedures

Aluminum 2024 alloy reinforced with SiO_2 and BA Casting process procedure

The whole process of aluminum casting held on at the foundry of Ethiopian technical university.

- Al2024 cuts into small pieces to make it suitable to put in the furnace
- The test specimens were prepared from wood at the wood workshop of Ethiopian technical university.
- The sand mould is prepared and dried for three days until it loses the moisture of the sand.
- The reinforcement pre-heat at temperature 1000^0c for 30 minutes for SiO_2 and BA before being added to the melt Aluminum alloy to remove moisture and gases from the reinforcement. Also, the Silica content in the ash increases with higher burning temperature [70,35].
- An electric induction furnace is used for the casting process
- To control the temperature pyrometer instrument which can read or sense the temperature from >5mm is used
- Melt the Al2024 in the furnace at 750 ^{0}C for 1hr, then add the silica sand with the prepared volume fraction ratio with a constant adding time difference, then the intended amount added in 10-sec gaps. Then it stirs about 5 min at 650rpm and add the bagasse ash to the melt aluminum alloy and silica sand in 10sec intervals and stirs about 10min at 650 rpm.
- For wettability of reinforcement and the matrix commercial pure Magnesium powder was used [22].
- To degasifying salt added to the molten composite
- Slag removed before pouring. Then the molten composite poured into the mold
- The mold crushed after 3 hours and pulled out the casted composite

Table 3.7: Materials and Equipment used during the manufacturing process

No.	Type	Material
1	**Reinforcement**	Silica sand, bagasse ash
2	**Matrix**	Al2024
3	**Additives**	Pure magnesium powder, Degasifying salt
4	**Equipment**	Sand Sieves 63µm, electric induction furnace, graphite crucible heat furnace, sand mixer, stirrer, mold, ram, sprue, runner, riser, brush, pyrometer, a digital scale, and weight balance

a) Al2024 work samples

b) Preheating the reinforcement in heat treatment furnace

c) Mixing the reinforcement into molten aluminum alloy

d) Adding salt and pure magnesium into the composite and removing the slag Stirring the reinforcement with the molten alloy by stainless steel stirrer

e) Pouring the molten composite into the mold and removed after 3hr

Figure 3.10: a) – e) Steps followed to manufacturing the composite test specimens

Pyrometer

In the casting process: to detect the temperature of the melting furnace Pyrometer was used. A pyrometer is a remote-sensing thermometer and non-contact measuring device for high temperatures. It is used to measure the high temperature up to 3500°C. Thermal radiations from the radiating object come inside the housing tube. These radiations fall on the concave mirror, and they reflected the hot junction of the thermocouple. Therefore, an e.m.f. produced in the thermocouple and is measured using a mile-voltmeter. This change in e.m.f. will give the measure of temperature. The advantages of using the pyrometer have high accuracy, no physical contact with the radiating object, and space among radiating things. Also, the pyrometer is negligible. Disadvantages it is not proper for very low-temperature measurement because of poor sensitivity. Dust, smoke, gases in between radiating objects and instruments will cause an error.

Table 3.8: Specifications of the aluminum melting furnace (electric induction furnace) Particulate Description

Temperature	12000 °C
Melting capacity	5-10 kg
Controller	Thyristorised PID temperature – 6 Kw with power pack
Crucible	Graphite
Power	230 volts, 6 kw

Heat Treatment - T3

The heat treatment process (temper T3 heat treatment) of cast specimens offers enhancement in its mechanical properties, which is often necessary for many uses. The T3 heat treatment has a three-step process. The castings first allowed heating solution at 450^0c for 9hr and then immediate quenching (w temper) at cold-water media. Next, it cooled at room temperature for 3days [71].

Figure.3.11: Heat treatment, quenching of the specimen, and test specimens

3.4.3 Introduction to test apparatus

Universal testing machine (UTM):

Electronic ranges of UTM Machines are fast, accurate, & simple to operate. Load and displacement are displayed on the digital display system in their respective engineering units in these machines. It is supported by Windows-based software, which can store, retrieve readings as and when required. Each includes a load unit with integrally mounted servo valves, actuator and the control system, and a hydraulic power unit, as illustrated in figure 3.12. The control system has three major parts: the system software running on a personal computer, the digital controller, and a remote station control panel. These functions work together to provide fully automated test control. The universal testing machine of model WP 310 has a test load capacity of up to 50 KN, with a maximum piston stroke of 150 mm at Bishoftu Defense College of engineering and a 6 mm/sec crosshead speed.

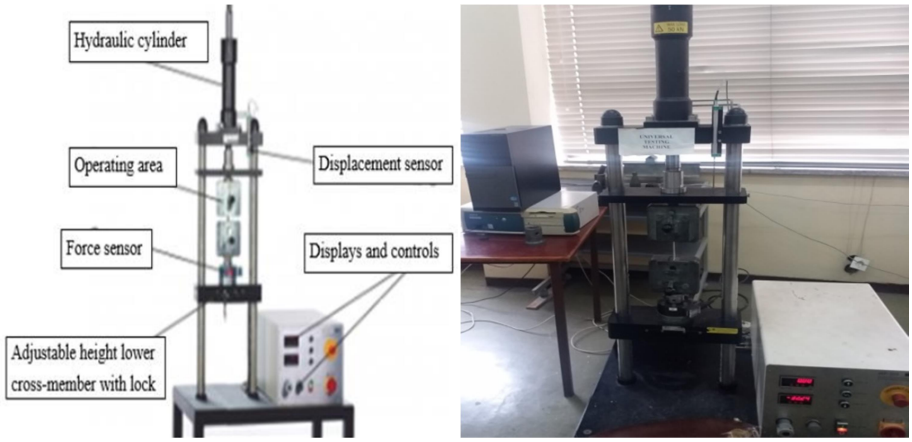

Figure 3.12: UTM for bending and tensile test

3.4.3.1 Testing Conditions

The experiment was conducted at constant strain rate values for tensile and flexural testing under constant room temperature. The next task was the experimental investigation of prepared test pieces on

UTM by varying a load from the dynamometer load cell. After each test, displacements at different load responses were generating in a data acquisition system as an output.

Five specimens are taken for each of the tests to show the results' repeatability by minimizing the experimental errors. The hardness, tensile strength, flexural strength, and optical microscope tests were prepared according to ASTM standard E18-15, E8/E8M-16a, and ASTM290.

The tensile test, a three-point bending test, was conducted along the longitudinal and horizontal direction of the metal matrices composite on a universal testing machine according to [72]. The hardness test was performed using a Rockwell hardness testing machine.

3.4.3.2 Tensile Strength Test

Tensile testing is a fundamental materials science test during which a sample is subjected to a controlled tension until failure is also known as tension testing. The results from the trial are usually used to choose a material for the associate application, for quality control, and to predict how a material can react under very different forces. The [73] was followed while preparing the tensile test specimens for the aluminum composite material test. Properties obtained from this test are Ultimate tensile strength, maximum elongation, and reduction in area. Properties like young's modulus and yield strength also are determined from these measurements.

The prepared specimens (rectangular cross-section 57 x 2.5 mm2 & length 200 mm) were carried out utilizing Universal Testing Machine for the tensile test. The experimental setup and samples for the tensile test are shown in figure 3.13 (a) and (b), respectively. Four specimens were tested in this machine.

$$\sigma = \frac{P}{Wt} \quad \text{.....(3.6)}$$

Where: σ = tensile stress, P= applied load, t= average thickness of the film, w= width of the test specimen

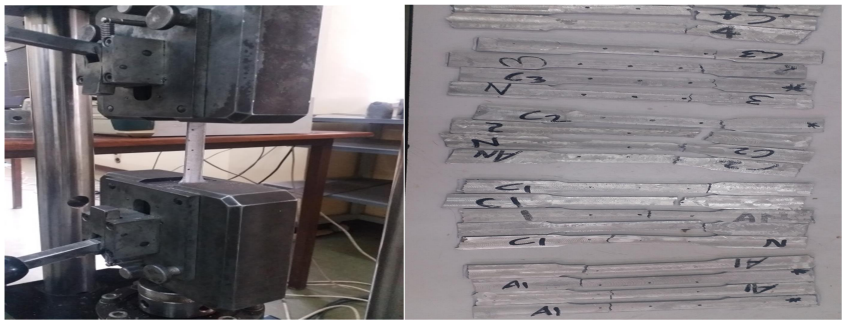

Figure 3.13: Tensile strength test

During the test, the specimens were placed in the grips of UTM. After griping the sample, the required data like thickness, gage length, width, material type, and date were added to the computer software of UTM. Then the machine started, and the load was automatically applied until the spacemen are failed. Finally, the stress-strain data are recorded during the test, and the values will be obtained from the software.

3.4.3.3 Flexural Bending Test

Flexural bending test (3-Point bending test) is one of the simplest bending tests used to determine flexural strength. Flexural strength is the ability of the material to resist bending loads applied perpendicular to its longitudinal axis. The stresses caused by the flexural load are a combination of tensile and compressive stresses. Bending tests were tested in the UTM machine that exists in Defense University Engineering College Lab. ASTM E290 was followed while preparing the 3-point bending test specimens for the aluminum composite material test. According to this standard, the dimension of each sample was 2.5 mm thickness, 20 mm of width, and 200 mm overall length. The experimental setup and specimens for the 3-point bending test are shown in figure 3.14 (a) And (b), respectively. Five samples were tested in this machine.

Figure 3.14: (a) Typical specimen under bending test on UTM, (b) Specimens after the test

The basic procedure involved during this test is that the supporting roller is prepared to depend on the dimension of the specimen. Next, the sample is fixed on the supporting roller by adjusting the supporting roller into the required gauge length dimension of the piece. Then the machine started, and the load was manually applied until the spacemen are failed. Finally, the software gives the recorded data during the test.

3.4.3.4 Hardness Test

Hardness test measurement was carried out on the base metal and composite samples using a standard Rockwell hardness test machine. The Rockwell scale is a hardness scale based on the indentation hardness of a material. The Rockwell test determines the hardness by measuring the depth of penetration of an indenter under a large load compared to the penetration made by a preload. Rockwell hardness measurements were carried out to investigate the influence of particulate volume fraction on the matrix hardness. First, the specimen surface is polished until it gets a smooth surface.

For each specimen, tests were taken at a different point, like two times the diameter of the other test point. The applied load was 100 kg, and the ball indenter used was 1/16' as the Aluminum Rockwell hardness test standard. Advantages of the Rockwell hardness method include the direct Rockwell hardness number display and fast testing time. Hardness test Rockwell scale B, indenter 1/6” ball Pmajor 100kg

HRX = Rx = M- $\frac{(h2-\ )}{0.002}$ Where M = 130 for B, E, M, R, etc. scales

Figure.3.15: Rockwell hardness testing machine and specimens after the test

3.4.3.5 Micro Structural Analysis

The optical microscopy test was performed to analyze the morphology of the base metal and the composite. Before testing, the specimen had to be polished in different glass paper (abrasive paper). The polishing process was continued until the sample get a clear face (like a mirror). The materials used to polish in different steps are 120,150,180, 220, CC400,1/0, 2/0 electro-coated waterproof abrasives. After applying those polishing steps, the specimen was washed by MP-2B grinder polisher with the addition of water and grade II, III abrasion gel. Finally, the sample was washed with sodium chloride and get dry for an optical microscopy test.

Figure.3.16: a) Grade II & III Polishing gel b) MP-2B Grinder Polisher c) the final specimens for test

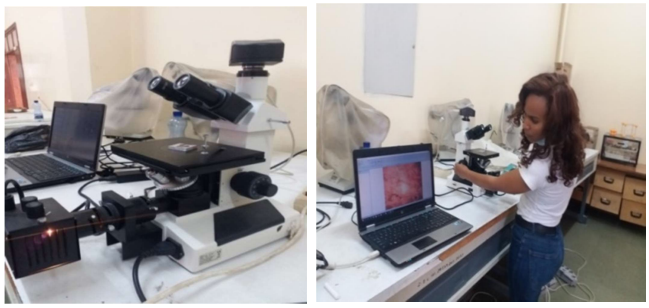

Figure 3.17: a) Optical microscope measuring instrument, b) performing optical microscopy test

3.5 Specification/Dimension of the Fuselage Skin Panel

3.5.1 Analytical Data

Considering the fuselage structural part fuselage-skin stiffened panel as the Al2024 alloy is the primary material to these application areas and standing from this, this research paper aims to model and apply static analysis and testing properties experimental test results. The practical test specimens were prepared as per ASTM standards. The aluminum ceramic matrix composite fuselage skin was designed with SOLIDWORK 2017 software, which is compatible with ANSYS 19.2 and imported to FEA, which

will have a high strength to weight ratio and lower stress of the current Al2024.

The selected Al2024 application and their specification are listed below.

Table3.9 Airbus A321 specification [74]

Dimensions	Overall length	44.51 m
	Cabin length	34.44 m
	Fuselage width	3.95 m
	Max cabin width	3.70 m
	Wingspan (geometric)	35.80 m with Shark lets

Capacity	Pax	Max seating	220
	Typical seating	170-210	
	Cargo	LD3 capacity underfloor	10 LD3-45W
	Max pallet number underfloor	10	
	Water volume	59 m^3	

Performance	Range	5950km with shark lets
	Maxi ramp weight	93.9 tons
	Max take-off weight	93.5 tons
	Max landing weight	77.8 tons
	Max zero fuel weight	73.8 tons
	Max fuel capacity	30030 liters

The type of panel stringer shape for fuselage structural application is hat stiffener. The specification of the hat stiffener for aluminum material is shown in table 3.9

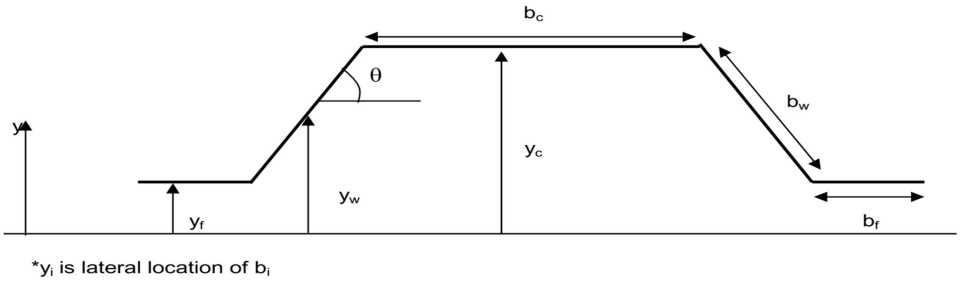

Figure 3.18 Geometry of a Hat Stiffener[75]

Table 3.10 Fuselage stiffened panel geometry value (aluminum) [75]

Parameter Designation	**Parameter Name and Description**	**Units**	**Narrow Body (NB) Value**	**Wide Body (WB) Value**
B	Panel Width	In	2.5	4.4
A	Panel Length	In	3.8	6.5

Parameter Designation	Parameter name and description	Units	Narrow Body(NB) Value	Wide Body (WB) Value
b_w	Stiffener Hat-Section Web Width	In.	0.35	0.70
b_f	Stiffener Hat-Section Flange Width	In.	0.30	0.45
b_e	Stiffener Hat-Section Cap Width	In.	0.70	1.40
θ	Stiffener Hat-Section Web Angle	Degrees	43	43

Table 3.11 Fuselage-skin stringer-panel geometry value (aluminum)

Structural Analysis: Hoop Stresses

Hoop stresses are the result of cabin pressure loads acting on the fuselage skin. This pressure force is a byproduct of the pressure differential between atmospheric pressure and internal cabin pressure, taken into account when sizing the fuselage-skin panel. Using the pressure load, the radius of the fuselage, and the thickness of the skins, the hoop stress was calculated using Equation 3.7.

Types of load, which are applied on the fuselage structural parts

According to [55,75], the fuselage dimension and the applied force were calculated to analyze the von-mises stress and deformation of the fuselage skin panel. The Calculation of force a differential pressure from 5psi – 31psi was considered for the current case. Due to the internal pressurization of the fuselage passenger cabin, the hoop stress would develop in the fuselage structure. The tension load generated inside the fuselage of the skin panel corresponding to pressurization is considered for the linear static analysis of the skin. The cabin pressure was converted into force and analyzed in this case.

The corresponding pressure value in the SI unit is N/m2. The calculated load is tabulated in Table 8.

$$\sigma hoop = \frac{pd}{2t} \quad \text{..... (3.7)}$$

P = the load in N/m2, d = the diameter, and t = was the thickness of fuselage skin.

Substituting P from above, d = 3.95m, and t = 0.0012m we find the hoop stress values. The hoop is defined as,

$$\sigma hoop = \frac{F}{A} \quad \text{..... (3.8)}$$

Where, F = the force value which has to be entered for analysis, and A = the area.

A = (Length of fuselage skin panel * skin thickness)

= (0.6604 * 0.0012) = 0.00079m2

$$F = \sigma hoop * A \quad \text{..... (3.9)}$$

Table 3.12: calculated load (N)

Pressure (psi)	Pressure($N/m^{2)}$	Load (N)
5psi	34,473.8	89,646.2438
10psi	68,947.573	179,292.418
15psi	103,421.359	268,938.626
17psi	117,258.740	304,921.582
20psi	137,895.146	358,584.84
27psi	186,234.444	484,287.15
28psi	193,132.042	502,223.78
30psi	206,842.719	537,877.253
31psi	213,824.761	556,033.472

According to [75] buckling effect of skin panel with and without frame research analysis, Al2024 T351 material properties [76] were used, and it shows excellent performance for this application area. Therefore, for this thesis work, Al2024 T351properties were chosen to compare with the reinforced new aluminum composite and unreinforced aluminum composite performance by applying pressure load on the materials.

Table 3.13: Mechanical properties of Al2024 T3, Al2024/ SiO_2/BA T3 composite & Al2024 T351

Materials	**AL Cu T3**		**AL Cu/SiO_2/BA T3**		**AL Cu T351**	
Mechanical properties	Values	Units	Values	Units	Values	Units
Density (ρ)	2.6555	g/m3	2.56	g/m3	2.78	g/m3
Young modulus (E)	70.887	GPa	78.894	GPa	71000	GPa
Poisson's ratio (v)	0.33		0.3		0.33	
Tensile yield strength (σy)	214.22	MPa	392.67	MPa	350	MPa
Ultimate tensile strength (σt)	320.22	MPa	560	MPa	480	MPa
Behaviour	Isotropic		Isotropic		Isotropic	

Allowable stress = yield strength/ factor of safety

- For Aluminium, alloy 2024-T3 we have Yield strength = 214.22 MPa

Allowable stress = 214.22/2

= 107.11 MPa.

- Also for Al2024/SiO_2/BA –T3 We have Yield strength = 392.67 MPa

Allowable stress = 392.67/2

= 196.335 MPa.

- For Aluminium, alloy 2024-T351 we have Yield strength = 350 MPa

Allowable stress = 350/2

= 175 MPa.

3.6 Modelling of Fuselage Skin Panel

After collecting the required data, which is discussed in section 3.1 up to section 3.4, the next step is modelling fuselage application. Finite Element Analysis is method is a numerical technique for solving engineering problems. It is the most powerful analysis tool used to solve simple to complicated issues. With the basic understanding of how finite element programs work, a finite element model must be created with appropriate parameters such as dimensions, loads, constraints, element choice, mesh selection, etc. In ANSYS, there are two completely different methods to construct the model. The first methodology is to create the model in a CAD environment like SOLIDWORKS or CATIA and save the model with a file format like IGES & ACIS. Then, the file is imported into ANSYS for setup and analysis. The second method is to use ANSYS internal drawing capabilities to build the model. However, the modelling functions in ANSYS are not as good as the other CAD programs; users often encounter

difficulties in making complex models due to interface limitations. In this study, the first method was used to model the system.

3.6.1 3D modelling of the fuselage skin panel with stiffener

The fuselage skin panel modelling was prepared on SOLIDWORK 2017. This software application is 3D mechanical design software for creating 3D prototypes, used to design, visualize and simulate the analysis. Various mechanical design and manufacturing operations were modelled using SOLIDWORK. This software allows the user to make changes very easily without going to the back at the beginning and updating all the drawings. Generally, SOLIDWORK is easy to use and feature-based parametric solid modelling software with many extended design and manufacturing applications.

In this specific research, based on the material dimension, the obtained theoretical calculation, and direct measuring data discussed in section 3.4, 3D modelling of the fuselage skin panel created with the help of SOLIDWORK 2017 solid modelling software and analysis performed by using ANSYS 19.2 workbench. Figure 3.19 shows the 3D modelling fuselage skin panel.

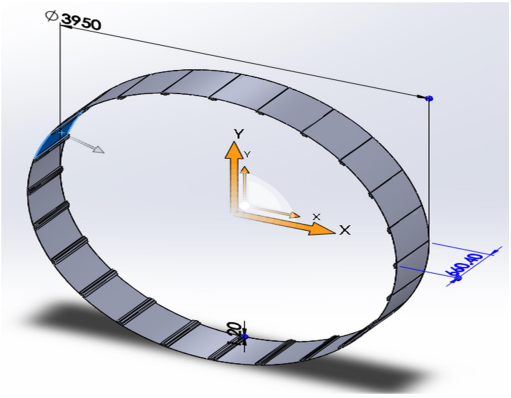

Figure3.19: Trimetric view of fuselage skin panel with stiffener using SOLIDWORK 2017

3.7 FEA of Fuselage Stiffener Panel

FEA is a numerical model of investigating a complex structure into very small parts called elements. The software implements equations that manage the character of these components and solves all of them, generating a complete description of how the system acts as a whole. This solution result can display in tabulated or graphical forms. This kind of analysis is typically used to design and improve a system that is too complicated to Analyze manually.

Applications of Finite Element tools:

- Static Analysis: - stress, deflections, forces, strains, & energies
- Dynamic Analysis: - stress, frequencies, deflections, forces, strain, and energies
- Heat Transfer Analysis: - thermal gradients, heat fluxes, Temperature, and heat flow from convection
- Fluid Analysis:- convection coefficients, Pressure, velocities gas, and temperature

- In aerospace engineering, the following types of FEA are common: dynamic analysis, static analysis, transient dynamics, aeroelasticity, aerodynamics fracture mechanics, creep and heat transfer and plasticity analysis, composite materials [48].

3.7.1 Static structure analysis

A static structural analysis determines the stresses, strains, displacements, and forces in structures. Steady loading and response conditions are assumed; that's, the loads and the structure's response are assumed to vary slowly concerning time.

The general assumption for analysis

It is essential to acknowledge the assumptions made to obtain this stage. First, the fuselage stiffened skin panel assumed circular as the fuselage structure is cylindrical with constant cross-section [56]. Second, as previously discussed, this analysis does not account for a stringer, frame, and others of the fuselage structure. Finally, this analysis does not account for non-pressurized areas, instead assumes
the full fuselage panel is pressurized. These assumptions simplify the overall research and ensure hypothesis completion; it gives a good representation of the overall fuselage-skin panel structure and provides a platform for FEA analysis.

3.7.1.1 Static analysis of Heat-treated Al2024 T3, Al2024/SiO_2/BA T3 composite, and Al2024 T351 fuselage stiffened panel

Define Engineering Data

This is completed by selecting the Engineering Data from the analysis tab of the ANSYS Workbench and inserting the corresponding values. The specific material property of the chosen Al2024, Al2024/SiO_2/BA composite, and Al2024 T35 material is stated in figure 3.20:

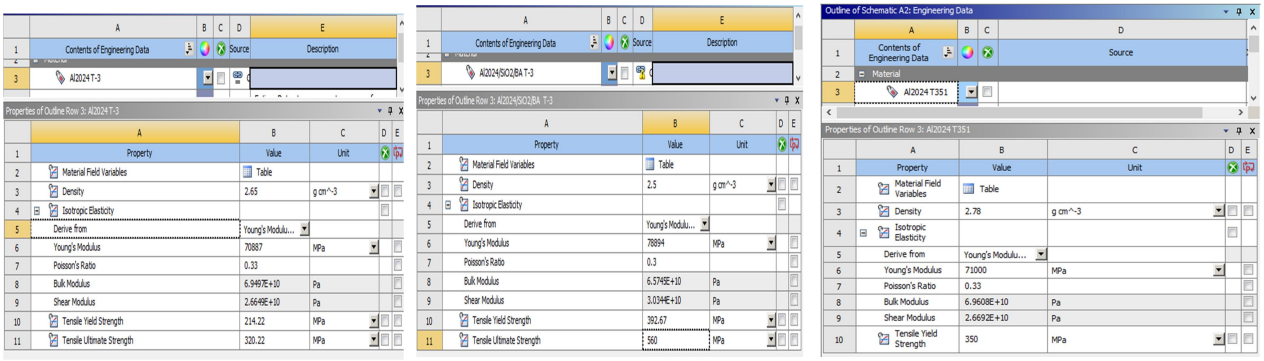

Figure 3.20: Material properties of heat-treated unreinforced Al2024, Al2024/SiO2/ BA composite, and Al2024 T351

Attach geometry

Using ANSYS as FEA analysis was conducted using the CAD model and applied loads. Due to the limitations of the software and the large geometry, the CAD model was reduced to a Single fuselage-skin panel figure 3.19. This reduces the computational requirements of the FEA model and significantly reduces the time required for each analysis. By verifying the structural integrity of this section, it is easy to justify the integrity of the entire structure. Attach geometry from a CAD system supported by

Workbench. Then the browsed solid model of the unreinforced AlCu, reinforced AlCu composite, and other AlCu T351 stiffened fuselage skin panel had done on SOLIDWORK 2017 present as shown in figures 3.21.

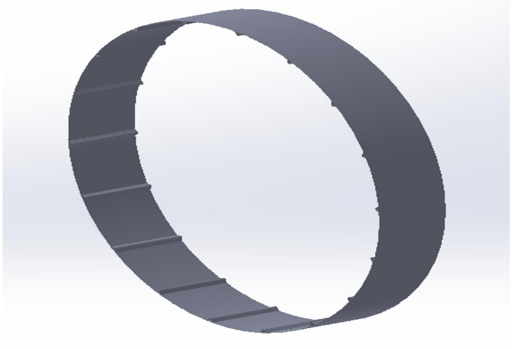

Figure 3.21: 3D model of the fuselage skin panel

Apply mesh controls/preview mesh

In the FEA, the basic concept is to analyze the structure, an assembly of discrete pieces called elements connected at a finite number of points called nodes. Meshing is the web between the features; this step divides the advanced geometry model into tiny elements that become solvable in an otherwise too advanced situation. Solid Modeling constitutes a part of the FEA. Thus, the sole purpose of Solid Modeling is to create the mesh of the geometry as conveniently and efficiently as possible. The meshing process is performed only after the specification of the element type.

After transferring the CAD geometry into the FEA software, the structure meshed using the coarse mesh setting. Using this setting, ANSYS constructs a mesh containing 33850 elements and 61956 nodes. While a finer mesh is possible, it significantly increases the required computation time, with a slight improvement in overall accuracy.

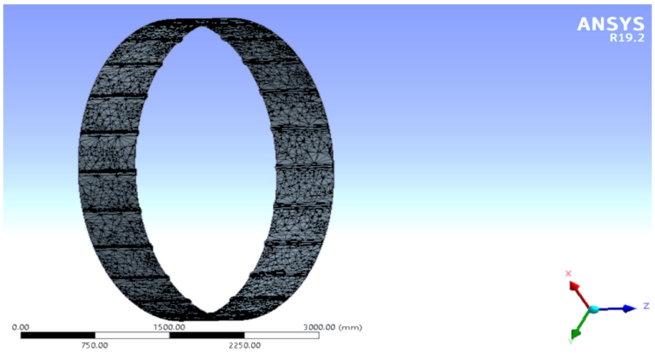

Figure 3.22: Meshed model of unreinforced AlCu T3, AlCu/SiO_2/BA composite & other AlCu T351 material

Apply Loads and Supports

In this step, load and boundary conditions are specified. The boundary and loading condition of the fuselage skin panel assumed one is fixed and load applied inside the panel [77]. Therefore, the rear and the front face of fuselage skin have the tension to deform when the load is applied on the fuselage skin,

and it can bend about the center of the fuselage.

To attain an accurate stress analysis for any application, the support and the load should define. This will ensure that the solution incorporates support of the domain [56]. The fuselage skin panel is mounted at the center of the fuselage structure, and it is considered fixed at one with other stiffened skin panels. The static load is applied inside the fuselage along the Fx direction, as shown in figure 3.23. For this analysis, the maximum applied load is 304KN for Al2024 T3, 502KN for Al2024 T351, and 556KN for Al2024/silica sand/bagasse ash T3 composite.

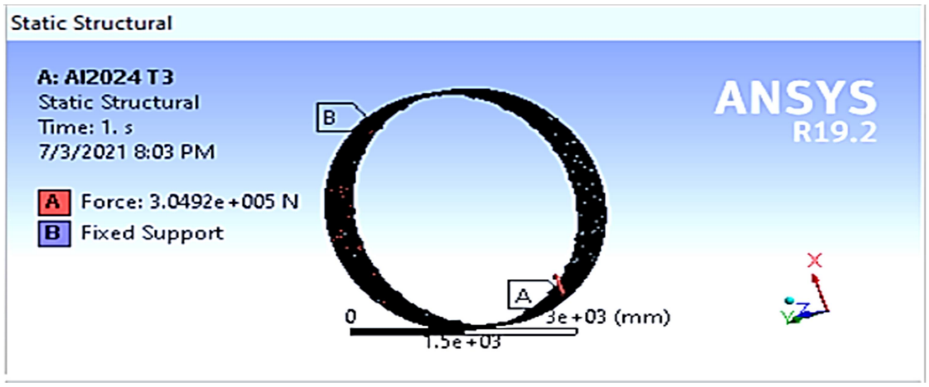

Figure 3.23: Boundary condition and applied load of Al2024 T3 at 17psi for the maximum allowable stress

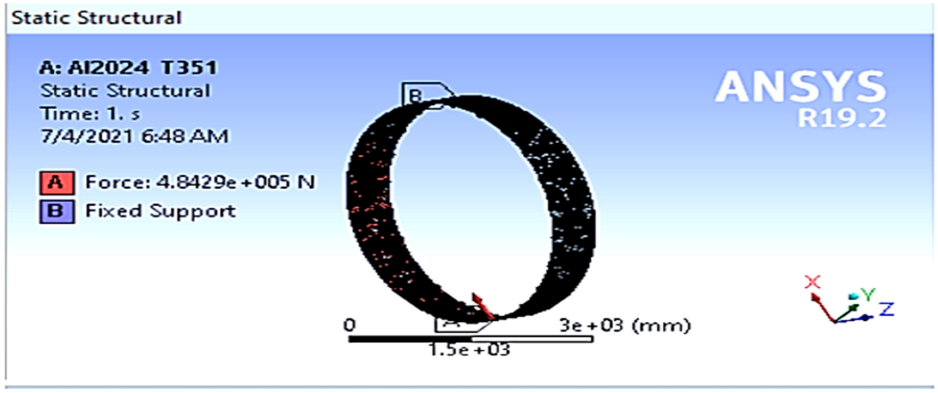

Figure 3.24: Boundary condition and applied load of Al2024 T351 at 27psi for the maximum allowable stress

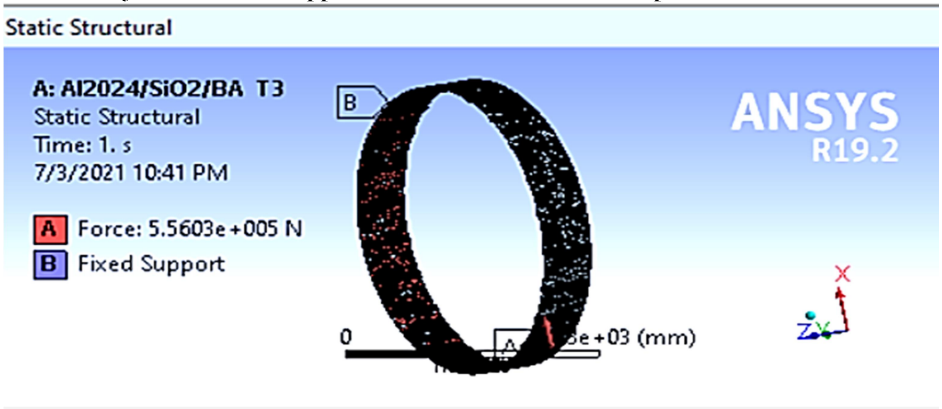

Figure 3.25: Boundary condition & applied load of Al2024/SiO_2/BA T3 composite at 31psi for the maxi allowable stress

Generate solution

In this step, the solution is generated from the above input parameters of the research. The total deformation and equivalent (Von Misses) stress are the essential variables to solve by this software analysis. Once the solution is generated, if there is a change of valuable information on the behaviour of the structural, the solution output is updated itself from the solver; the detailed solution of each dependent parameter can display one by one for both materials. Once the solution generates, each dependent parameter is solved and ready to be seen and interpreted.

CHAPTER FOUR
4. Results and Discussions

4.1 Results

4.1.1.1 Tensile test

For tensile strength evaluation, there were five specimens of aluminum ceramic reinforced composite with matrix/reinforcement particle ratio (Al2024 85%, SiO_2 10%vf, and BA5%vf) tested. While the typical UTS and composite vol.fraction ratio of aluminum ceramic reinforced composite specimens under tensile is presented in figure 3.13. Each of the five samples results showed a small difference among their result output.

The modulus of elasticity (Young's Modulus) is the ratio of stress in MPa to strain in millimetres per millimetre (mm/mm.) as computed from the graph.

$$E = \frac{\sigma}{\varepsilon} \quad \text{..... (4.1)}$$

Where: E is young's modulus in GPa, σ is engineering stress in GPa and ε is engineering strain

Therefore, the maximum tensile strength and tensile modulus of the Al2024 85%, SiO_2 10% & BA 5% of particle reinforced isotropic aluminum ceramic composite material is 560 MPa and 78.887 GPa.

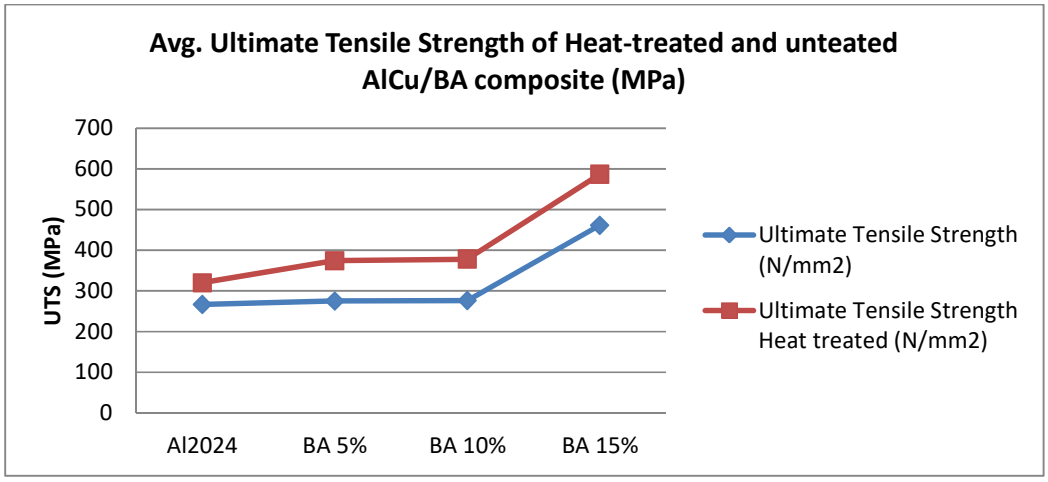

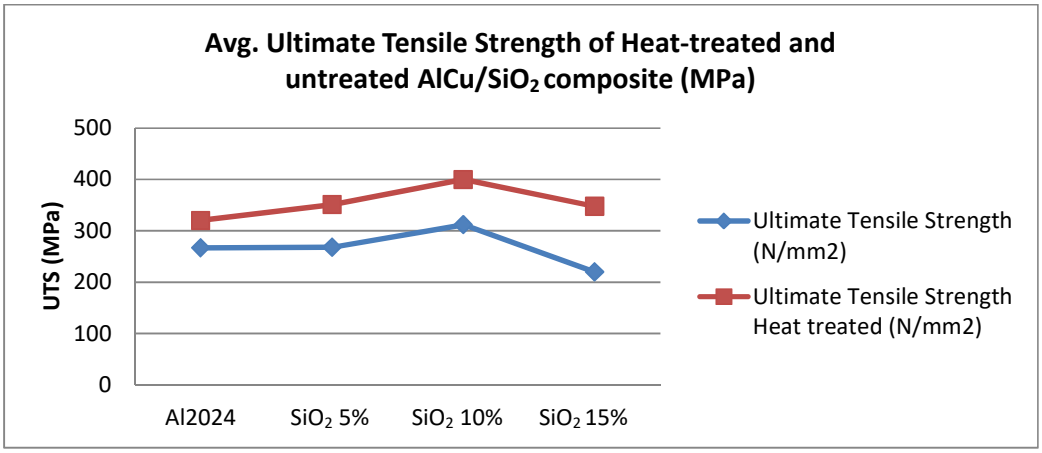

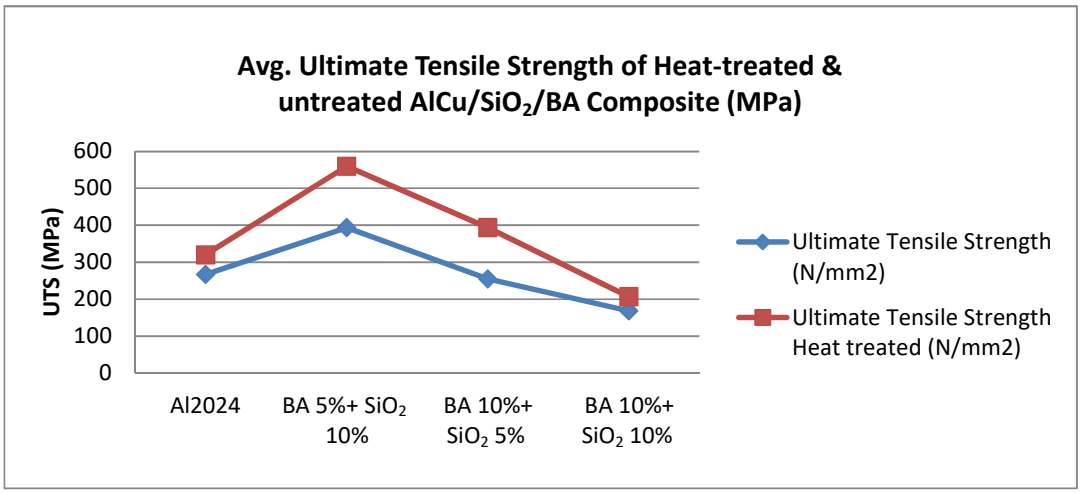

Figure 4.1: Tensile strength of AlCu/BA, AlCu/SiO_2 & AlCu/SiO_2/BA heat-treated & untreated composite, respectively.

4.1.1.2 Hardness test

Hardness test Rockwell scale B, indenter 1/6" ball Pmajor 100kg

$$HRX = Rx = M - \frac{(h2 - h)}{0.002} \quad \text{..... (4.2)}$$

Where M = 130 for B, E, M, R, etc. scales

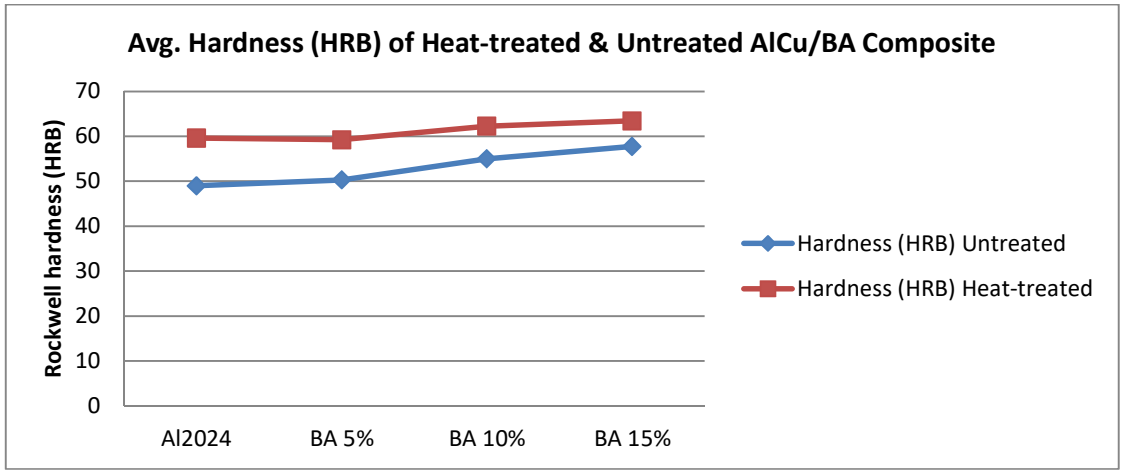

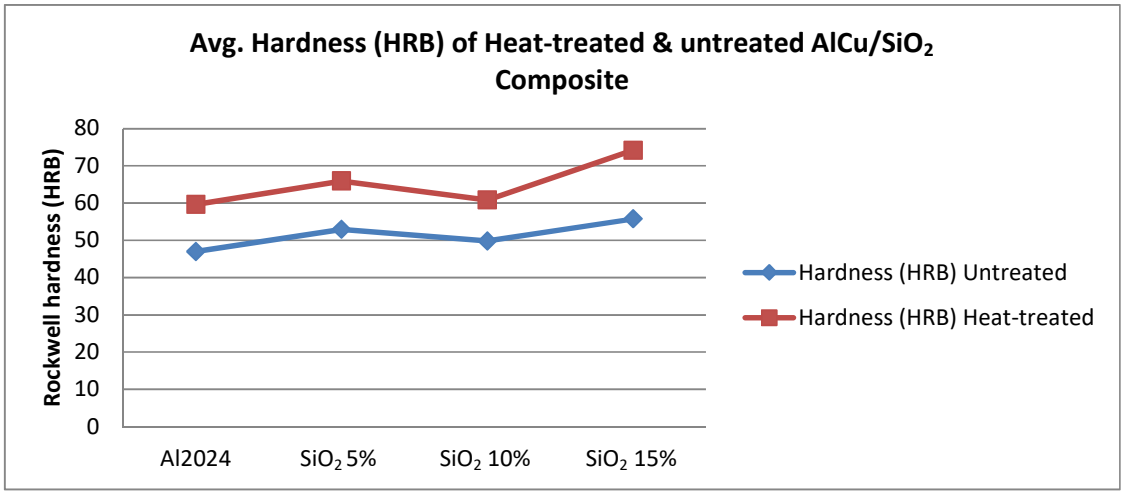

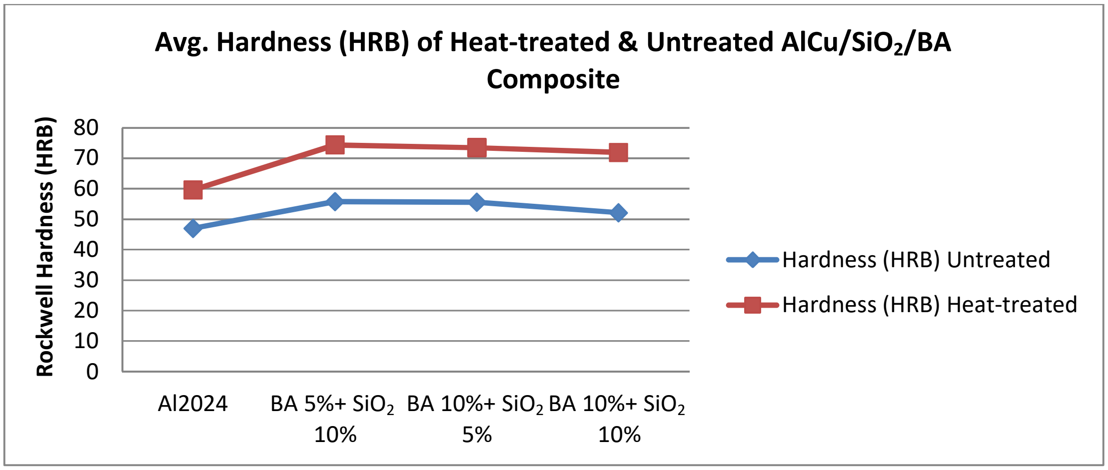

Figure: 4.2. Rockwell hardness results of AlCu/BA, AlCu/SiO_2 & AlCu/SiO_2/BA composite, respectively.

The hardness of unreinforced and reinforced Al2024 composite was determined according to ASTM E18-15 at room temperature of 20^0c.

4.1.1.3 Flexural/ Bending test

The flexural test measures the load required to bend a beam in three-point loading conditions. The data records are frequently used to select elements for parts that will maintain loads without inflection. Flexural modulus is used as a sign of a material's stiffness once inflection. Three-point bend test carried out in a UTM machine under ASTM E290 standard to measure the flexural strength of the aluminum ceramic reinforced composites. Five specimens were prepared for repeatability. In addition, each of the five specimens' results showed that there is no big difference among their result output. Bending test performed with DIN 50110 under three-point bending in figure 3.12 when the load P applied at mid-span of a rectangular specimen of span L between two rollers, the highest flexural strength (σ_{bf}) determined by:

$$\sigma bf = \frac{3LP}{2(bd2)} \dots \dots \dots \dots \dots \dots \dots \dots \dots \dots \dots \dots \dots \dots \dots \dots \dots \dots \dots \dots \dots \dots \dots \quad (4.3)$$

Where: P = load at a given point on the load-deflection curve, N L= support span of the specimen, mm, b = width of the specimen tested, mm and d = depth of the specimen, mm

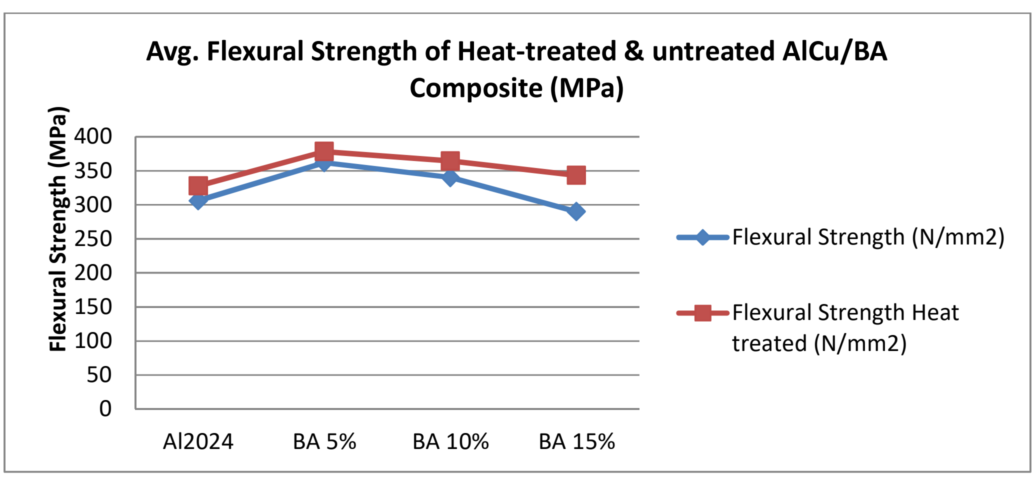

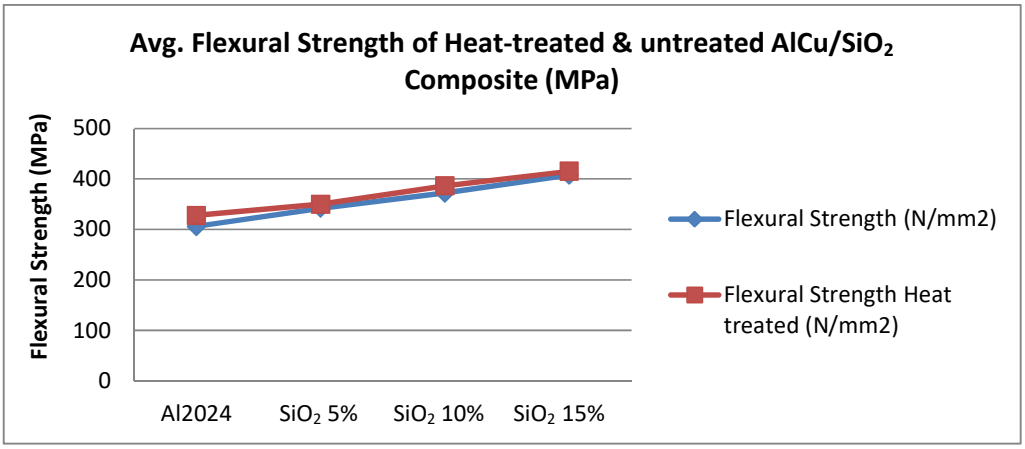

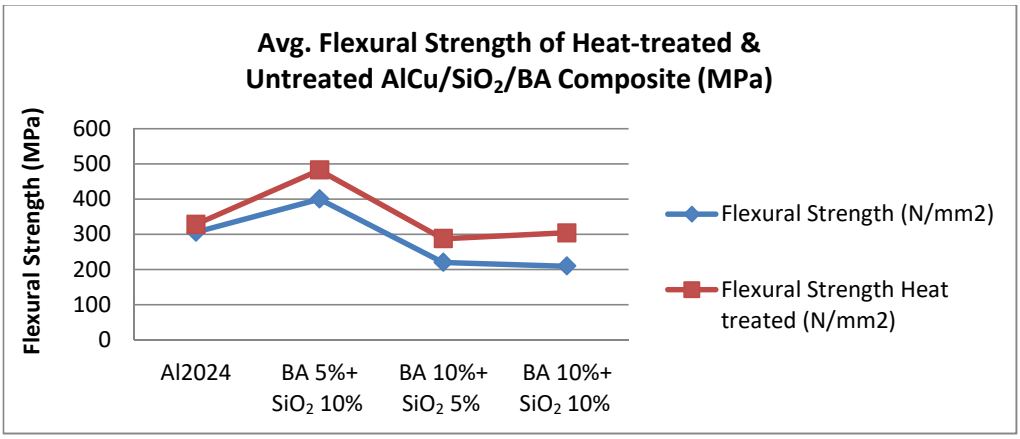

Figure 4.3: Flexural strength of AlCu with SiO_2, BA, & AlCu/SiO_2/BA composite, respectively.

4.1.1.4 Microstructural Analysis Result

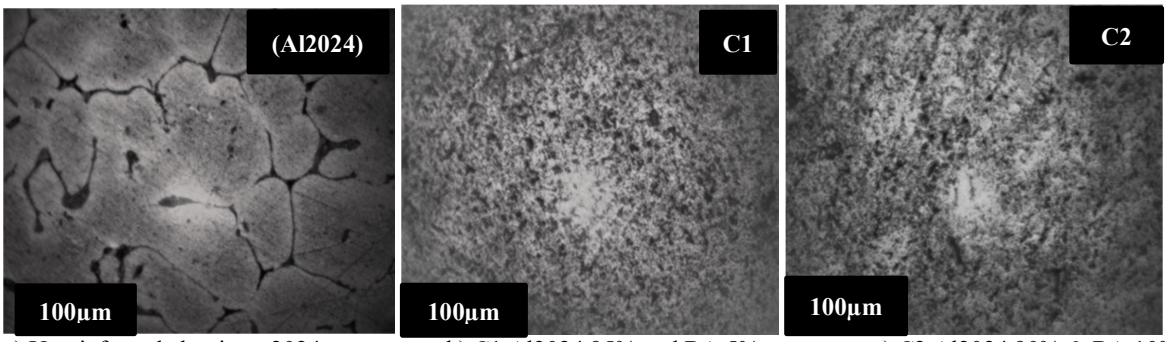

a) Unreinforced aluminum2024 b) C1 Al2024 95% and BA 5% c) C2 Al2024 90% & BA 10%

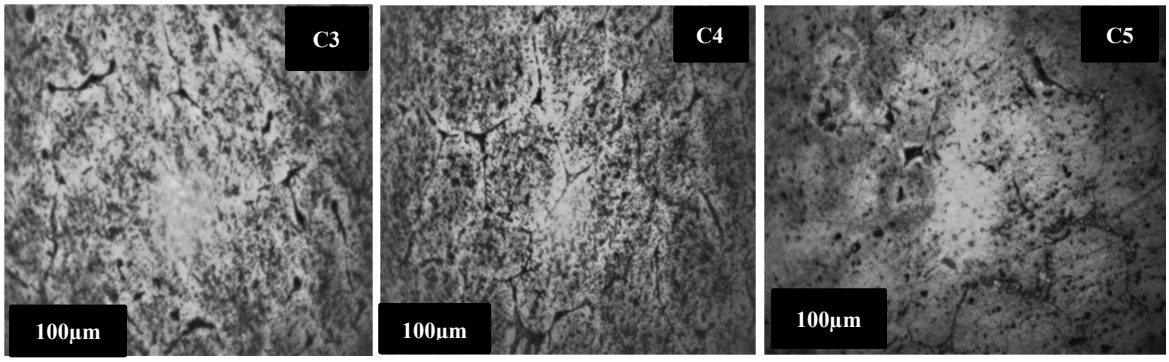

d) C3 Al2024 85% & BA 15% e) C4 Al2024 95% and SiO_2 5% f) C5 Al2024 90% & SiO_2 10%

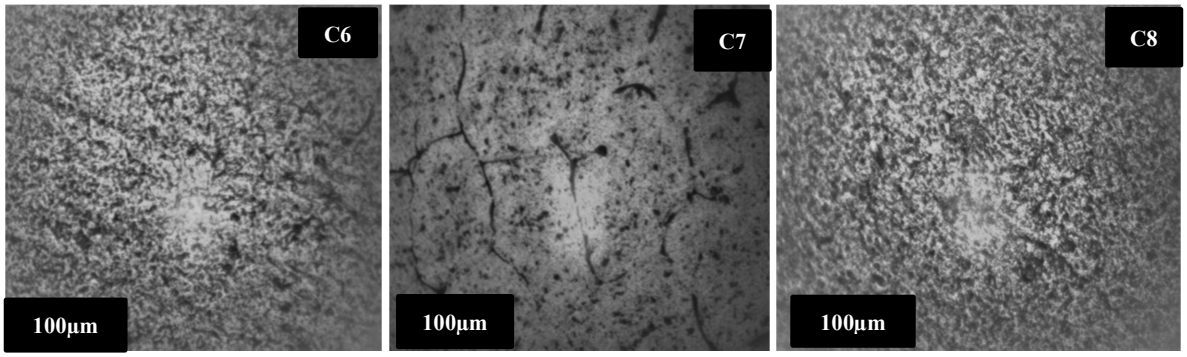

g) C6 Al2024 85% & SiO_2 15 h) C7 Al2024 85%, SiO_2 10% & BA 5% i) C8 Al2024 85%, SiO_2 5% & BA 10%

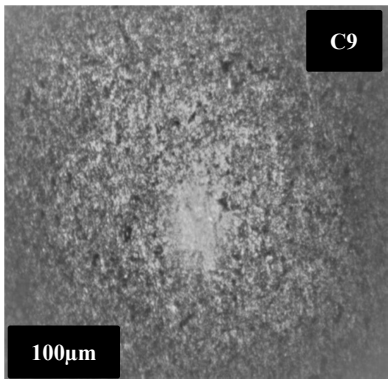

j) C9 Al2024 85%, SiO_2 10% & BA 10%

Figure 4.4: (a-j) optical microphage of heat-treated reinforced and unreinforced aluminum composite

4.1.2 The static structural analysis result

Stress is defined as the average force per unit area that some particle of a body exerts on an adjacent particle across an imaginary surface that separates them.

a) Equivalent (von- mises) stress (MPa)

The equivalent (Von Misses) stress values of all the Al2024 and reinforced matrix of FEA respectively look like in the following figures.

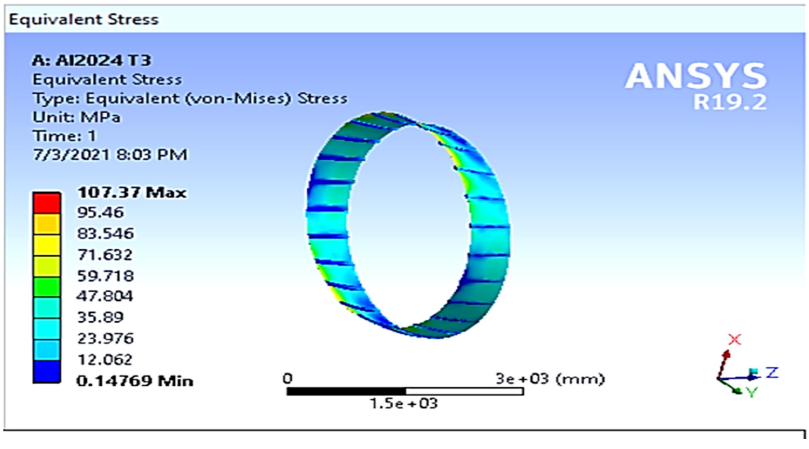

Figure 4.5: Equivalent (Von Mises) stress of Al2024 T3 at 20psi maximum allowable stress

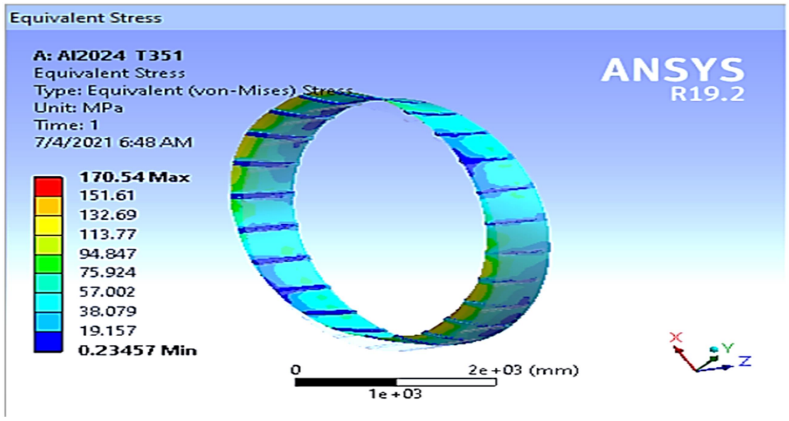

Figure 4.6: Equivalent (Von Mises) stress of Al2024 T351 at 27psi maximum allowable stress

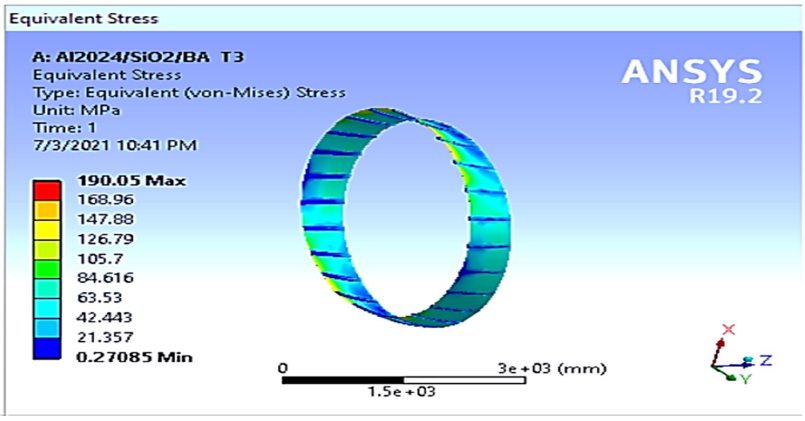

Figure 4.7: Equivalent (Von Mises) stress of reinforced metal matrix (Al2024/silica sand/bagasse ash) T3at 31psi for maximum allowable stress

As shown in figure 4.6- 4.8, the maximum von - Mises stress is 107.37 MPa for Al2024 T3, 170.5MPa for Al2024 T351 fuselage panel, and 190.05 MPa reinforced Aluminum composite fuselage. The minimum von – mises stress is 0.148MPa, 0.2346 & 0.271MPa for Al2024 T3/T351 fuselage panel and reinforced Aluminum composite fuselage panel, respectively. The result shows that the composite fuselage skin panel is rigid and safe according to the failure theory analysis, which means the working stress is far below the yield strength of the materials [77].

b) Deformation

The deformation values of both the Al2024 T3/T351 fuselage panel and reinforced Aluminum composite fuselage panel of FEA respectively looks like in the following figures (4.8 - 4.10)

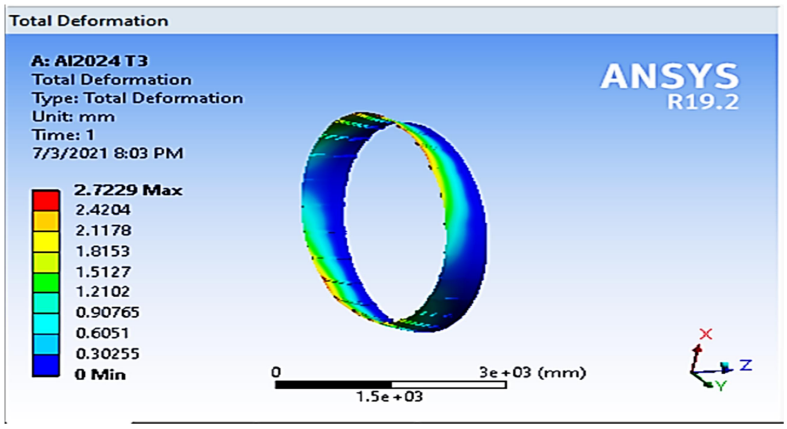

Figure 4.8: Deformation of Al2024 T3 at 17psi for maximum allowable stress.

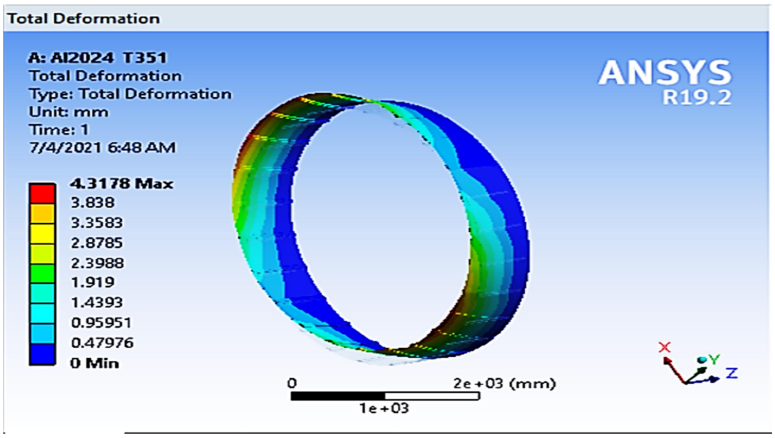

Figure 4.9: Deformation of Al2024 T351 at 27psi for maximum allowable stress.

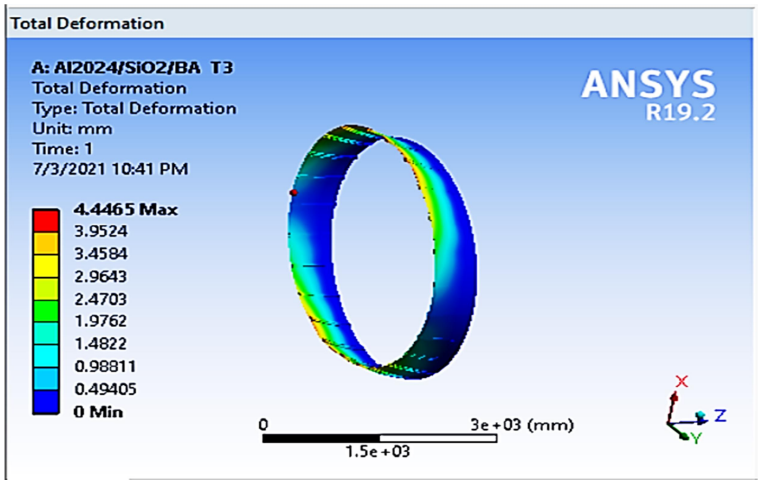

Figure 4.10: Deformation of reinforced Aluminum composite Al2024/silica sand/bagasse ash T3 at 31psi for maximum allowable stress.

Figure 4.8-10 shows that the total deformation is 2.7229mm, 4.317 for Al2024 T3/T351 fuselage skin panel, and 4.446mm reinforced Aluminum composite fuselage skin panel at their maximum allowable stress.

4.2 Discussions

4.2.1. Tensile test

The tensile properties evaluated from the tensile test are the UTS (σ), strain (ε), elongation, and Youngs' modulus. As a result, it shows, the tensile strength of the Al2024 primary alloy and the formed composites are increase linearly with the rise in SiO_2 10 Vf% and BA 5 Vf% particle content. The addition of reinforcement in matrix alloy generates a significant amount of disorder densities throughout solidification because of the thermal mismatch among matrix alloy and reinforcement particles. Hence, the SiO_2 & BA particles reinforcement could productively work as a barrier to dislocation movement. Therefore, it enhances the UTS, youngs modulus, and yield strength of the produced composites [78]. The best strength is obtained at Al2024/10 Vf. % SiO_2/ 5 Vf % BA AMCs by increasing from 320.22 MPa unreinforced alloy to 560 MPa reinforced material. As the silica volume fraction increased in the matrix, tensile strength shows a better mechanical performance [27,36]. Also, adding and increasing the volume fraction of bagasse ash in the matrix gives a good result in enhancing the tensile strength of the composite [79].

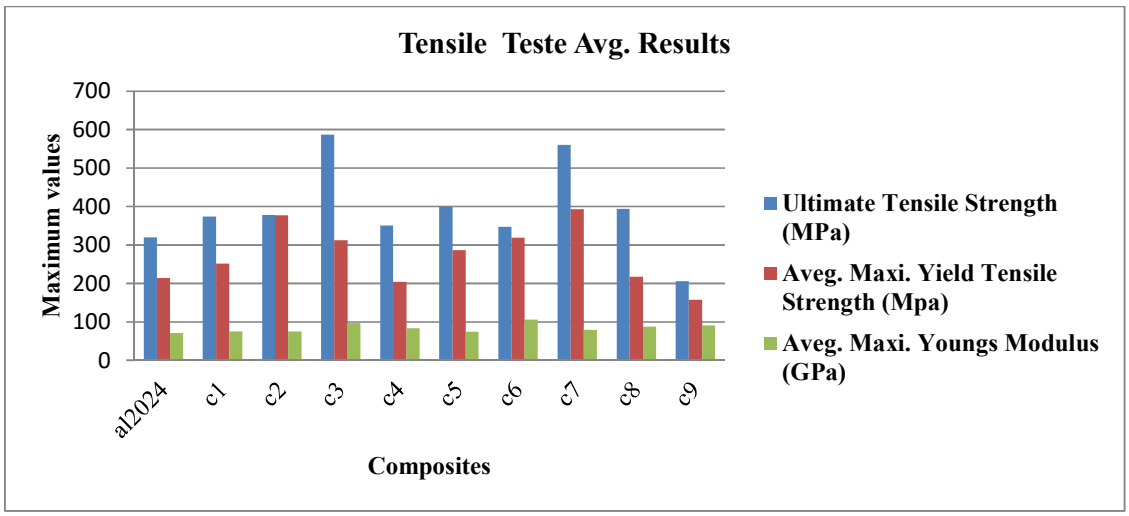

Figure 4.11: Tensile test specimen's ultimate tensile strength and young's modulus peak value.

Also, from the experimental, the ultimate tensile strength, yield strength, Young modulus were obtained from tensile test reports. The average UTS for all samples is 560 MPa and its young's modulus 78.894 GPa for Al2024/silica sand/bagasse ash composite.

$$E = \frac{\text{stress}}{\text{strain}} = \frac{\sigma}{\varepsilon} \quad \text{..... (4.4)}$$

Where: E – youngs modulus, σ - Tensile stress, ε – Tensile strain

For the selected application of this thesis, cast7 composition was determined. Then, with this Al2024/silica sand/bagasse, ash composite materials property finite element analysis for fuselage-skin panel application was investigated.

4.2.2. Hardness test

Figure 4.2: showed the peak values of hardness at the maximum and minimum values for all hardness test specimens. From average values of Hardness specimens, the maximum hardness value 74.36 (HRB) and the minimum value 59.26 (HRB), the output force is 100kg as the Rockwell hardness test indenter scale for soft and Aluminum type material. When the reinforcement is added to the matrix, it shows the hardness properties increasing except at the composition of BA 5%. In general, it is concluded that Al2024/SiO_2/BA composite material has a higher or improved mechanical properties hardness than the Al2024 unreinforced Alloy [78]. The hardness values increased with an increasing percentage of bagasse ash particle additions. This may be due to the presence of the hard ceramic phase of the bagasse ash in the ductile matrix [41,79].

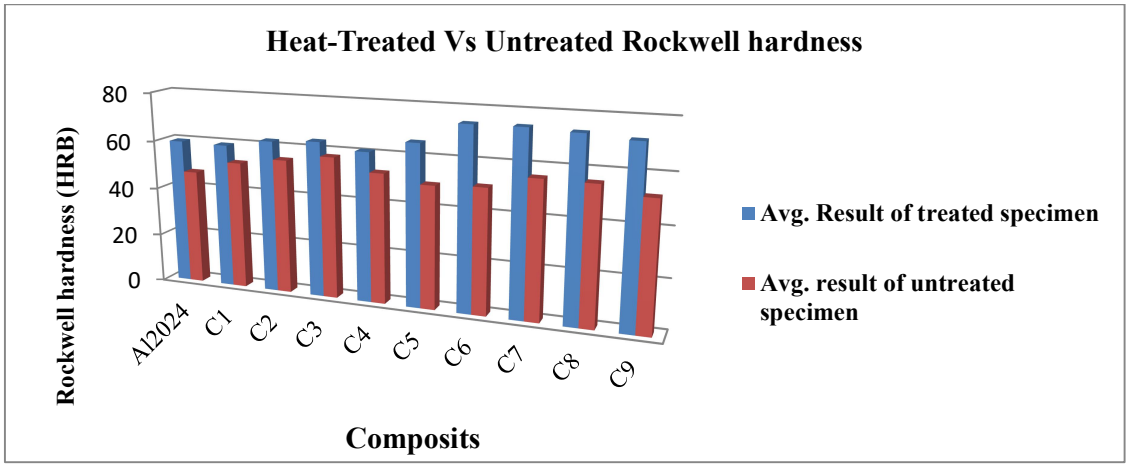

Figure 4.12: Hardness test specimen's peak value.

4.2.3 Flexural test

Figure 4.3: shows the highest flexural strength and maximum output force for all flexural test specimens. From the average values of flexural specimens, the maximum bending strength value is 482 MPa in the transverse direction, and the maximum output force is 28 kN. As it shows the addition of volume fraction ratio in the matrix increases the material resistance to bending load, in this experiment, the composition of silica at 5%, 10% also silica 5%+ bagasse 10%, silica 10% +bagasse 10% revealed the bending resistance of a material is reduced. It may be due to the weight of ceramic particles in the matrix. Here is also the best result recorded at the cast7 composition chosen for the fuselage skin analysis investigation.

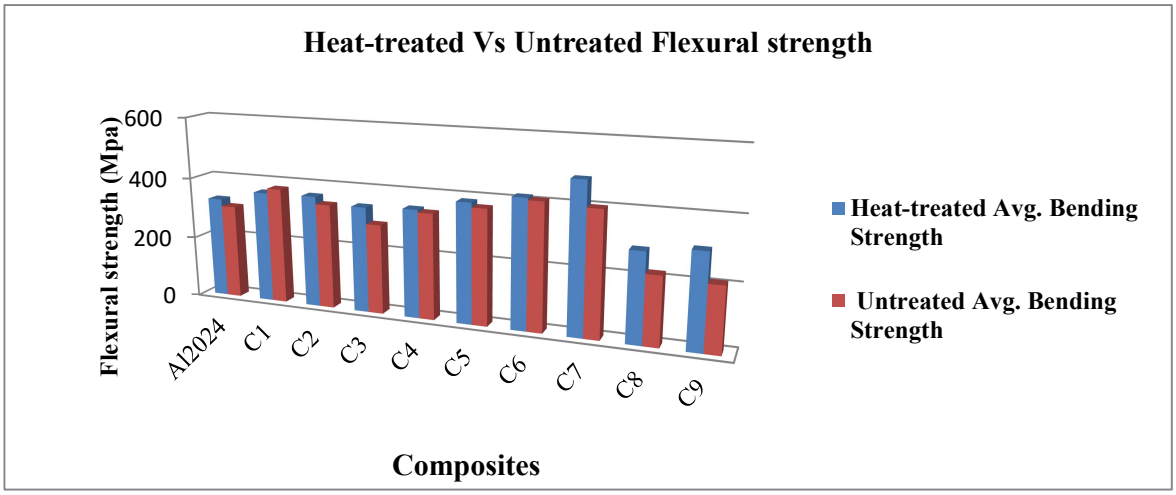

Figure 4.13: Flexural strength test specimen's peak value.

4.2.4. Micro-Structural Analysis

Optical microphage for aluminum composite reinforced with silica sand and bagasse ash represent in the fig (4.4). It shows the reinforcing particles are visible and uniformly distributed as particulate in the aluminum matrices. It also shows there is a high volume of particulate spread in the matrices. Most of the microphage result shows a good dispersion of particulate in the aluminum matrices in all composition of composite. This result shows the best result achieved in the stir casting method for particulates to get a great uniform distribution in the matrices. The optical microphage investigation showed a reasonably uniform distribution of BA and SiO_2 particles and a small macro-segregation of particles in certain spaces. The dispersion of BA and SiO_2 particles is influenced by the better wettability of the BA and SiO_2 by the molten metal and great interfacial attachment among BA and SiO_2 particles and the metal matrix material fig. 4.4 [22,80].

During the casting, it is observed that of the composites, increasing the vol. %. BA and SiO_2 particles above 10-vol%, the fluidity of the mixture became thick and the flow of the molten matrix composite reduced. The microstructure shows small breaks and a reasonably identical BA and SiO_2 particles dispersion in the metal matrix. The silica and Bagasse ash (ceramic) phase was revealed as dark points (fig.4.4, (b-j)). Although, the metal alloy phase is white fig 4.4 (a).

The microstructure of the MMCs displays a uniform dispersion of BA & SiO_2 in the matrix with some breaks as the vol.% additions of the reinforcement is raised beyond 10 vol% faction ratio figure 4.4 (c, d, f, g, i & j) [78].

In the composites investigation, no effects of unwanted occurrences were observed, which often form the structures of cast composites, such as the residue of fluid out of the reinforcing phase, also the growth of particle agglomerates or gas bubbles formation. This revealed that there is good interfacial bonding among the BA & SiO_2 particles and matrix; this good interfacial bonding may occur due to the Mg in the matrix, which helps in improving the wettability of the ceramic phase in the metal matrix

figure (e, f & h) [22]. Aluminum alloy-based SiO2 & BA mixtures. It must be well-known that the existence of the ceramic particles in the metal matrix alloy outcomes in much smaller grain size in the cast composites compared to the matrix alloy as we can see in figure (a) and the rest of composites grain structure.

The density of BA & SiO_2 was 1.77 g/cm3 and 2.197 g/cm3, respectively. The overall density of BA & SiO_2 particle reinforced composites reduced with vol.fraction ratio additions of particles. Composite density reduced with rising vol% additions of reinforcement particles.

Hardness values improved with an addition vol.fraction of reinforcement. This is due to the hard ceramic phase of the SiO_2 & BA in the ductile matrix figure 4.4 (g, i & j) as the hardness property of composite shows adding reinforcement particles in the matrix can raise the strain energy in the boundary of the particles in the medium. And tendencies may occur by forming the disorder at the boundary of ceramic reinforcing particles by a change in the thermal expansion coefficient among matrix & ceramic reinforcing particles [31]. The dislocations produced rising in hardness and residual stress in the mixtures. It is understood if there is a greater quantity of the ceramic reinforcing particles in the medium, the greater density of dislocation; as a result, the greater the hardness in the composite [41].

The ultimate tensile strength and yield increased with increasing vol. fraction ratio of reinforcement particles additions up to maximum values of 377.1 N/mm2 yield strength at 10%vf BA addition & the maximum ultimate strength is obtained 586.9 at BA 15%vf addition [41]. It reduced at the other components of vol. fraction ratio figure 4.4 (a-j). The maximum values for both yield strength and ultimate tensile obtained in cast seven composites composition (10% silica sand/ 5% bagasse ash). As compared to the decreased value of these properties of cast 8 (10% BA + 5% SiO_2) & cast 9 and (10% BA + 10% SiO_2) [78].

Reinforcement addition is attributed to the uniform distribution of the particles at 10%silica sand and 5% bagasse ash in the microstructure figure 4.4 (h). Related to the microstructure of composite with 10% BA + 5% SiO_2 and 10% BA + 10% SiO_2 addition, figure 4.4 (I & j).

The results indicate that Al2024/10% silica sand/5% bagasse ash particle samples have 43% and 45.4% rises in ultimate tensile strength and yield than that of unreinforced Al2024 alloy, respectively [78]. The percent elongation was reduced with the increase in volume fraction of silica sand and bagasse ash, figure 4.4 (h).

Validating the results with other works

As a conclusion of the discussion, several types of research made on ceramic particle reinforced aluminum alloys as related to my result are here in the figure: 4.14.

- The SiO_2 UTS aluminum alloy, LM25 matrix and fused silica-SiO_2 particulates as the reinforcement (size 150-250μm) in the matrix compared. The reinforcement added ranges from 4 to 12wt% in steps of 4% [27].

- The effect of Bagasse ash (BAp) particle reinforcement on the wear behaviour of Al-Cu-Mg alloy has been studied. Bagasse ash particles were varied from 0 wt. pct-10 wt. pct. with an interval of 2 wt. pct. [34].

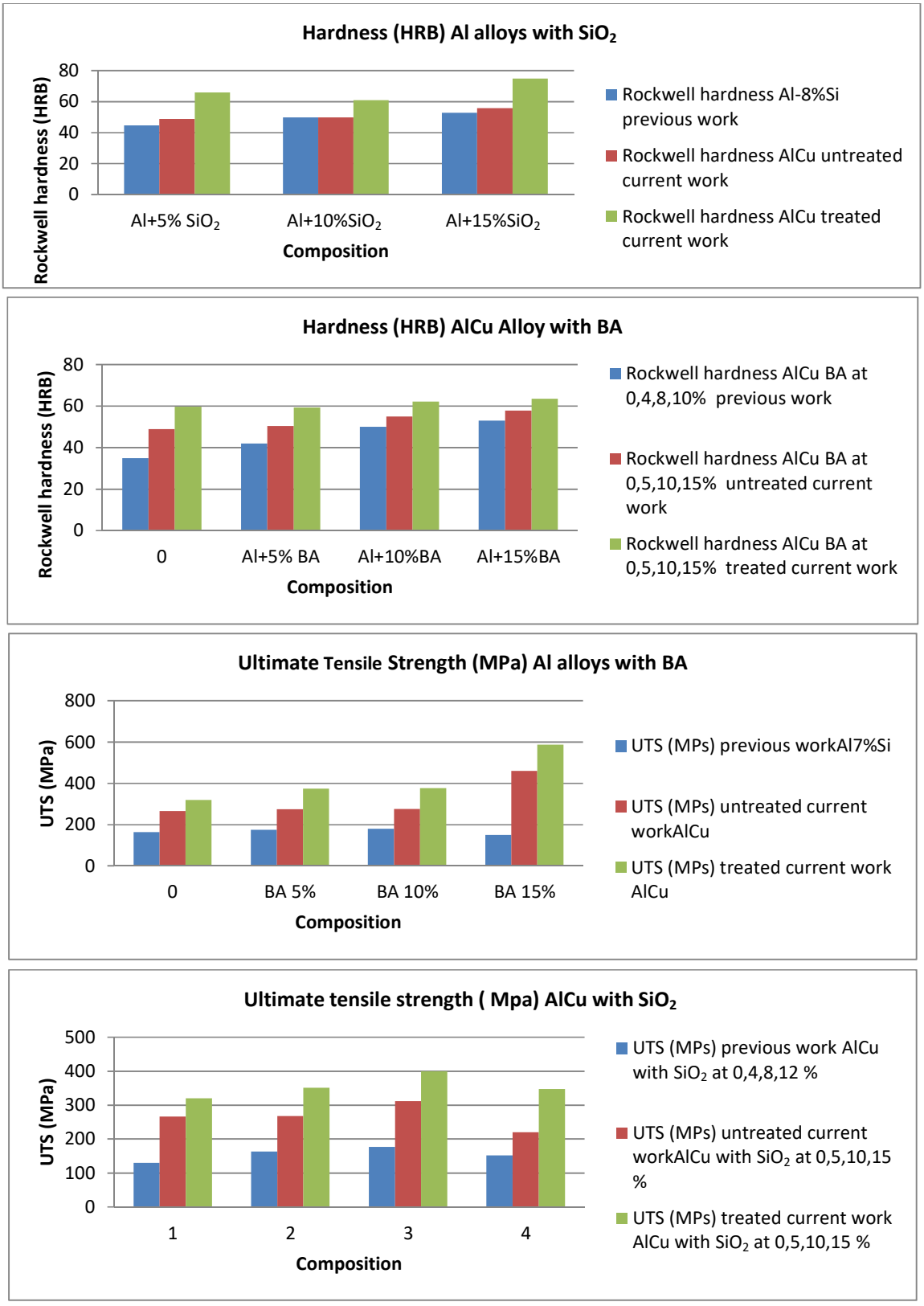

Figure 4.14: Relative work comparison [81] [27] [35][33]

4.2.5 Numerical analysis discussion

This section of the paper specifies the result obtained from the ANSYS software carried out by making everything the same for both Al2024 T3/T351 and the reinforced composite, except material properties; i.e. at the same loading type and the same specimen dimension boundary condition and the same method of finite element analysis. The FEA result shows different stress types and deformation due to the applied load on the application. Three different materials for fuselage skin panel, namely Al2024 T3/T351 and Al2024/silica sand/bagasse ash composite for fuselage skin panel, compared each other as next shown.

Table 4.1 Static analysis result in summary

Applied load in N	Aluminum 2024 alloy - T3		Al2024 T351		Al2024/SiO2/BA T3	
	Maximum stress (MPa)	Maximum deformation (mm)	Maximum stress (MPa)	Maximum deformation (mm)	Maximum stress (MPa)	Maximum deformation (mm)
89,646.24	31.568	0.8	31.568	0.799	30.64	0.7169
179,292.42	63.136	1.601	63.136	1.598	61.28	1.4338
268,938.63	94.704	2.402	94.704	2.397	91.92	2.1506
304,921.58	107.37	2.7229	107.37	2.7186	104.22	2.438
358,584.84			126.27	3.197	122.56	2.867
484,287.15			170.54	4.3178	163.53	3.87
502,223.78			176.85	4.4777	171.66	4.016
537,877.25					183.84	4.3
556033.472					190.05	4.446

The Table 4.1 shows the three material performances of resisting the applied load until it reached their yield tensile strength. It shows that the heat-treated ceramic particle reinforced Al-2024 has a better performance of tensile strength over the unreinforced heat-treated aluminum alloys.

The persuaded Von-Mises stress in the material must be lower than the allowable stress to design fuselage structural components such as skin, frame, stringers, and bulkhead against the loading and internal pressurization and buckling failure. Therefore, failure load under pressurization condition for skin panel found to be greater than 17psi 304KN for Al2024 T3 alloy, 27psi 484KN Al2024 T351, and 31psi or 556KN for Al2024/SiO_2/BA T3 composite.

As shown from table 4.1, the static analysis result using ANSYS 19.2 Workbench software shows the value of allowable stress with different pressurization loads. As a result, the maximum von - mises stress and deformation is at 304KN load 107.37MPa and 2.7(mm), respectively. If a more significant load is applied to it, it will fail and create considerable damage to materials and lives.

In the newly designed isotropic metal-ceramic composite, as shown in table 4.1, the maximum von misses stress and deformation is at 556KN load 190.05MPa and 4.4mm, respectively. As is seen here, the unreinforced Al2024 T3 & Al2024 T351 tensile yield strength has the lowest value allowable stress

for the applied load on the fuselage skin panel. It fails at more than 304KN & 502KN compared with the reinforced Al2024/silica sand/Bagasse ash composite. The new composite load resistance is more than 43.5 % & 10.3% than the Al2024 T3 and Al2024 T351 alloys, respectively.

Depending on static analysis results, the equivalent (Von-Mises) stress of the new ceramic reinforced aluminum composite material fuselage-skin panel is the yield strength has excellent resistance to one compared to that of the unreinforced aluminum metal alloy. In addition, the maximum displacements of the Al2024/silica sand/bagasse ash composite material fuselage-skin panel have the lowest deformation value compare with that of the unreinforced alloys under the same FEA. This indicates that the new composite material fuselage-skin panel has less stress, less density, and better performance.

4.2.5.1 Graphical comparison for load failure of Al2024 alloys & the new composite

Load Versus Von- Misses Stress

The comparison of Load versus von-misses stress of Al2024 T3/T351 and Al2024/silica sand/bagasse ash composite fuselage stiffened panel graph is clearly illustrated in figure 4.15. Load showed on the chart at the x-axis. Whereas: - the stress for Al2024/ and composite material is taken on the y-axis. Observation of the graph indicates the different stress levels of two other materials at a given loading condition; this implies that the unreinforced Al2024 alloy is highly stressed than that of the Al2024/silica sand/bagasse ash composite fuselage-skin material. In addition, due to the less al2024 yield strength, it fails before the reinforced one.

Table 4.2: finite element maximum (von-mises) stress result

Applied load (KN)	(Von-Mises) stress Maximum stress (MPa)		
	Al2024 T3	Al2024 T351	Al2024/SiO_2/BA T3
89KN	31.568	31.568	30.64
179KN	63.136	63.136	61.28
268KN	94.704	94.704	91.92
304KN	107.37	107.37	104.22
358KN		126.27	122.56
484KN		170.54	163.53
502KN		176.85	171.66
537KN			183.84
556KN			190.05

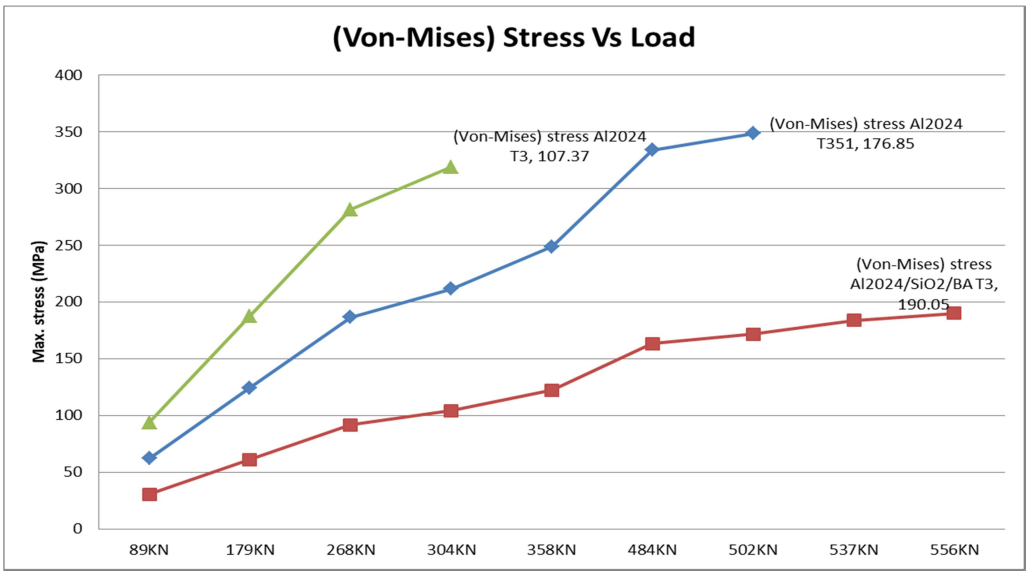

Figure 4.15: Comparison Load versus Von-mises stress of Al2024 T3/T351 & Al2024/SiO_2/BA T3

Load versus Total Deformation

The comparison load versus deformation of Al2024 and the new composite fuselage skin panel is shown in figure 4.16. It shows that the deformation in unreinforced aluminum-alloy fuselage skin panel is higher than the new reinforced composite fuselage skin for the given loading conditions.

Table 4.3: finite element maximum deformation result

Applied load in N	Max. Deformation of materials		
	Al2024 T3 (mm)	Al2024 T351 (mm)	Al2024/SiO_2/BA T3 (mm)
89KN	0.8	0.799	0.7169
179KN	1.601	1.598	1.4338
268KN	2.402	2.397	2.1506
304KN	2.7229	2.7186	2.438
358KN		3.197	2.867
484KN		4.3178	3.87
502KN		4.4777	4.016
537KN			4.3
556KN			4.446

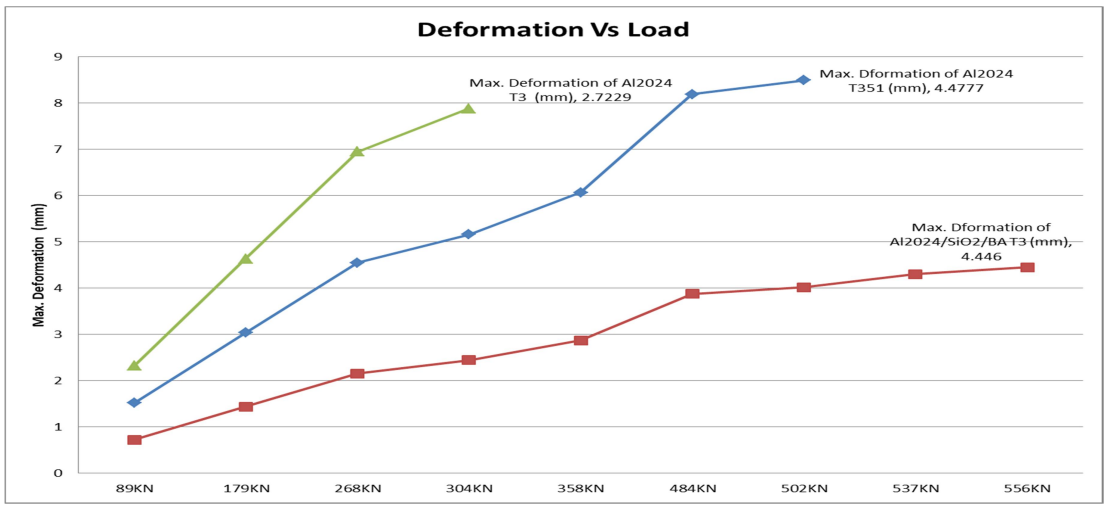

Figure 4.16: Comparison Load Versus Deformation of Al2024 T3/T351 and Al2024/silica sand/bagasse ash T3 fuselage-skin panel

Comparison of weights

As the finite element analysis, the mass of Al2024 T3 & T351 is 103.74(Kg), 108.42(Kg), and the new reinforced aluminum composite masse is 99.838(Kg). This comparison of the bar chart shows that the weight reduction in the fuselage skin panel is observed. This implies that the new Al2024/Silica Sand/ Bagasse ash composite material is lightweight than those of the unreinforced aluminum fuselage skin panel by 3.9% from Al2024 T3 & 7.9% Al2024 T351 weight reduction.

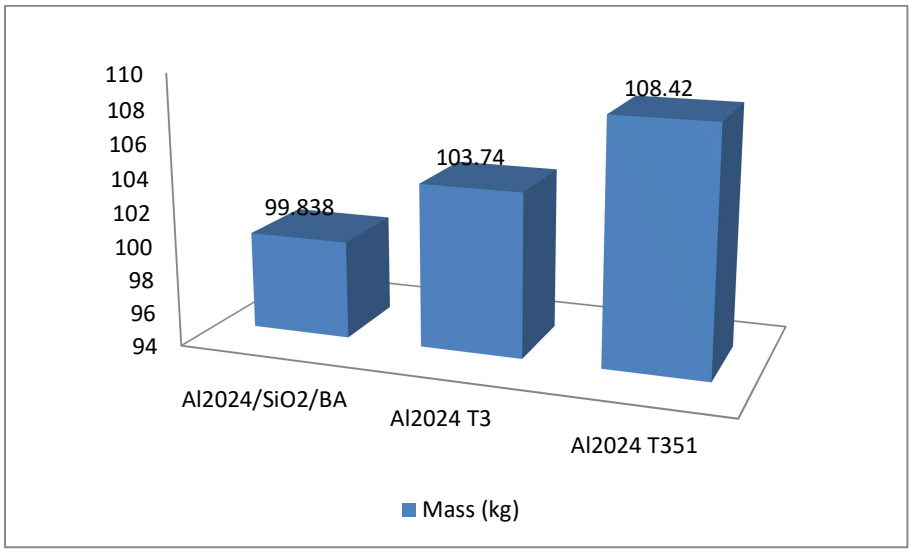

Figure 4.17: Comparison of weights

CHAPTER FIVE

5. Conclusion, Recommendation, and Future Work

5.1 Conclusion

The main objective of this thesis is to improve Al2024 mechanical properties by reinforcing with the hard ceramic particle silica sand and the agro-waste bagasse ash. The selected application area of the Al2024 is aircraft fuselage-skin panel as the alloy currently and mainly uses as aerospace application. The analysis was accomplished by using experimental and finite element analysis.

The Al2024/Silica-sand/Bagasse ash was manufactured by the stir casting method with a different composition ratio and investigated the tensile, bending, and hardness of its mechanical performance and the characterization optical microscope test performed. Then, as a result, obtained from the performed tests, the composition of Al2024/with the volume ratio of 10vf silica sand and 5vf bagasse ash gave better results than the other compositions by its hardness flexural strength performance. Based on the experimental results, the composite was selected for the application of fuselage structural part.

The Al2024 and the reinforced composite 3D modelling performed with SOLIDWORK 2017 and the mechanical property analysis of the material result analyzed. In addition, a comparative study has been made concerning stresses and deformation between Al2024 T3/T351 and composite fuselage panel structure. As general, the effect of the addition of SiO_2 & BA particles and temper-T3 condition on mechanical properties of Al2024 alloy is investigated. Based on the results, the following conclusions are drawn.

The addition of SiO_2 and BA particles reduces the density of the matrix. The composite density was less than before to a maximum of 3.39 % compared to the base aluminum alloy. It observed that density reduction as compared to unreinforced Alloy.

The significant improvement in the tensile performance of the material was obtained with the combination of Al2024 and BA particles at 15%Vf BA content. And maximum yield strength was obtained at 10%Vf BA. Hardness values were found to increase with the reinforcement addition and heat-treating. The Al-2024 alloy reinforced with 10%Vf SiO_2 and 5%Vf BA shows a significant improvement in the hardness, tensile and flexural strength compared to other composition percentages. The addition of SiO_2 and BA particles increases the hardness property of the matrix alloy by about 25.4%.

Moreover, increase its performance by increasing tensile strength 560 MPa, increasing flexural strength 482 MPa, and increasing hardness from 59.6 to 74. Also, in the structural analysis of aircraft fuselage-skin panels, when the safety factor is two, it reduces stress. On von Mises stress, the maximum allowable yield strength stress is 190.05MPa and maximum deformation 4.4mm recorded for the Al2024/SiO_2/BA composite. In addition, the maximum permissible stress was 107.37 MPa, 170.54 the-

maximum deformation 2.72 & 4.48 mm for unreinforced Al-Cu-Mg T3/T351, respectively. Hence this combination can be used for lightweight & high-strength applications[82].

As a result, composite Al2024/SiO_2/Bagasse ash composite aircraft fuselage-skin panel has high-stress resistance than the Al2024 T3/T351 alloys with similar dimensions and load capacity. It also shows the composite material has better resistance for the high amount of applied load as a structural material. Generally, using ceramic particles and agro-west ash could improve the current aerospace materials property instead of changing them; it is better to keep them with their un-replaceable character by other materials.

5.2. Recommendations

Other tests such as wear test, corrosion resistance test, fatigue test, thermal and electrical conductivity test, etc., must conduct to characterize the composites fully. The interest in a material with lightweight and high performance is increasing unexpectedly from time to time. Therefore the properties of composite materials, like high strength to weight ratio and high specific stiffness, are attractive for the construction of lightweight, fuel-efficient, and environmentally, economically safe aerospace and automotive components. The finite element analysis result shows that the heat-treated Al2024/SiO_2/BA composite fuselage-skin panel has much better performance than the Al2024 T3 alloys. Moreover, the tensile, bending, hardness strength and density reduction are the highest results of the Al2024/SiO_2/Bagasse ash T3 composite fuselage structure.

5.3 Future Work

As future work, many works could be considered because of the new Al2024/SiO_2/BA. Composite shows a better result and creates good motivations to work on other industrial and agro-waste as a raw material for high industrial applications. In this investigation, better mechanical properties were achieved, such as density reduction, stress resistance, high strength, and increased hardness. The Al2024/SiO_2/BA composite material can be used for a different application area based on its material property; such application areas would be an automotive application with a necessary inspection and more investigation. Based on this perception, Al2024/SiO_2/BA composite material aircraft and automotive products can be made and developed in the future, which this study could not address.

- Investigate other mechanical tests to improve the material performance in all aspects of fuselage parts.
- Investigate the effect of heat treatment on aluminum ceramic composite for fuselage structural parts.
- Based on the material mechanical property, it could implement on more automotive parts like a brake disc.

Reference

[1] C. Wu, K. Ma, J. Wu, P. Fang, G. Luo, and F. Chen, "Materials Science & Engineering A In fl uence of particle size and spatial distribution of B 4 C reinforcement on the microstructure and mechanical behavior of precipitation strengthened Al alloy matrix composites," *Mater. Sci. Eng. A*, vol. 675, pp. 421–430, 2016, doi: 10.1016/j.msea.2016.08.062.

[2] S. Nudvi and B. S. Motgi, "Study on Mechanical Properties of Al6063 Reinforced with Sic & Tur Husk," *IRJET.*, vol. 7, no. 09, pp. 1534–1539, 2020.

[3] Onyechi P. C., Asiegbu K., Igwegbe C. A., and Nwosu M. C., "Effect of volume fraction on the mechanical properties of Periwinkle Shell Reinforced Polyester Composite (PRPC) ," *Am. J. Mech. Eng. Autom.*, vol. 2, no. 1, pp. 1–15, 2015.

[4] M. Nagaral, V. Bharath, and V. Auradi, "Effect of Al 2 O 3 Particles on Mechanical and Wear Properties of 6061al Alloy Metal Matrix Composites," *J Material Sci Eng.,* vol. 2, no. 1, pp. 2–5, 2013, doi: 10.4172/2169-0022.1000120.

[5] M. Imran, A. R. A. Khan, S. Megeri, and S. Sadik, "Study of hardness and tensile strength of Aluminium-7075 percentage varying reinforced with graphite and bagasse-ash composites," *Resour. Technol.*, vol. 2, no. 2, pp. 81–88, 2016, doi: 10.1016/j.reffit.2016.06.007.

[6] I. M. Astika, "Hardness improvement of aluminum alloy 2024 t3 after artificial aging treatment," *IOP Conf. Ser. Mater. Sci. Eng.*, vol. 539, no. 1, 2019, doi: 10.1088/1757-899X/539/1/012004.

[7] K. Ravi Kumar, T. Pridhar, and V. S. Sree Balaji, "Mechanical properties and characterization of zirconium oxide (ZrO2) and coconut shell ash(CSA) reinforced aluminium (Al 6082) matrix hybrid composite," *J. Alloys Compd.*, vol. 765, pp. 171–179, 2018, doi: 10.1016/j.jallcom.2018.06.177.

[8] H. S. Kumaraswamy, V. Bharat, and T. Krishna Rao, "Influence of Mechanical &tribological BehaviourOf Al 2024 MMC Fabricated by Stir Casting Technique-A Review," *Mater. Today Proc.*, vol. 5, no. 5, pp. 11962–11970, 2018, doi: 10.1016/j.matpr.2018.02.170.

[9] O. Bacarreza, M. H. Aliabadi, and A. Apicella, "Robust design and optimization of composite stiffened panels in post-buckling," *Struct. Multidiscip. Optim.*, vol. 51, no. 2, pp.

409–422, 2015, doi: 10.1007/s00158-014-1136-5.

[10] S. Yadav, "Design and Static Structural Analysis of Aircraft Floor Beam," *GRD Journals- Glob. Res. Dev. J. Eng.*, vol. 04, no. 08, pp. 7–10, 2019.

[11] A. T. Submitted, I. N. Partial, F. Of, R. For, and T. H. E. Degree, "Metal Matrix Composite

Production and Characterisation of Aluminium-Fly Ash Composite Using Stir Casting Method Production and Characterisation of Aluminium-Fly Ash Composite Using Stir Casting Method," *Mater. Eng.*, no. 10404002, pp. 1–57, 2008.

[12] B. Rebba and N. Ramanaiah, "Evaluation of Mechanical Properties of Aluminium Alloy (Al-2024) Reinforced with Molybdenum Disulphide (MOS 2) Metal Matrix Composites," *Procedia Mater. Sci.*, vol. 6, no. Icmpc, pp. 1161–1169, 2014, doi: 10.1016/j.mspro.2014.07.189.

[13] R. P. M, R. Saravanan, and M. Nagaral, "Fabrication and Wear Behavior of Particulate Reinforced Metal Matrix Composites-An Overview," *IOSR-JMCE*., vol. 14, no. 1, pp. 10–20, 2017, doi: 10.9790/1684-1401041020.

[14] S. Madhusudan, M. M. M. Sarcar, and N. B. R. M. Rao, "Mechanical properties of Aluminum-Copper(p) composite metallic materials," *J. Appl. Res. Technol.*, vol. 14, no. 5, pp. 293–299, 2016, doi: 10.1016/j.jart.2016.05.009.

[15] Surappa M.K., "Aluminium Matrix Composites: Challenges and Opportunities // Sadhana. Department of Metallurgy, Indian Institute of Science, Bangalore 560 012, India," vol. 28, no. 1–2, pp. 319–334, 2003.

[16] V. V. K. Lakshmi, K. V. Subbaiah, B. S. Babu, B. N. Chakravarthy, and S. Kaundinya, "Effect of hydrated mg-al-silicate ceramic particle on microstructure and compressive properties of Al6063 MMC," *Mater. Today Proc.*, vol. 5, no. 9, pp. 19424–19430, 2018, doi: 10.1016/j.matpr.2018.06.303.

[17] N. Saba, M. Jawaid, and M. T. H. Sultan " An Overview of Mechanical and Physical Testing of Composite Materials*"*. *Mechanical & Physical Testing of Biocomposites, Fibre-Reinforced Composites & Hybrid Composites*., vol. 08, no. 4. pp. 1-12, doi.org/10.1016/B978-0-08-102292-4.00001-1, 2018.

[18] M. Sambathkumar, P. Navaneethakrishnan, K. Ponappa, and K. S. K. Sasikumar, "Mechanical and Corrosion Behavior of Al7075 (Hybrid) Metal Matrix Composites by Two Step Stir Casting Process," *Lat. Am. J. Solids Struct.*, vol. 14, no. 2, pp. 243–255, 2017, doi:

10.1590/1679-78253132.

[19] P. M. Composite, C. M. Composites, and M. Composites, "Composite Materials," *Technologies* , vol. 37, no. 4. doi:10.3390/technologies4040037, 2016.

[20] H. Kala, K. K. S. Mer, and S. Kumar, "A Review on Mechanical and Tribological Behaviors of Stir Cast Aluminum Matrix Composites.," *Procedia Mater. Sci.*, vol. 6, no. Icmpc, pp. 1951–

1960, 2014, doi: 10.1016/j.mspro.2014.07.229.

[21] Deepak C Patil, "Mechanical Property Evaluation of an Al-2024 Alloy Subjected to HPT Processing," *Mater. Sci. Eng*., pp. 63 012085, 2014, doi: 10.1088/1757-899X/63/1/012085 IOP 6th Conf. Ser.:

[22] U. G. Scholar, "CHARACTERIZATION OF CERAMIC PARTICLE REINFORCED ALUMINIUM METAL MATRIX COMPOSITES – A CRITICAL REVIEW," IJMET., vol. 10, no. 11, pp. 168–176, 2019.

[23] K. Omar Cooke, "Introductory Chapter: Structural Aluminum Alloys and Composites," *Alum. Alloy. Compos.*, pp. 1–20, 2020, doi: 10.5772/intechopen.90569.

[24] T. Satish Kumar, S. Shalini, K. K. Kumar, R. Thavamani, and R. Subramanian, "Bagasse Ash Reinforced A356 Alloy Composite: Synthesis and Characterization," *Mater. Today Proc.*, vol. 5, no. 2, pp. 7123–7130, 2018, doi: 10.1016/j.matpr.2017.11.377.

[25] P. D. Srivyas and M. S. Charoo, "Role of Reinforcements on the Mechanical and Tribological Behavior of Aluminum Metal Matrix Composites - A Review," *Mater. Today Proc.*, vol. 5, no. 9, pp. 20041–20053, 2018, doi: 10.1016/j.matpr.2018.06.371.

[26] C. U. Atuanya and V. S. Aigbodion, "Evaluation of Al-Cu-Mg alloy/bean pod ash nanoparticles synthesis by double layer feeding-stir casting method," *J. Alloys Compd.*, vol. 601, pp. 251–259, 2014, doi: 10.1016/j.jallcom.2014.02.086.

[27] S. Thirumalvalavan and N. Senthilkumar, "Evaluation of mechanical properties of aluminium alloy (Lm25) reinforced with fused silica metal matrix composite," *Indian J. Eng. Mater. Sci.*, vol. 26, no. 1, pp. 59–66, 2019.

[28] M. O. Bodunrin, O. P. Oladijo, O. O. Daramola, K. K. Alaneme, and N. B. Maledi, "Porosity measurement and wear performance of aluminium hybrid composites reinforced with silica sand and bamboo leaf ash," *Ann. Fac. Eng. Hunedoara*, vol. 14, no. 1, p. 231, 2016.

[29] P. P. Kulkarni, B. Siddeswarappa, and K. S. H. Kumar, "A Survey on Effect of Agro Waste Ash as Reinforcement on Aluminium Base Metal Matrix Composites," *Open J. Compos. Mater.*, vol. 09, no. 03, pp. 312–326, 2019, doi: 10.4236/ojcm.2019.93019.

[30] V. S. Aigbodion, S. B. Hassan, and J. E. Oghenevweta, "Microstructural analysis and properties of Al-Cu-Mg/bagasse ash particulate composites," *J. Alloys Compd.*, vol. 497, no. 1–2, pp. 188–194, 2010, doi: 10.1016/j.jallcom.2010.02.190.

[31] V. Dardare and S. G. Kulkarni, "Effect of bagasse ash reinforcement on Al356 matrix composite manufactured by two stage stir casting process," *Int. J. Curr. Eng. Technol.*, vol. 8, no. 04, pp. 911–915, 2018, doi: 10.14741/ijcet/v.8.4.3.

[32] K. P. Gowda, J. N. Prakash, S. Gowda, and B. S. Babu, "Effect of Particulate Reinforcement on the Mechanical Properties of Al2024-WC MMCs," *J. Miner. Mater. Charact. Eng.*, vol. 03, no. 06, pp. 469–476, 2015, doi: 10.4236/jmmce.2015.36049.

[33] V. S. Aigbodion, S. B. Hassan, T. Ause, and G. B. Nyior, "Potential Utilization of Solid Waste (Bagasse Ash)," *Jornal of Minerals & Materials Characterization & Engineering*., vol. 9, no. 1, pp. 67–77, 2010.

[34] V. S. Aigbodion, S. B. Hassan, G. B. Nyior, and T. Ause, "Effect of Bagasse ash reinforcement on the wear behaviour of Al-Cu-Mg/Bagasse ash particulate composites," *Acta Metall. Sin. (English Lett.*, vol. 23, no. 2, pp. 81–89, 2010, doi: 10.11890/1006-7191-102-81.

[35] A. M. Usman, A. Raji, N. H. Waziri, and M. A. Hassan, "Production and Characterisation of Aluminium Alloy - Bagasse Ash Composites," *IOSR J. Mech. Civ. Eng.*, vol. 11, no. 4, pp. 38–44, 2014, doi: 10.9790/1684-11433844.

[36] R. Raja, S. Jannet, and M. A. Thampy, "Synthesis and characterization of AA5083 and AA2024 reinforced with SiO2 particles," *Bull. Polish Acad. Sci. Tech. Sci.*, vol. 66, no. 2, pp. 127–132, 2018, doi: 10.24425/119066.

[37] A. Chaubey, P. Konda Gokuldoss, Z. Wang, S. Scudino, N. Mukhopadhyay, and J. Eckert, "Effect of Particle Size on Microstructure and Mechanical Properties of Al-Based Composite Reinforced with 10 Vol.% Mechanically Alloyed Mg-7.4%Al Particles," *Technologies*, vol. 4, no. 4, p. 37, 2016, doi: 10.3390/technologies4040037.

[38] V. K. Varma, S. V. Kamat, Y. R. Mahajan, and V. V. Kutumbarao, "Effect of reinforcement size on low strain yielding behaviour in Al-Cu-Mg/SiCp composites," *Mater. Sci. Eng. A*, vol. 318, no. 1–2, pp. 57–64, 2001, doi: 10.1016/S0921-5093(01)01337-5.

[39] B. Bakthavatchalam, K. Habib, N. Patil, and O. A. Hussein, "Microstructural analysis of Al6063/sic with calcium additives for hardness enhancement," *MATEC Web Conf.*, vol. 225, pp. 1–6, 2018, doi: 10.1051/matecconf/201822503007.

[40] K. K. . M. and A. C. Ravindra Mamgain, Alakesh Manna, "Effect of volume fraction (Al2O3) on tensile strength of Aluminium 6061 by varying stir casting furnace parameters: A Review," *Int. J. Sci. Eng. Res.*, vol. 6, no. 5, pp. 189–198, 2015.

[41] T. Satish Kumar, S. Shalini, K. K. Kumar, R. Thavamani, and R. Subramanian, "Bagasse Ash Reinforced A356 Alloy Composite: Synthesis and Characterization," *Mater. Today Proc.*, vol. 5, no. 2, pp. 7123–7130, 2018, doi: 10.1016/j.matpr.2017.11.377.

[42] V. Mohanavel, K. Rajan, S. Suresh Kumar, A. Chockalingam, A. Roy, and T. Adithiyaa, "Mechanical and tribological characterization of stir-cast Al-SiCpcomposites," *Mater. Today Proc.*, vol. 5, no. 1, pp. 1740–1746, 2018, doi: 10.1016/j.matpr.2017.11.271.

[43] K. Almadhoni, S. Khan, and P. D. Student, "Review of Effective Parameters of Stir Casting Process on Metallurgical Properties of Ceramics Particulate Al Composites," *IOSR J. Mech. Civ. Eng.*, vol. 12, no. 6, pp. 2278–1684, 2015, doi: 10.9790/1684-12642240.

[44] J. J. Moses, I. Dinaharan, and S. J. Sekhar, "Prediction of influence of process parameters on tensile strength of AA6061 / TiC aluminum matrix composites produced using stir casting," *Trans. Nonferrous Met. Soc. China*, vol. 26, no. 6, pp. 1498–1511, 2016, doi: 10.1016/S1003-6326(16)64256-5.

[45] ASM Handbook Committee, "ASTM B93/B93M-09, Standard Specification for Magnesium Alloys in Ingot Form for Sand Castings, Permanent Mold Castings and Die Castings, steel," *ASM Int.*, vol. 2, pp. 1–9, 2009, doi: 10.1361/asmhba000.

[46] D. S. Mackenzie, "Heat Treating Aluminum for Aerospace Applications," *Journal of Materials Science and Engineering*., vol.10, no. 2, pp (3-4) (2020) 53-59 doi: 10.17265/2161-6213/2020.3-4.002

[47] Z. Aburas, "Microstructural Characterisation and Corrosion Studies of Excimer Laser-Treated Aluminium Alloy AA2024-T351," pp. 1–295, 2013, [Online].

[48] K. Sree Lakshmi, O. Prashanth Rao, and M. Dr. Satyanarayana Gupta, "Design and Static Stress Analysis of Fuselage Structure for a Military Transport Aircraft," *Int. J. Eng. Technol. Manag. Res.*, vol. 3, no. 9, pp. 485–490, 2016.

[49] S. S. Karthik and Gurusiddayya, "Design and Optimization of Fuselage of an aircraft for Static and dynamic loads," *Int. J. Eng. Res. Technol.*, vol. 3, no. 19, pp. 1–8, 2015.

[50] D. Kumar, M. Ko, R. Roy, and J. Kweon, "AFP Mandrel Development for Composite Aircraft Fuselage Skin," *Int'l J. of Aeronautical & Space Sci*., vol. 15. no. (1), pp. 32–43 (2014), doi: 10.5139/IJASS.2014.15.1.32.

[51] M. Karuskevich, "Fatigue Failure Prediction for Fuselage Skin Made of Alclad,"., *Science-based technologies*. vol. 18, no.2. November 2013, 2016, doi: 10.18372/2310-5461.18.4868.

[52] . C. B. S., "Fatigue Life Estimation of Rear Fuselage Structure of an Aircraft," *Int. J. Res. Eng. Technol.*, vol. 04, no. 07, pp. 347–354, 2015, doi: 10.15623/ijret.2015.0407056.

[53] S. Desai and A. Desai, "Structural Design of Fuselage,"., *IJTIMES* , vol. 3, no. 5, pp. 43–48, 2017.

[54] Sanmati Vikas T L and Athrey S Katti, "Finite Element Analysis of Skin-Stringer Panel for Typical Fuselage Structure," *Int. J. Eng. Res.*, vol. V9, no. 04, pp. 386–393, 2020, doi: 10.17577/ijertv9is040313.

[55] R. Abbishek, B. R. Kumar, and H. S. Subramanian, "Fatigue analysis and design optimization of aircraft's central fuselage," *IOP Conf. Ser. Mater. Sci. Eng.*, vol. 225, 2017, doi: 10.1088/1757-899X/225/1/012031.

[56] B. Karthick, S. Balaji, and P. Maniiarasan, "Structural Analysis Of Fuselage With Lattice Structure," *Int. J. Eng. Res. Technol.*, vol. 2, no. 6, pp. 1909–1913, 2013.

[57] A. K. R. Kothapalli, A. Mohanty, and S. R. K. Adika, "Finite Element Modeling And Analysis Of Fuselage Stiffened Panel Subjected To Cabin Pressurization," *Researchgate.Net*, no. January, pp. 678–681, 2012, [Online].

[58] B. Raghu, B. Rajesh, C. H. Swathi, D. Rishikesh, and G. A. Kadir, "Modelling and Analysis of Fuselage." IRJAT., vol. 8, no. Issue 6, pp. 860–880, 2020.

[59] K. B. Mohamed and H. Mohammed, "Design, Analysis and Optimization of Fuselage Floor Beam," IJSRD., Vol. 4, Issue 06, 2016 | ISSN (online): 2321-0613

[60] M. M. Manjunath, G. K. Vijeth, R. Hoque, K. P Mohanan, A. Kumar A, and S. Gouda, "Stress Analysis And Fatigue Estimation Of Centre Fuselage Of An Aircraft," *Int. J. Innov. Res. Sci. Eng. Technol.*, vol. Vol. 4, no. Issue 5, pp. 3182–3188, 2015, doi: 10.15680/IJIRSET.2015.0405101.

[61] A. Y. Qwam Alden and R. Almamalook, "Impact of fuselage cutouts on the stress and deflection behavior: Numerical models and statistical analysis," *IOP Conf. Ser. Mater. Sci. Eng.*, vol. 454, no. 1, 2018, doi: 10.1088/1757-899X/454/1/012063.

[62] I. Sen, "Aircraft Fuselage Design Study - Parametric Modeling, Structural Analysis, Material Evaluation and Optimisation for an Aircraft Fuselage (MSc thesis)," p. 180, 2010.

[63] S. Zhang and F. Wang, "Comparison of friction and wear performances of brake material dry sliding against two aluminum matrix composites reinforced with different SiC particles," *J. Mater. Process. Technol.*, vol. 182, no. 1–3, pp. 122–127, 2007, doi: 10.1016/j.jmatprotec.2006.07.018.

[64] G. G. Sozhamannan, S. B. Prabu, and V. S. K. Venkatagalapathy, "Effect of Processing Paramters on Metal Matrix Composites: Stir Casting Process," *J. Surf. Eng. Mater. Adv. Technol.*, vol. 02, no. 01, pp. 11–15, 2012, doi: 10.4236/jsemat.2012.21002.

[65] A. M. Usman, A. Raji, M. A. Hassan, and N. H. Waziri, "A Comparative Study on the Properties of Al-7%Si-Rice Husk Ash and Al-7%Si-Bagasse Ash Composites Produced by Stir Casting," *Int. J. Eng. Sci.*, vol. 3, no. 8, pp. 1–7, 2014, [Online]. Available: http://theijes.com/papers/v3-i8/Version-1/A03810107.pdf.

[66] O. F. F. L. Y. Ash, B. A. S. H. Al-mmcs, M. Anas, and M. Z. Khan, "COMPARISION OF HARDNESS AND STRENGTH Comparison of Hardness and Strength of Fly Ash and Bagasse Ash Al-MMCs," IJSART., Volume 1 Issue 7, pp. 88–93, 2016.

[67] S. Soltani, R. Azari Khosroshahi, R. Taherzadeh Mousavian, Z. Y. Jiang, A. Fadavi Boostani, and D. Brabazon, "Stir casting process for manufacture of Al–SiC composites," *Rare Met.*, vol. 36, no. 7, pp. 581–590, 2017, doi: 10.1007/s12598-015-0565-7.

[68] ASTM E8, "ASTM E8/E8M standard test methods for tension testing of metallic materials 1," *Annu. B. ASTM Stand. 4*, vol. i, no. C, pp. 1–27, 2010, doi: 10.1520/E0008.

[69] O. O. Daramola, A. A. Adediran, and A. T. Fadumiye, "Evaluation of the mechanical properties and corrosion behaviour of coconut shell ash reinforced aluminium (6063) alloy composites," *Leonardo Electron. J. Pract. Technol.*, vol. 14, no. 27, pp. 107–119, 2015.

[70] G. Narasaraju and D. L. Raju, "Characterization of Hybrid Rice Husk and Fly ash-Reinforced Aluminium alloy (AlSi10Mg) Composites," *Mater. Today Proc.*, vol. 2, no. 4–5, pp. 3056–3064, 2015, doi: 10.1016/j.matpr.2015.07.245.

[71] P. Maibusab, H. K. Shivanand, M. M. G., S. H.A., and S. B. G., "Evaluation of Wear Properties of Heat-treated Al 7075/Graphite Powder/Bagasse ash Hybrid Metal Matrix Composites," *Int. J. Sci. Res. Sci. Technol.*, vol. 6, no. 3, pp. 201–210, 2019, doi: 10.32628/ijsrst1196338.

[72] M. Z. Khan, M. Anas, A. Hussain, M. Irshadul Haque, and K. Rasheed, "Effect on Mechanical Properties of Aluminium Alloy Composites on Adding Ash as Reinforcement Material," *J. Met. Mater. Miner.*, vol. 25, no. 2, pp. 1–7, 2015.

[73] ASTM E8, "ASTM E8/E8M Standard Test Methods For Tension Testing Of Metallic Materials 1," *Annu. B. ASTM Stand. 4*, vol. i, no. C, pp. 1–27, 2010, doi: 10.1520/E0008.

[74] Sreenivasa R, 2Kallesh S S, 3Naveen Kumar K H, 4Sandeep S H "Study the Effect of Buckling on Aircraft Fuselage Skin Panel with or without Airframe,". *IJSDR*., vol. 1, no. 6, pp. 346–353,

2016.

[75] S. S. Karthik and Gurusiddayya, "Design and Optimization of Fuselage of an aircraft for Static and dynamic loads," *Int. J. Eng. Res. Technol.*, vol. 3, no. 19, pp. 1–8, 2015.

[76] J. Singh and A. Chauhan, "Characterization of hybrid aluminum matrix composites for advanced applications – A review," *Integr. Med. Res.*, vol. 5, no. 2, pp. 159–169, 2015, doi: 10.1016/j.jmrt.2015.05.004.

[77] V. S. Aigbodion, S. B. Hassan, and J. E. Oghenevweta, "Microstructural analysis and properties of Al-Cu-Mg/bagasse ash particulate composites," *J. Alloys Compd.*, vol. 497, no. 1–2, pp. 188–194, 2010, doi: 10.1016/j.jallcom.2010.02.190.

[78] O. B. Fatile, J. fedayo AkinruliI, and A. A. Amori, "Microstructure and Mechanical Behaviour of Stir-Cast Al-Mg-Sl Alloy Matrix Hybrid Composite Reinforced with Corn Cob Ash and Silicon Carbide," *Int. J. Eng. Technol. Innov.*, vol. 4, no. 4, pp. 251–259, 2014, [Online]. Available: https://doaj.org/article/3ff98d13a11042498fb5fe293ccaae35%0Ahttp://ojs.imeti.org/index.php/IJETI/article/view/42.

[79] V. Mahesh Kumar and C. V. Venkatesh, "Effect of ceramic reinforcement on mechanical properties of aluminum matrix composites produced by stir casting process," *Mater. Today Proc.*, vol. 5, no. 1, pp. 2466–2473, 2018, doi: 10.1016/j.matpr.2017.11.027.

APPENDIX

Table: 1. Flexural strength result

Composite	Treated											Untreated	
	T1	T2	T3	T4	T5	Avg. Applied Force (KN)	T1	T2	T3	T4	T5	Avg. Bending Strength	Applied Force (KN)	Bending Strength
Base Alloy	190	216	190	196	192	19.867	312	360	312	326	320	328	18.5	306
C1	240	230	214	252	245	22.8	400	380	306	420	408	362	18.5	378
C2	220	204	233	230	230	21.9	365	340	388	306	306	364	20.4	340
C3	196	190	236	192	233	20.7	326	312	392	320	388	343	17.4	290
C4	144	432	144	322	192	24.0	240	570	240	536	320	350	11.5	342
C5	233	230	245	240	240	23.6	368	384	408	400	400	386.7	21.1	372
C6	252	250	246	245	250	24.9	420	416	410	408	416	415	24.5	408
C7	322	245	302	302	322	28.97	536	408	502	536	416	482	24.0	400
C8	192	150	175	214	144	17.2	320	250	292	306	240	287	13.2	220
C9	168	192	190	192	192	18.3	280	320	312	320	320	304	12.6	210

Table: 2. Rockwell Hardness test results

Composite	T1	T2	T3	T4	T5	Avg. Result of the treated specimen	Avg. result of untreated specimen
Al2024	59.9	57	61.9	60.6	58.7	59.62	47
C1	61.8	82.2	61.9	48.9	41.5	59.26	52.3
C2	56.4	65.5	64.5	66.3	58.7	62.28	55
C3	66.6	67.8	68.5	58.6	59.9	63.48	57.76
C4	58.5	59.3	64	60.9	61.9	60.92	52.92
C5	67.4	61.8	58.8	62.4	78.8	65.84	49.84
C6	94.5	71.3	69.3	63	73	74.22	50.76
C7	76.3	79.3	76.6	70.6	69	74.36	55.8
C8	67.8	75.3	72.8	74.4	78.2	73.5	55.58
C9	69.8	77.9	69.9	69	73	71.98	52.12

Table: 3. heat-treated tensile test results

Composites	Ultimate Tensile Strength (MPa)	Avg. Maxi. Yield Tensile Strength (MPa)	Avg. Maxi. Youngs Modulus (GPa)
Al2024	320.2	214.2	70.88654
c1	373.99	251.56	75.25593
c2	378	377.1	75.3329
c3	586.9	312.2	96.22054
c4	351.1	204.2	83.32525
c5	400.1	286.2	74.97025
c6	347.67	318.7	105.5475
c7	560	392.67	78.89429
c8	394	217.7	87.6683
c9	206.35	157.7	91.28042

Reinforcement Composition comparisons

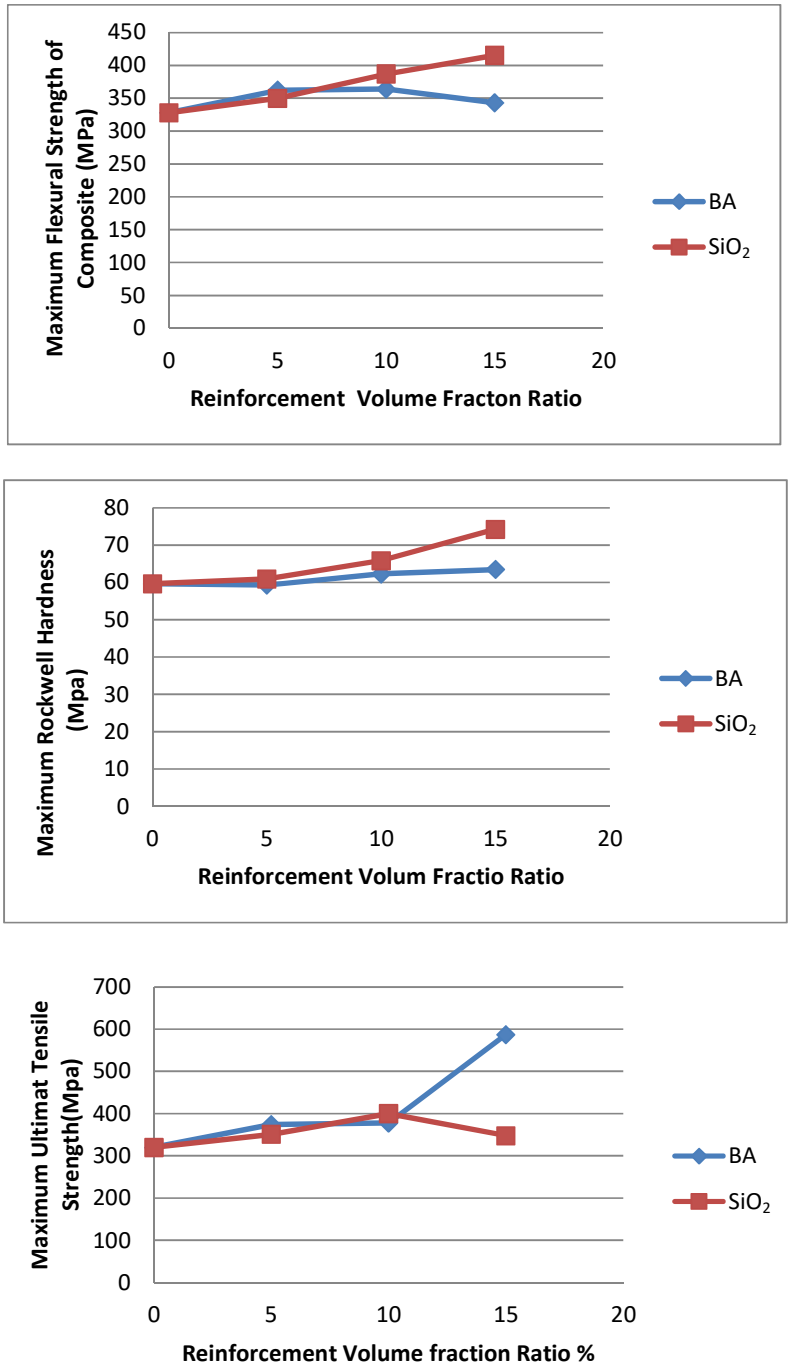

Figure 1. Reinforcement Composition comparisons

Some of the ANSYS test result

15psi Al2024 T3

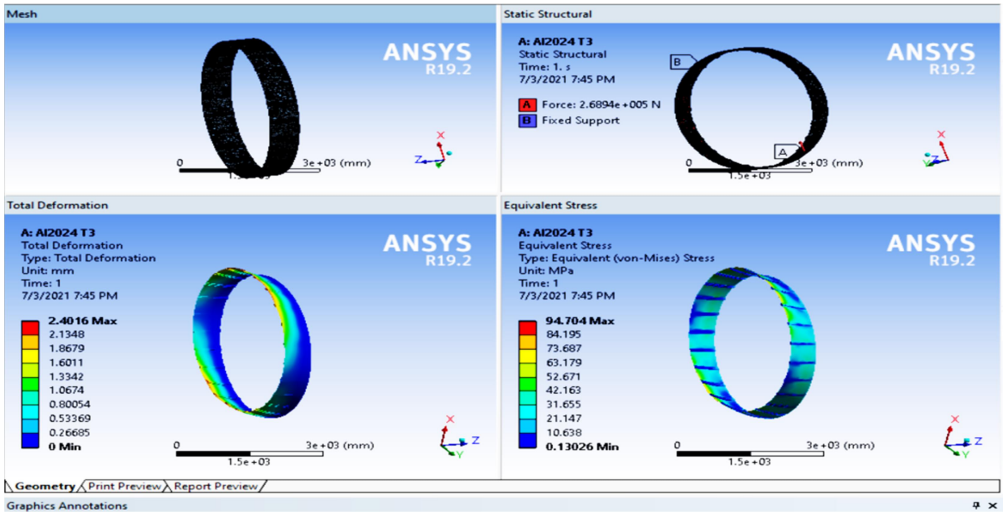

17psi Al2024 T3

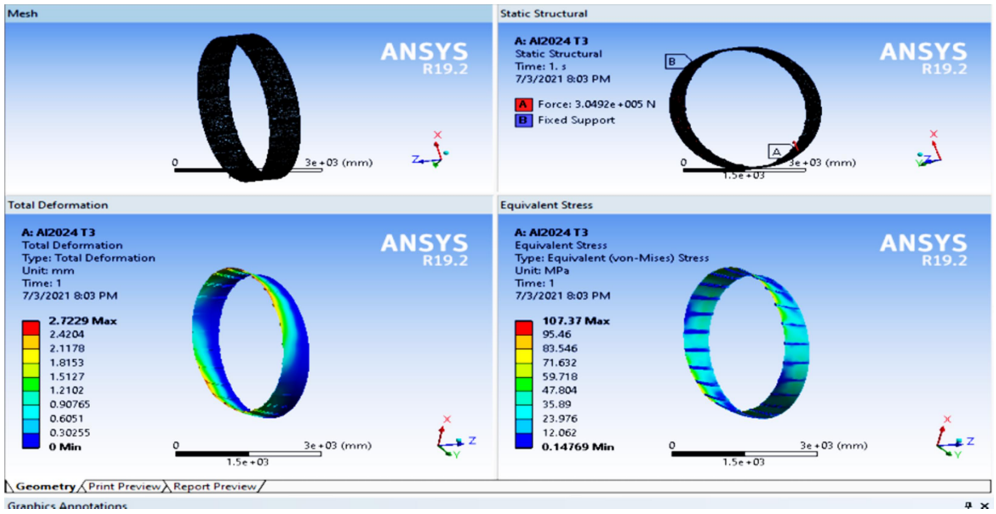

Length X	3952.4 mm
Length Y	3952.4 mm
Length Z	660.4 mm
Properties	
Volume	3.8999e+007 mm³
Mass	103.74 kg
Centroid X	-0.14239 mm
Centroid Y	-1.8134 mm
Centroid Z	330.08 mm
Moment of Inertia Ip1	2.0447e+008 kg·mm²
Moment of Inertia Ip2	2.0393e+008 kg·mm²
Moment of Inertia Ip3	4.0086e+008 kg·mm²
Statistics	
Nodes	61956
Elements	33850

Figure 2. 15 & 17 psi Al2024 T3

10psi Al2024 T351

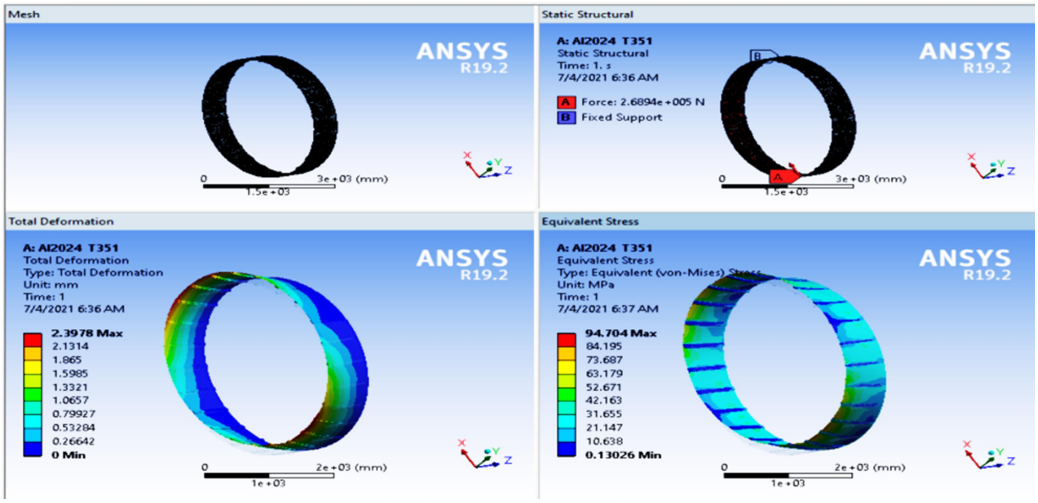

27psi Al2024 T351

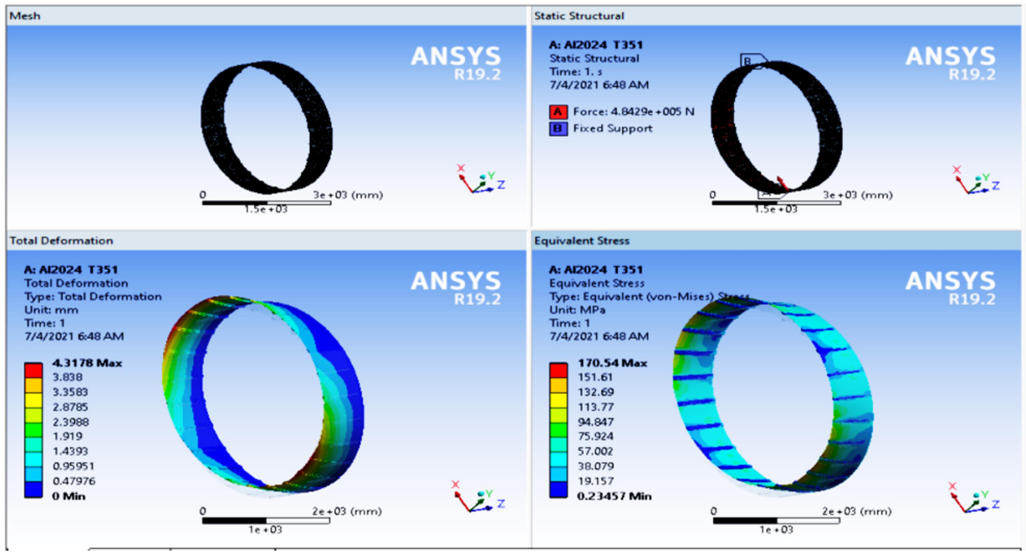

Length Y	3952.4 mm
Length Z	660.4 mm
Properties	
Volume	3.8999e+007 mm³
Mass	108.42 kg
Centroid X	-0.14239 mm
Centroid Y	-1.8134 mm
Centroid Z	330.08 mm
Moment of Inertia Ip1	2.1369e+008 kg·mm²
Moment of Inertia Ip2	2.1313e+008 kg·mm²
Moment of Inertia Ip3	4.1894e+008 kg·mm²
Statistics	
Nodes	61956
Elements	33850

Figure 3. 10 & 27psi Al2024 T351

5psi Al2024/SiO_2/BA T3

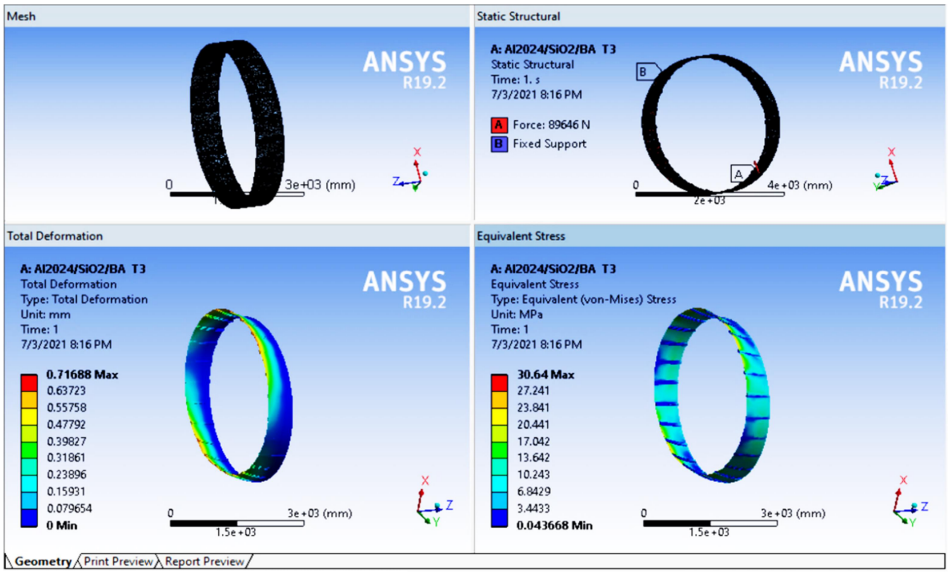

31psi Al2024/SiO_2/BA T3

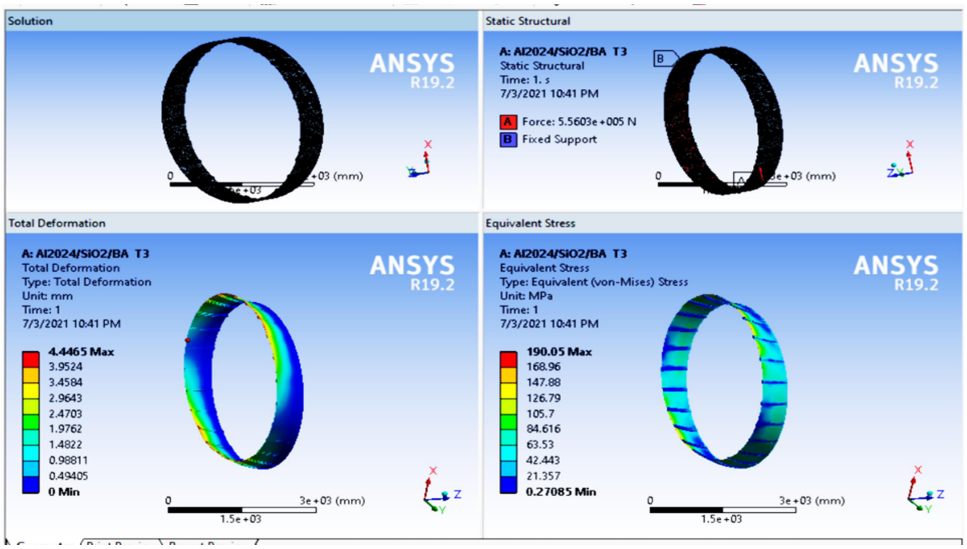

Length Y	3952.4 mm
Length Z	660.4 mm
Properties	
Volume	3.8999e+007 mm³
Mass	99.838 kg
Centroid X	-0.14239 mm
Centroid Y	-1.8134 mm
Centroid Z	330.08 mm
Moment of Inertia Ip1	1.9678e+008 kg·mm²
Moment of Inertia Ip2	1.9627e+008 kg·mm²
Moment of Inertia Ip3	3.8579e+008 kg·mm²
Statistics	
Nodes	61956
Elements	33850

Figure 4. 5 & 31psi Al2024/SiO_2/BA T3

Stress-Strain graphical representation

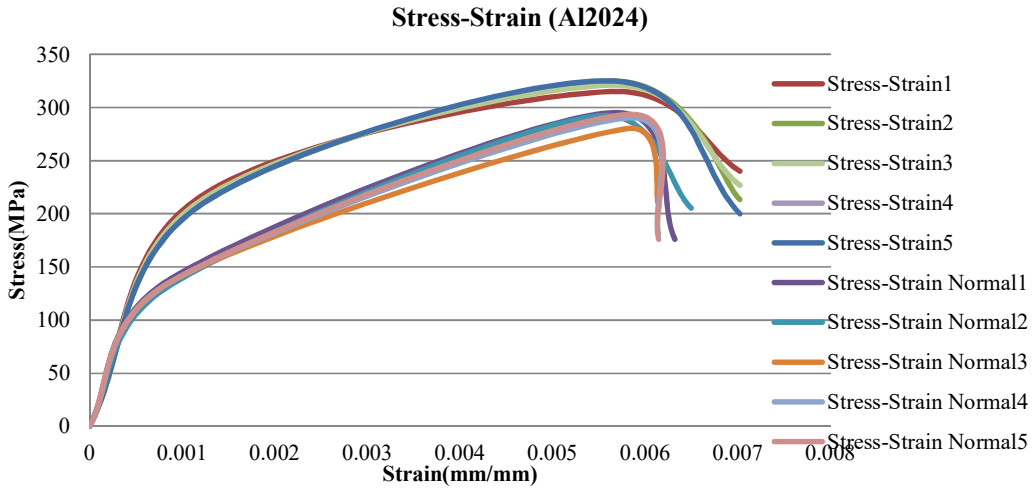

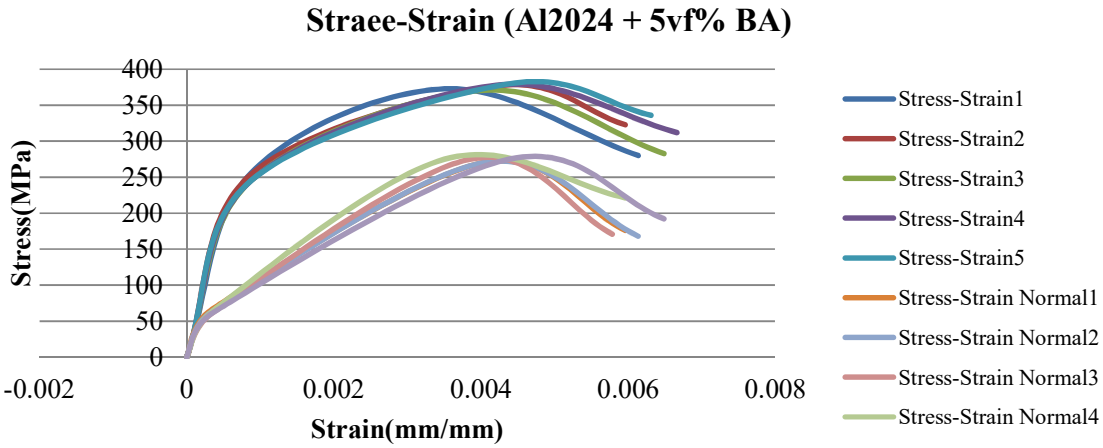

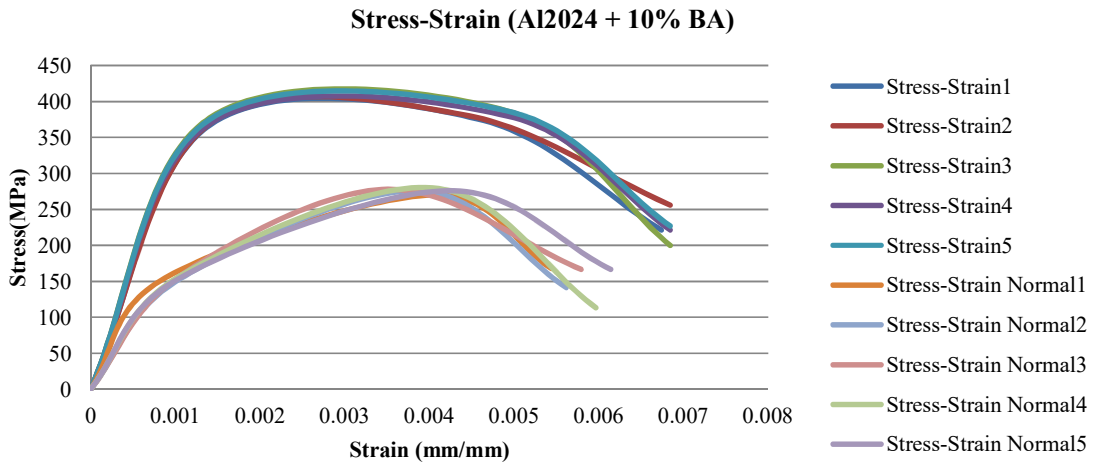

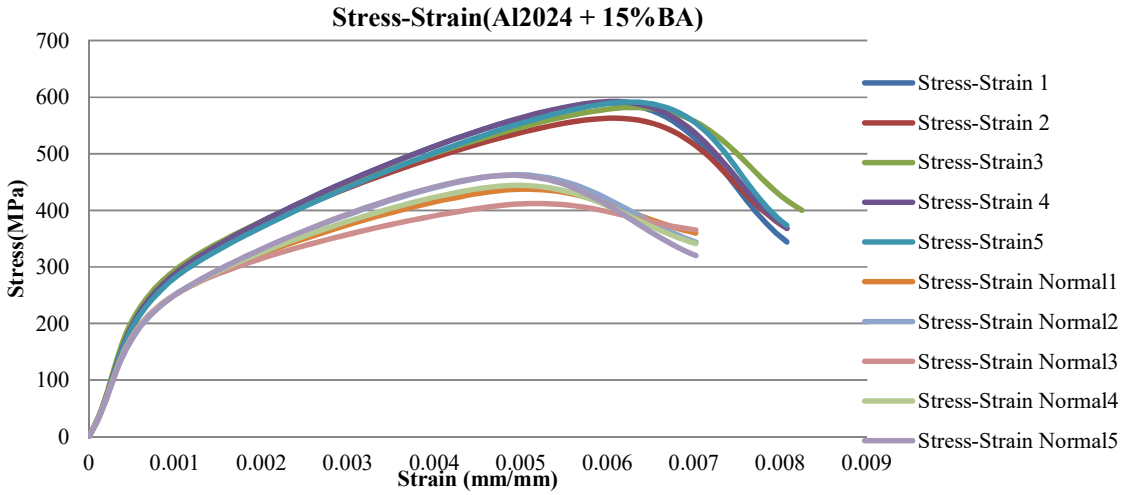
Stress-Strain(Al2024 + 15%BA)
Stress(MPa)
Strain (mm/mm)
Stress-Strain 1
Stress-Strain 2
Stress-Strain3
Stress-Strain 4
Stress-Strain5
Stress-Strain Normal1
Stress-Strain Normal2
Stress-Strain Normal3
Stress-Strain Normal4
Stress-Strain Normal5

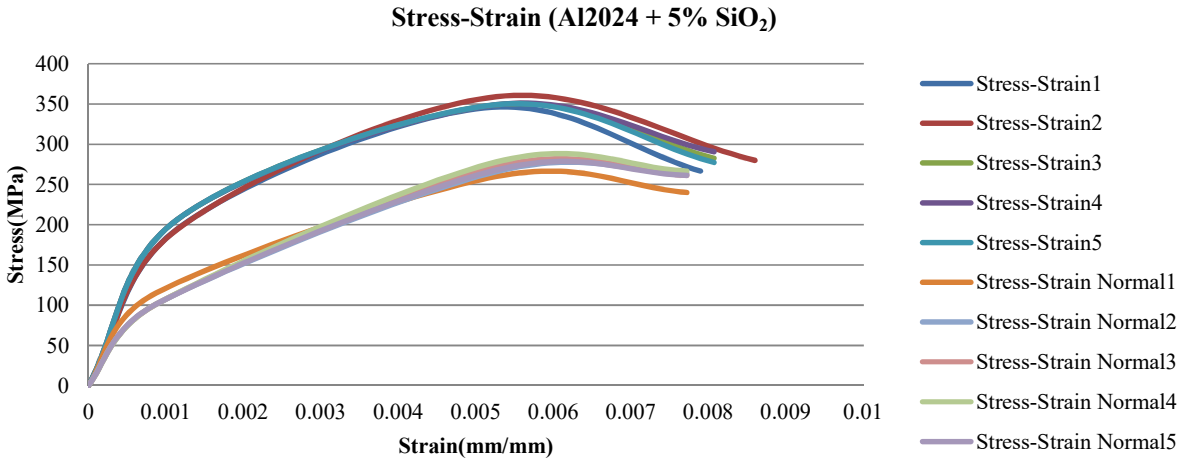
Stress-Strain (Al2024 + 5% SiO2)
Stress(MPa)
Strain(mm/mm)
Stress-Strain1
Stress-Strain2
Stress-Strain3
Stress-Strain4
Stress-Strain5
Stress-Strain Normal1
Stress-Strain Normal2
Stress-Strain Normal3
Stress-Strain Normal4
Stress-Strain Normal5

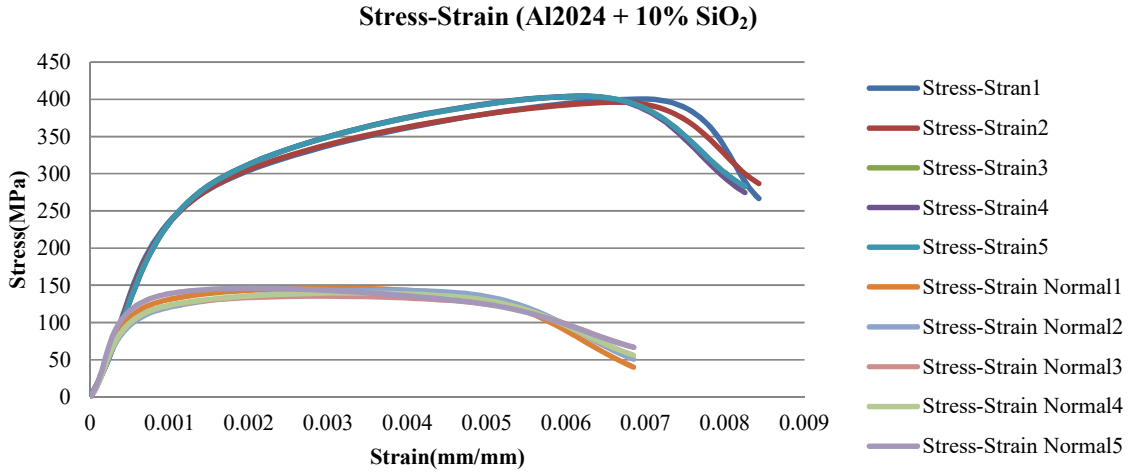
Stress-Strain (Al2024 + 10% SiO2)
Stress(MPa)
Strain(mm/mm)
Stress-Stran1
Stress-Strain2
Stress-Strain3
Stress-Strain4
Stress-Strain5
Stress-Strain Normal1
Stress-Strain Normal2
Stress-Strain Normal3
Stress-Strain Normal4
Stress-Strain Normal5

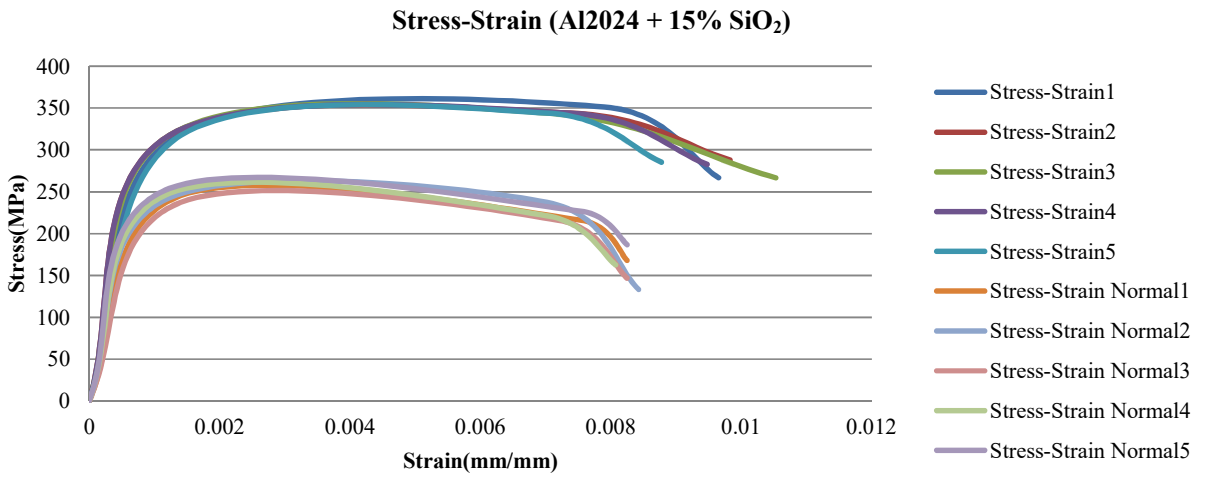
Stress-Strain (Al2024 + 15% SiO2)
Stress(MPa)
400
350
300
250
200
150
100
50
0
0
0.002
0.004
0.006
0.008
0.01
0.012
Strain(mm/mm)
Stress-Strain1
Stress-Strain2
Stress-Strain3
Stress-Strain4
Stress-Strain5
Stress-Strain Normal1
Stress-Strain Normal2
Stress-Strain Normal3
Stress-Strain Normal4
Stress-Strain Normal5

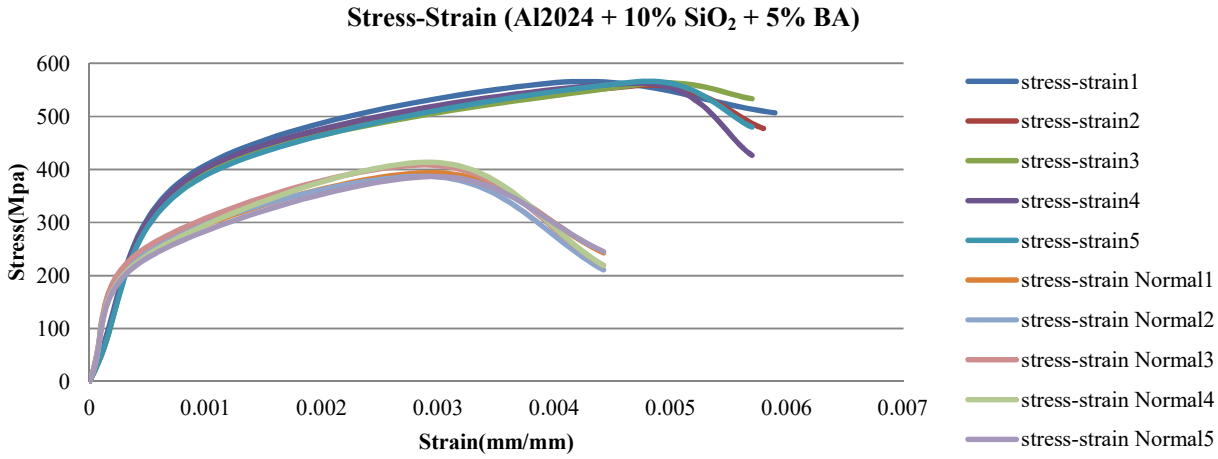
Stress-Strain (Al2024 + 10% SiO2 + 5% BA)
Stress(Mpa)
600
500
400
300
200
100
0
0
0.001
0.002
0.003
0.004
0.005
0.006
0.007
Strain(mm/mm)
stress-strain1
stress-strain2
stress-strain3
stress-strain4
stress-strain5
stress-strain Normal1
stress-strain Normal2
stress-strain Normal3
stress-strain Normal4
stress-strain Normal5

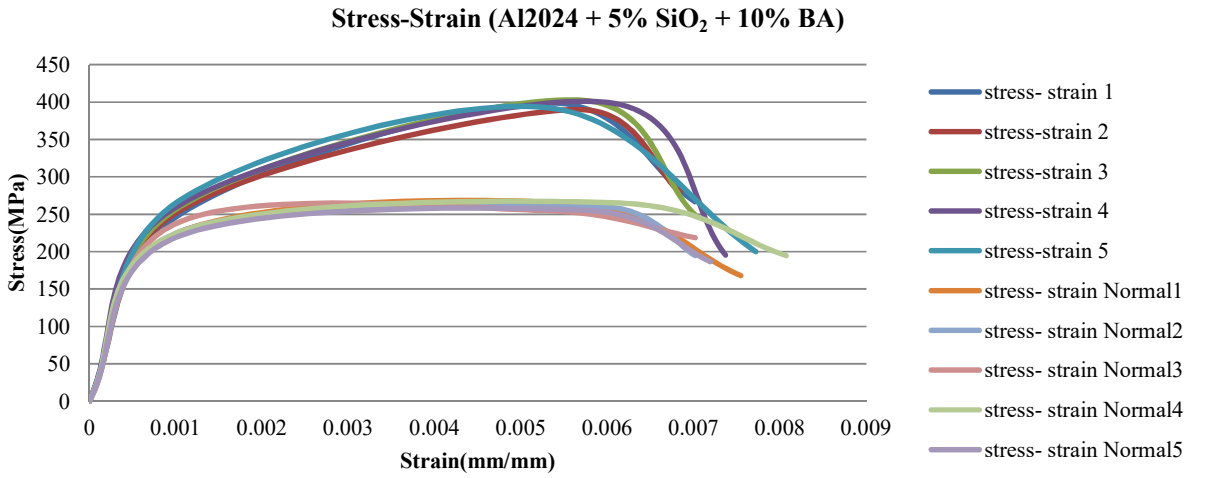
Stress-Strain (Al2024 + 5% SiO2 + 10% BA)
Stress(MPa)
450
400
350
300
250
200
150
100
50
0
0
0.001
0.002
0.003
0.004
0.005
0.006
0.007
0.008
0.009
Strain(mm/mm)
stress- strain 1
stress-strain 2
stress-strain 3
stress-strain 4
stress-strain 5
stress- strain Normal1
stress- strain Normal2
stress- strain Normal3
stress- strain Normal4
stress- strain Normal5

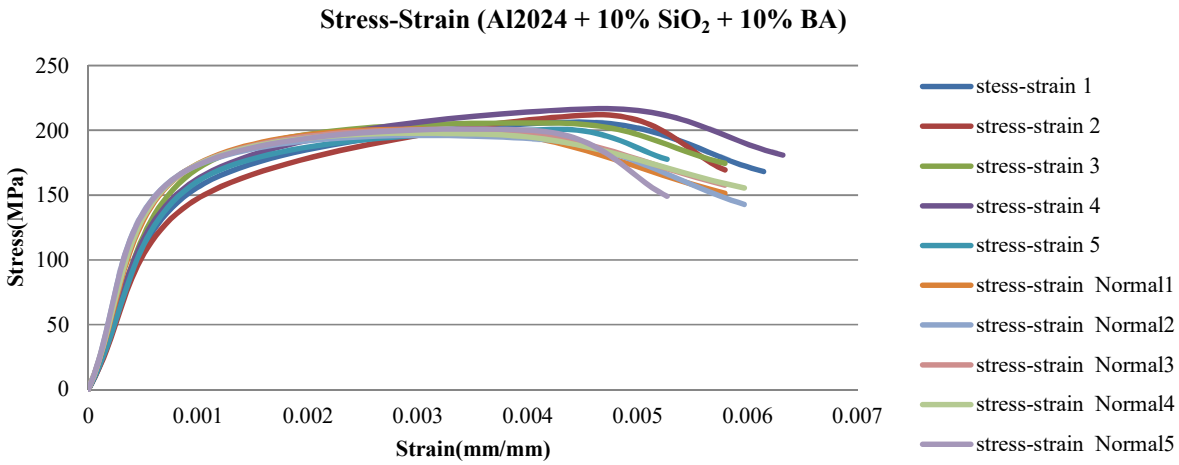

Figure 5. Stress-Strain graphical representation